

NATIONAL AERONAUTICS AND SPACE ADMINISTRATION

Space Programs Summary No. 37-37, Volume III

for the period November 1, 1965 to December 31, 1965

The Deep Space Network

FACILITY FORM 802

N66-18023

(ACCESSION NUMBER)

(THRU)

(PAGES)

(CODE)

(NASA CR OR TMX OR AD NUMBER)

(CATEGORY)

NASA CR70636

GPO PRICE \$ _____

CFSTI PRICE(S) \$ _____

Hard copy (HC) 3.00

Microfiche (MF) .45

ff 653 July 85

jpl

JET PROPULSION LABORATORY
CALIFORNIA INSTITUTE OF TECHNOLOGY
PASADENA, CALIFORNIA

January 31, 1966

NATIONAL AERONAUTICS AND SPACE ADMINISTRATION

Space Programs Summary No. 37-37, Volume III

for the period November 1, 1965 to December 31, 1965

The Deep Space Network

JET PROPULSION LABORATORY
CALIFORNIA INSTITUTE OF TECHNOLOGY
PASADENA, CALIFORNIA

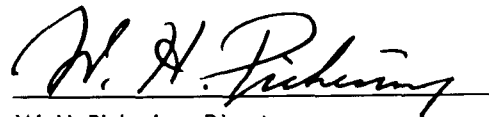
January 31, 1966

Preface

The *Space Programs Summary* is a six-volume, bimonthly publication that documents the current project activities and supporting research and advanced development efforts conducted or managed by JPL for the NASA space exploration programs. The titles of all volumes of the *Space Programs Summary* are:

- Vol. I. The Lunar Program (Confidential)
- Vol. II. The Planetary-Interplanetary Program (Confidential)
- Vol. III. The Deep Space Network (Unclassified)
- Vol. IV. Supporting Research and Advanced Development (Unclassified)
- Vol. V. Supporting Research and Advanced Development (Confidential)
- Vol. VI. Space Exploration Programs and Space Sciences (Unclassified)

The *Space Programs Summary*, Vol. VI consists of an unclassified digest of appropriate material from Vols. I, II, and III; an original presentation of technical supporting activities, including engineering development of environmental-test facilities, and quality assurance and reliability; and a reprint of the space science instrumentation studies of Vols. I and II.



W. H. Pickering, Director
Jet Propulsion Laboratory

Space Programs Summary No. 37-37, Volume III

Copyright © 1966, Jet Propulsion Laboratory, California Institute of Technology
Prepared under Contract No. NAS 7-100, National Aeronautics & Space Administration

Contents

I. Introduction	1
II. DSN Systems Design	3
A. Communications Theory Model of the DSN Ground Communications System	3
B. High-Speed Data System	5
C. Simulation Data Conversion Center	7
D. <i>Mariner</i> Master Data Library	8
III. Communications Engineering Developments	12
A. S-Band Implementation for DSIF: Acquisition Aid for Ascension Island	12
B. 100-kw S-Band Final Amplifier	12
C. Multiplier Chains (Phase and Amplitude Stability)	13
D. Phase Response of the RF Carrier Tracking Loop (CTL) S-Band Transponder Ranging Station	16
E. Amplitude Stabilized Signal Source	31
References	32
IV. Communications Research and Development	33
A. Experimental Closed Cycle Refrigerator for Masers	33
B. Continuous Wave (CW) Signal Power Calibration With Thermal Noise Standards	35
C. Simultaneous Lobing Radiometric Tracking System	39
D. Microwave Maser Development	44
E. Frequency Generation and Control: S/X-Band Central Frequency Synthesizer	47
F. Information Processing	47
G. Combinatorial Communication Research	49
H. Venus Station Operations	50
V. Tracking Stations Engineering and Operations	55
A. Goldstone Operations	55
B. Antenna Dish Resurfacing at Woomera	58
C. Systems Engineering and Integration at Ascension Island	59
D. Aircraft Masking Exercise at Tidbinbilla	60

I. Introduction

1. General

The Deep Space Network (DSN) is a precision communication system which is designed to communicate with, and permit control of, spacecraft designed for deep space exploration. The DSN consists of the Deep Space Instrumentation Facility (DSIF), the Space Flight Operations Facility (SFOF), and the DSN Ground Communication System (GCS).

The DSN is a NASA facility, managed by JPL through a contract between NASA and the California Institute of Technology. The Office of Tracking and Data Acquisition is the cognizant NASA office.

It is the policy of the DSN to continuously conduct research and development of new components and systems and to engineer them into the DSN to maintain a state-of-the-art capability.

The DSN has facilities for simultaneously controlling a newly launched spacecraft and a second one already in flight. Within a few months, it will be able to control simultaneously either two newly launched spacecraft plus two in flight or the operations of four spacecraft in flight at the same time. The DSIF is equipped with 85-ft antennas having gains of 53 db at 2300 Mc and a system

temperature of 55°K, making it possible to receive significant data rates at distances as far as the planet Mars. To improve the data rate and distance capability, a 210-ft antenna is under construction at the Goldstone Mars Station and two additional antennas of this size are planned for installation at overseas stations.

The DSIF utilizes large antennas, low-noise phase-lock receiving systems, and high-power transmitters located at stations positioned around the Earth to track, command, and receive data from deep space probes. Overseas stations are generally operated by personnel of the respective countries. The DSIF stations are:

I.D. No.	Name	Location
11	Goldstone, Pioneer	Barstow, California
12	Goldstone, Echo	Barstow, California
13	Goldstone, Venus (R&D)	Barstow, California
14	Goldstone, Mars (under construction)	Barstow, California
41	Woomera	Island Lagoon, Australia
42	Tidbinbilla	Canberra, Australia
51	Johannesburg	Johannesburg, South Africa
61	Madrid (under construction)	Madrid, Spain
71	Spacecraft Monitoring	Cape Kennedy, Florida
72	Spacecraft Guidance and Command (under construction)	Ascension Island

The SFOF is located in a three-story building at the Jet Propulsion Laboratory in Pasadena, California, and utilizes operations control consoles, status and operations displays, computers, data processing equipment for analysis of spacecraft performance and space science experiments, and communication facilities to control space flight operations. This control is accomplished by generating trajectories and orbits, and command and control data, from tracking and telemetry data received from the DSIF in near real-time. The SFOF also reduces the telemetry, tracking, command and station performance data

recorded by the DSIF into engineering and scientific information for analysis and use by the scientific experimenters and spacecraft engineers.

The DSN Ground Communication System consists of voice, normal and high data rate teletype circuits provided by the NASA World-Wide Communications Network between each overseas station and the SFOF; teletype and voice circuits between the SFOF, Goldstone Stations, and Cape Kennedy; and a microwave link between the SFOF and Goldstone, provided by the DSN.

II. DSN Systems Design

A. Communications Theory Model of the DSN Ground Communications System

Engineering analyses of system capability and adequacy are often performed with models which separate the major functions of a system; e.g., telemetry data handling, analog data handling, and command data handling are often analyzed separately. The analysis is thereby simplified and yet yields results which give a valid estimate of adequacy. The separate functions of the system can be combined later to appraise the adequacy of the elements which treat the functionally different data streams as a whole (usually sequentially). For the study of the DSN Ground Communications System, certain tools for performing system analyses are required. Some initial results of attempts to provide general, yet useful, models of digital data transmission systems are presented here. The model developed here has resulted from both kinds of analysis: that of functionally defined data paths, and that of partially integrated data handling systems.

The model has an empirical basis, since it was from the study of existing systems and operations that a knowledge of the necessary relationships and operations between elements was acquired. Therefore, the general formal model is a generalization of some particular operational

models, and its generality may be thereby limited. (An evaluation of the capabilities and limitations of this formal scheme when applied to cases of interest remains to be accomplished.) The ground telemetry data handling system (somewhat simplified) given in Fig. 1 represents the type of system intended for generalization. The system operates in essentially real or near-real time, since magnetic tape recorders and other storage capabilities are not shown explicitly; however, these limitations are recognized, and the system shown is only intended to be illustrative.

Design simplicity, consistent with reasonable assumptions for the system which the model is intended to describe, is a desirable goal in model development. In the development of a digital data system model, one would like to reduce the number and/or complexity of the functional blocks in the system representation as much as possible while still retaining the usefulness of the model. The model discussed here involves a single, general "block" element (Fig. 2), which is actually a collection of relationships and operations sufficiently inclusive to represent most of the functional elements of a digital system.

Assume that a signal leaving a source is represented by the function $y_0(t)$, which will be the input to the first block of the system. Within the representation of the system, the $y_i(t)$ will represent the signals which leave

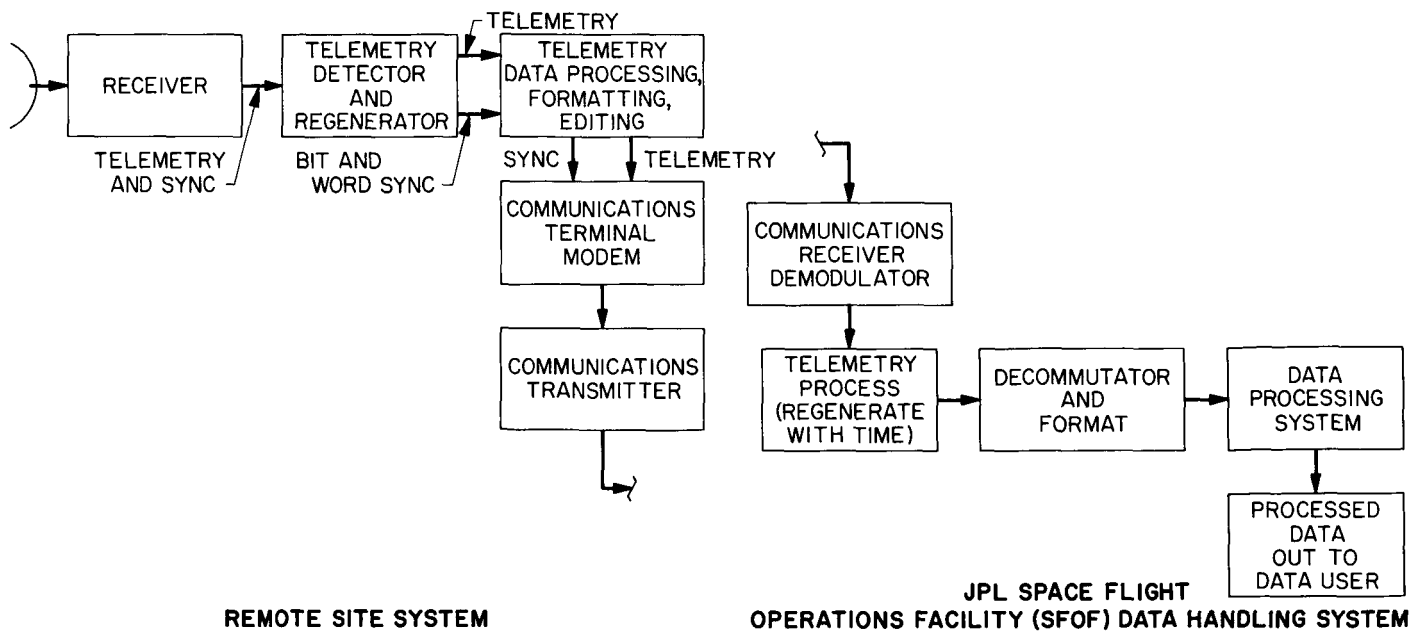


Fig. 1. Typical ground telemetry data handling system

one element and are presented to the succeeding element (which implies that signal flow is unidirectional and well-defined). In the absence of noise, the mappings T_k (considered purely deterministic) are:

$$T_k: y_{k-1} \rightarrow y_k, \quad k = 1, 2, \dots, n,$$

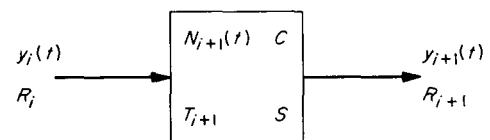
where n is the number of elements. However, consider that additive noise is to be included in the system such that, in functional notation,

$$y_k = T_k y_{k-1} + N_k.$$

Hence, recursively,

$$\begin{aligned} y_1 &= T_1 y_0 + N_1, \\ y_2 &= T_2 y_1 + N_2 = T_2 \cdot (T_1 y_0 + N_1) + N_2, \\ &\vdots \\ y_n &= T_n y_{n-1} + N_n, \end{aligned}$$

and where the center dot symbol (\cdot) represents the operation for combining mappings T_i . It is clear that the noise contribution at the i th stage is mapped forward by the transformation T_{i+1} at the $(i+1)$ th stage; however, the T_i are often linear transformations (or can be approximated over a useful range by a linear transformation), and the N_i are frequently normally distributed contributions. A linear transformation of a normally distributed variate is again a normally distributed variate, and the



$N(t)$ = NOISE CONTRIBUTION OF THE INDIVIDUAL ELEMENT
 T = MAPPING OF THE SIGNAL (OR SIGNAL AND NOISE) FORWARD
 C = DIGITAL CAPACITY OF THE ELEMENT
 S = STORAGE CAPACITY OF THE ELEMENT
 R_i = DATA RATE OF INPUT DATA ($i = 0, 1, 2, \dots$)
 R_{i+1} = DATA RATE OF OUTPUT DATA
 $y_i(t)$ = INPUT DATA SIGNAL
 $y_{i+1}(t)$ = OUTPUT SIGNAL

Fig. 2. Block representation of communications system element

transformations over several (or all) stages may be represented as:

$$y_m = \mathcal{G} y_k + \mathcal{N},$$

where

$$\mathcal{G} = T_m \cdot T_{m-1} \cdot \dots \cdot T_{k+1},$$

and where \mathcal{N} , the total noise contribution between the k th and the m th stages, is a linear combination of the N_i , $i = k+1, \dots, m$.

It should be noted that major transformations on the signal occur in modulator-encoder and demodulator-

decoder stages of a system. Formally, these transformations may be written:

$$y_k(t) = \mathcal{M}[y_{k-1}(t)],$$

$$y_{k+1}(t) = \mathcal{D}[y_k(t)],$$

where the demodulation transformation \mathcal{D} is ideally the inverse of the modulation transformation \mathcal{M} . Therefore, in the absence of noise in the ideal case,

$$y_{k+1}(t) = y_{k-1}(t).$$

In cases of interest, however, noise enters the system described by these equations, and the $y_k(t)$ presented to the demodulator is the $y_k(t) + N_k$ from the modulator output, or:

$$y_k(t) = \mathcal{M}[y_{k-1}(t)],$$

$$y_{k+1}(t) = \mathcal{D}[y_k(t) + N_k].$$

Hence,

$$y_{k+1}(t) = y_{k-1}(t) + \Delta y_{k-1}(t),$$

where

$$\Delta y_{k-1} = \mathcal{D}N_{k-1}.$$

In general, these processes are nonlinear and, in the simplest cases, represent frequency transformations. For n elements in a system including one modem sequence, the output y_n can be written:

$$y_n(t) = \mathcal{I}_2 \cdot \mathcal{D} \{ \mathcal{I}_1 \cdot \mathcal{M} [\mathcal{I}_0 y_0(t - \ell) + N_0] + N_1 \} + N_2,$$

where \mathcal{I}_2 , \mathcal{I}_1 , and \mathcal{I}_0 represent the "products" of transformations after the demodulator, between the modulator and the demodulator, and from the source to the modulator, respectively; N_i , the noise contributions corresponding to the respective \mathcal{I}_i ; and ℓ , the total delay time from the source to the receiver. Often, y_n represents as true a reproduction of y_0 as possible within system limitations. The expression for the ultimately received signal can frequently be simplified to

$$y_n(t) = A[y_0(t - \ell) + \Delta y(t)],$$

where A is a linear transformation (usually an approximation to the gain) and $\Delta y(t)$ is the total noise contribution of the system.

The digital capacity C of the element is often redundant if both R_i and R_{i+1} are known, since R_{i+1} usually implies C directly. However, there are situations in which R_{i+1} is not of particular interest; instead, variables which contribute to C , such as service time and holding times, are of interest. Such cases arise when the element is a memory or buffering device in the system. In these cases, the storage (or memory) capacity S of the element is also of interest.

B. High-Speed Data System

For high-speed data communications, various modulation methods are utilized for the transmission of digital information over telephone-type audio channels. The most significant advantage of this technique over other transmission methods such as teletype or analog is that of bit-rate capacity. For example, a given high-speed system operating over a 3-kc voice channel can transmit a volume of data equivalent to 80 teletype channels operating simultaneously.

Communications channels to and from the JPL Space Flight Operations Facility (SFOF), the various Deep Space Instrumentation Facility (DSIF) tracking stations, and various NASA and contractor organizations are provided by the DSN Ground Communications System (GCS), which utilizes a portion of the NASA Communications (NASCOM) Facility. NASCOM has the responsibility for implementation and technical control of the new GCS high-speed data system (HSDS). The HSDS, as presently being implemented by NASCOM, is composed of two related subsystems (Fig. 3):

- (1) Full duplex modem units, which provide separate receive/transmit capabilities for passage of digital data over 3-kc audio channels at standard data rates of 2400, 1200, and 600 bits/sec.
- (2) Error detection coder units, which provide for error detection coding of the digital data prior to data transmission by the modem subsystem and error detection decoding after the data reaches its destination.

Thus, these two subsystems provide for digital data transmission on an error-encoded block-by-block basis, with the capability of error-rate determination on a block

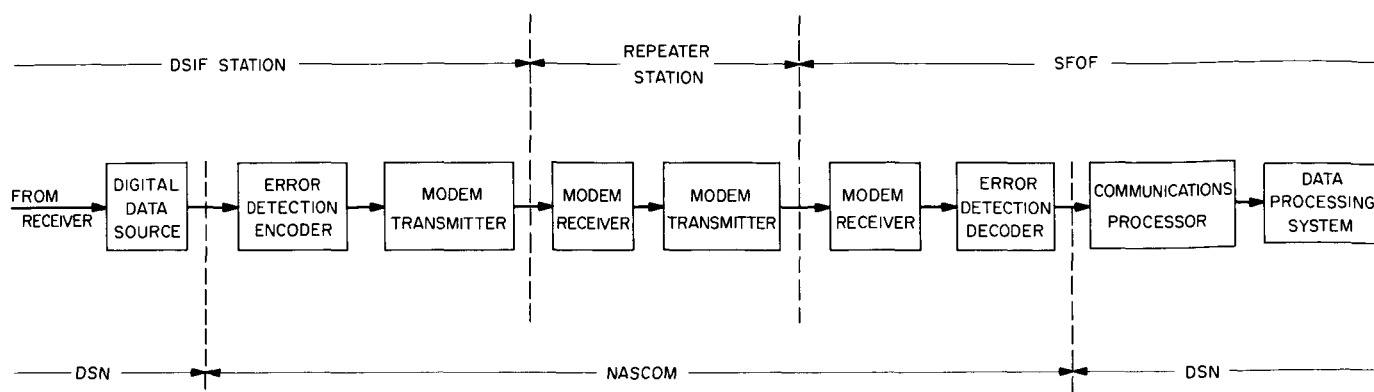


Fig. 3. High-speed data system

basis irrespective of data formats within the data block. Inclusion of error detection coding provides the user with *a priori* knowledge of blocks containing errors and enables communications personnel to perform circuit evaluation and trouble isolation without interrupting the data stream.

The HSDS is scheduled for installation at the NASCOM Facility by summer 1966. As the system becomes operational, further implementation will provide for GCS compatibility with the NASCOM high-speed message switching system (to be discussed in detail in a future issue of the SPS, Vol. III).

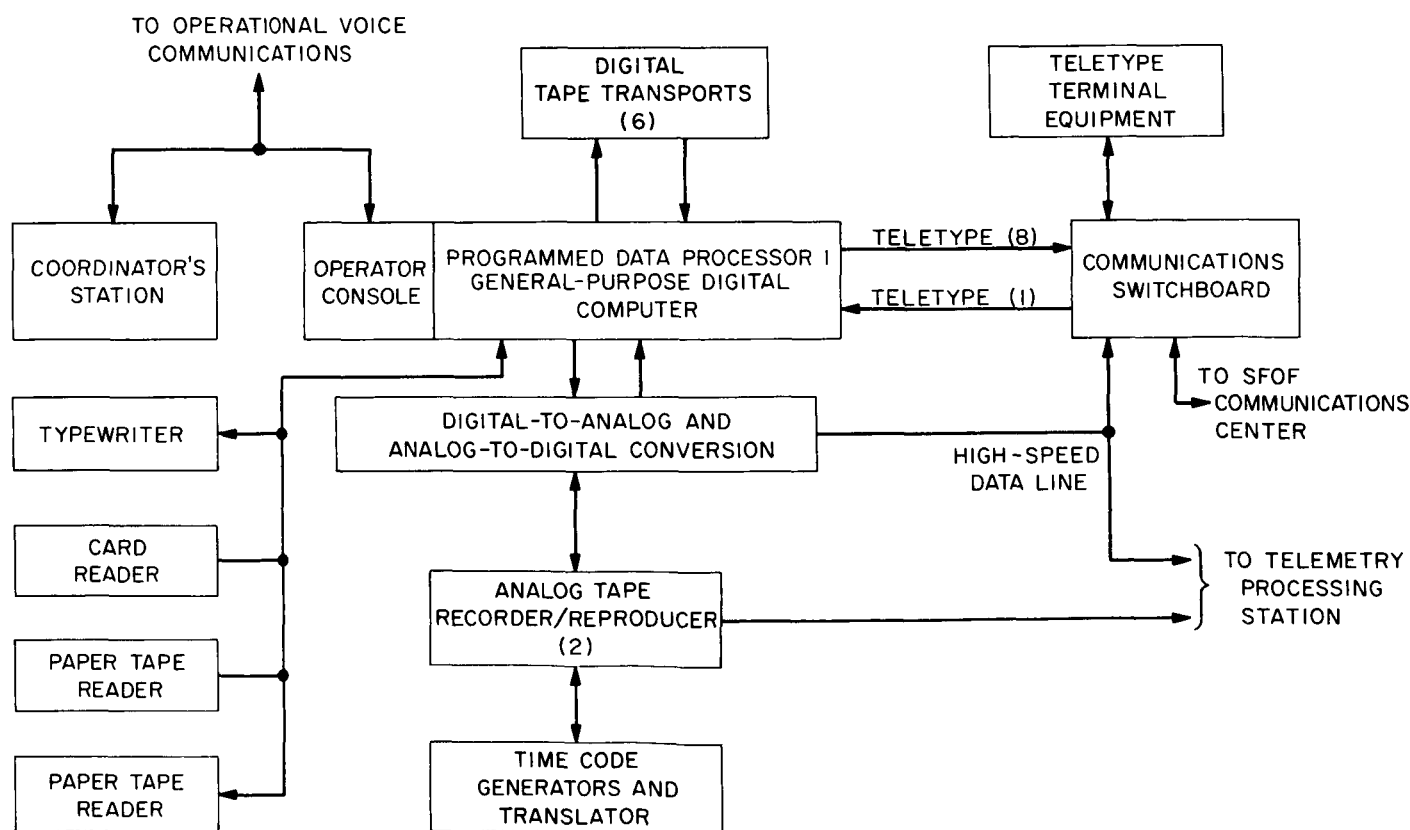


Fig. 4. Simulation data conversion center, Phase I configuration

C. Simulation Data Conversion Center

The Simulation Data Conversion Center (SDCC) of the JPL Space Flight Operations Facility (SFOF) was described in SPS 37-35, Vol. III, pp. 31-34. Described here are recent changes which have occurred and their relationship to the over-all objectives of the DSN Mission Simulation System.

1. Phase I Development (Fig. 4)

The mission-independent Phase I SDCC has been in use since mid-1965 in support of *Surveyor* and *Pioneer* Project operational tests. In November 1965, the facility was relocated in a larger area of the SFOF. Concurrent with the move, which caused only a short interruption in operational use, two new IBM Model 729-VI tape transports were installed on the Programmed Data Processor 1 (PDP-1) digital computer. Also, suitable modifications

were made to the computer tape control circuits to permit them to handle the new tape transports as well as the four Potter tape transports which were already installed. A third IBM 729-VI transport will be put into service in the near future.

2. Phase II Development (Fig. 5)

The Phase II SDCC development is proceeding as described in SPS 37-35, with emphasis being placed on its timely development, including a smooth transition from the Phase I capability. The need for almost continuous use of the facility during 1966 and 1967 has modified planning so as to ensure minimum interference with operations. In particular, the PDP-1 computer and other units now in use will be retained in the Phase II design. The present capability will be augmented by the addition of other units (SPS 37-35), including a larger, faster digital computer. Procurement specifications have been issued, and purchase of such a computer is anticipated in the near future.

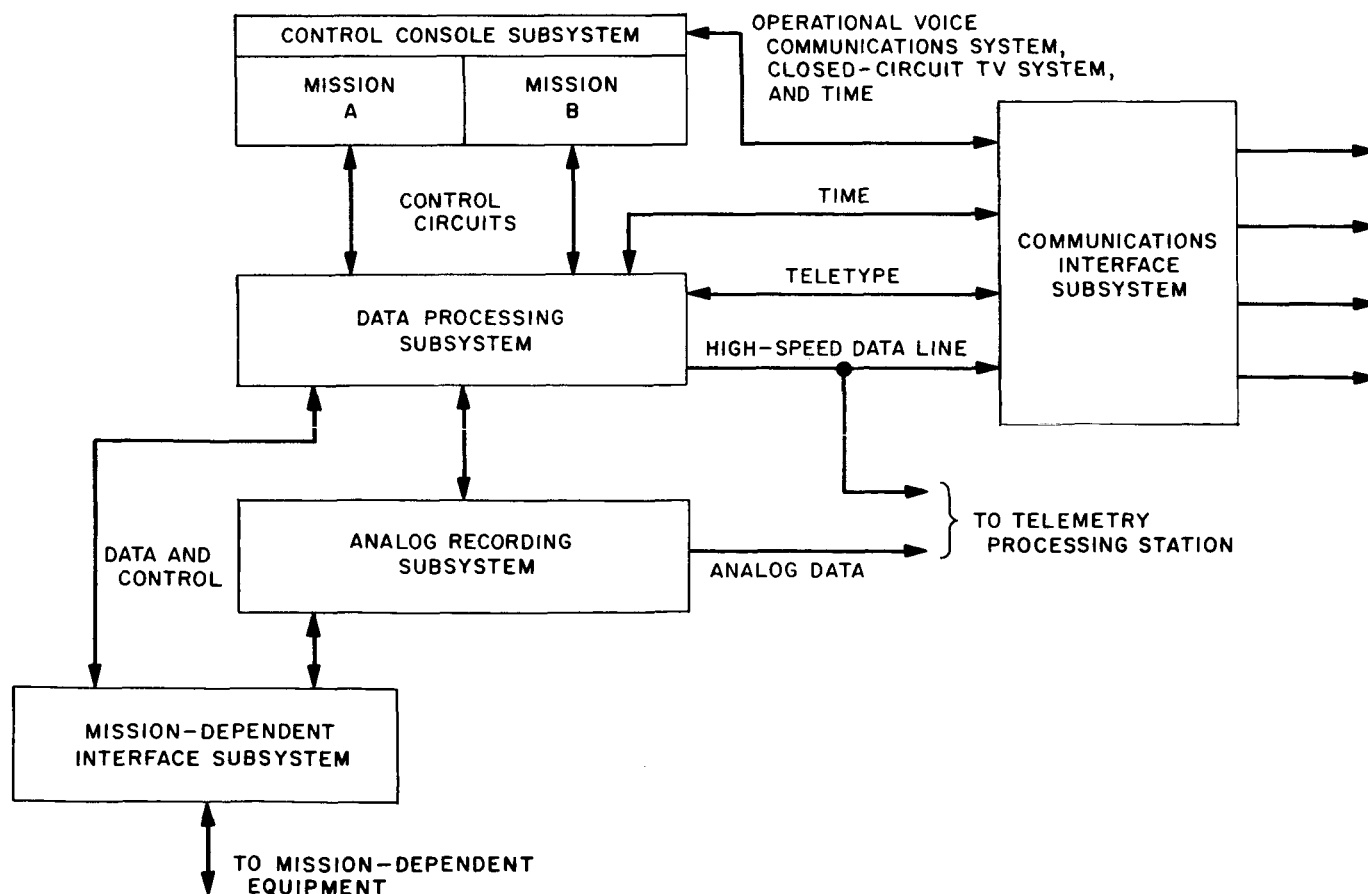


Fig. 5. Simulation data conversion center, Phase II functional diagram

To aid in the orderly development of the center, a new functional specification has been prepared which describes system functions on a slightly different level than that previously employed, but does not significantly alter the actual functions to be performed. Subsystems in the Phase II design are presently as follows: (1) control console, (2) data processing, (3) analog recording, (4) communications interface, and (5) mission-dependent interface. The subsystem functions described in this way serve not only to expedite the design and use of the facility in SFOF internal tests, but also to facilitate its use in connection with simulation capabilities to be developed at the remote sites.

D. Mariner Master Data Library

1. Introduction

The processing system; the telemetry, tracking, and comment data tables; and the JPL facilities required to develop the *Mariner* master data library (MDL) were described in SPS 37-35, Vol. III, pp. 34-37. The present status of the MDL will be presented here, including the status of the telemetry data processing, which non-real-time data are being processed, the percent of recovery for the telemetry data that have been processed, and a listing and status of the records that shall become part of the MDL.

2. Data Processing and Retrieval

The *Mariner IV* spacecraft telemetry system operated in four modes during the Mars mission:

- (1) Mode 1, used during maneuvers with only engineering data sampled. The time periods for Mode 1 were 339:14:35:00 to 339:14:37:14 and 340:14:25:00 to 340:16:15:20 GMT¹ 1964 and 196:11:53:53 to 196:13:01:58 GMT 1965.
- (2) Mode 2, used during launch, initial acquisition, and cruise. Blocks of engineering data 140 bits long were alternated with blocks of science data 280 bits long.
- (3) Mode 3, used during encounter phase while the TV system was scanning the planet. In this mode, only the science data were sampled.
- (4) Mode 4, during which the stored TV and science data recorded on the spacecraft tape machine were played back. The time periods for Mode 4 were 196:13:01:58 to 215:03:20:33 and 243:02:00:46 to 245:06:36:52 GMT 1965.

The *Mariner IV* mission covered a period of 44 wk, for which the non-real-time telemetry data from Modes 2 and 3 are being processed for the MDL. The status of the processing is as follows:

Status	Mission weeks covered by data
Released to user: data that have been extracted from the MDL final composite merge master tapes and put onto extract tapes for delivery to the scientific community	1-4, 6-15
In production: extract tapes of the data contained on the MDL final composite merge master tapes	5, 16-27
In production: MDL final composite merge master tapes, following acceptance by the MDL Acceptance Committee of the percent of data recovered by the composite merge of the data for these weeks	28-33, 36-38
Being processed: non-real-time data to produce a composite merge	39-44
Not processed: non-real-time data [The real-time data processing (during Mode 4) was determined as sufficient.]	34, 35

Data evaluation and data outage summaries are prepared for all data processed to point out when the outages occurred and to provide explanations for them. These summaries are reviewed by the MDL Acceptance Committee, which shall, based on comparisons with the real-time data records, the quantity and quality of the data, and the amount of data retrieved during periods of high scientific interest, either accept the data or recommend that additional processing be done. Table 1 summarizes the amount of data retrieved from the data processed thus far.

¹Day of year:hr:min:sec.

Table 1. *Mariner MDL data retrieval summary*

Mission week(s)	Percent of time receiver(s) was in lock ^a	Percent of spacecraft data received ^b	Percent of received data retrieved ^c	Percent of spacecraft data retrieved ^d	Mission week(s)	Percent of time receiver(s) was in lock ^a	Percent of spacecraft data received ^b	Percent of received data retrieved ^c	Percent of spacecraft data retrieved ^d
1 ^a	99.95	99.68	99.66	99.34	21	99.89	99.67	99.96	99.63
2	100.00	98.85	99.49	98.34	22	99.43	99.07	99.93	99.01
3	99.99	99.64	99.73	99.37	23	99.11	98.90	99.91	98.81
4	99.93	99.63	99.91	99.54	24	99.64	98.81	99.84	98.68
5 (1964)	99.95	99.81	99.71	99.51	25	99.70	99.22	99.77	98.99
5 (1965) ^f	99.96	99.88	99.37	99.24	26	99.91	99.14	99.70	98.84
5, 6 ^g , 7 ^g	99.52	98.91	99.86	92.36	27	99.89	99.60	99.95	99.54
8, 9	99.74	98.72	99.94	98.66	28	99.88	99.35	99.86	99.22
10 ^h	99.63	98.30	100.00	98.29	29	99.20	99.64	99.64	99.28
11 ^h	97.22	96.03	99.93	70.78	30	99.79	99.32	99.88	99.20
12 ^h	98.77	99.37	98.79	65.86	31	99.86	99.51	99.73	99.25
13 ⁱ	97.29	96.53	94.87	91.57	32	99.95	99.90	99.96	99.86
14	98.06	95.60	99.76	95.37	33	99.98	98.61	99.95	98.56
15 ^j	98.41	99.38	100.00	74.32	34 ^k , 35 ^k	—	—	—	—
16 ^j	99.23	99.17	99.87	71.53	36	99.93	99.80	99.86	99.66
17 ^j , 18, 19	99.74	99.28	99.88	93.62	37	98.40	97.69	99.89	97.58
20	99.87	99.43	99.46	98.89	38	99.66	99.32	100.00	99.32
					39-44 ^l	—	—	—	—

^aBased on the total number of minutes per day actually committed to *Mariner IV* tracking. During full coverage, a 1440-min day was used. This information was derived from post-track reports generated by each station. The data presented here were obtained from Catichio, A., *Mariner IV Raw Telemetry Summary*, Technical Section 337 Interoffice Memorandum, Jet Propulsion Laboratory, Pasadena, California, October 6, 1965.

^bBased on the spacecraft data transmitted during the time that the Deep Space Instrumentation Facility (DSIF) was actually committed to *Mariner IV* tracking. This information represents the ratio of the received data to the total data transmitted by the spacecraft during DSIF coverage. Received data are defined as those data transmitted by the spacecraft when the receiver(s) was in lock.

^cRepresents the ratio of the data actually recovered by the MDL system to the data actually received at the DSIF station(s) during a given period.

^dRepresents the ratio of the data retrieved by the MDL system to the data transmitted by the spacecraft during a given period.

^eMode 1.

^fEnd of high-rate data.

^gOnly two prime stations tracking for Passes 43-46.

^hOnly two prime stations tracking for Passes 72-86. Percents of spacecraft data retrieved affected for this interval.

ⁱProblems encountered with Johannesburg Tracking Station maser.

^jOnly two prime stations tracking for Passes 101 and 103-118. Percents of spacecraft data retrieved affected for this interval.

^kMode 4.

^lData still being processed.

3. MDL Records

A listing of the records to be kept in the *Mariner IV* MDL is given in Table 2. The main records shall, of course, be the station merge master magnetic tapes and the final composite merge master magnetic tapes. All computer programs used in processing the data shall be stored for possible future use.

Because of time and equipment-availability limitations, the tracking data section of the MDL has been redefined. The records that shall become part of the tracking data MDL are the tracking data paper tapes from the DSIF

stations, the processed real-time tracking data on magnetic tapes, and a TELPRT computer program for use by anyone desiring to process portions of the data. Operating on selected input data only, the TELPRT program shall convert tracking data in Baudot code on digital magnetic tape to binary-coded-decimal (BCD) data on digital magnetic tape, and shall be capable of reading in the BCD tapes and selecting data for output. The selection of both the input and output data shall be based on one or more of the following parameters: spacecraft identification, DSIF station identification, and sampling rate.

Table 2. Description and status of MDL records

Record	Content	Status
Magnetic tapes		
DSIF-station analog tapes	Voice label Telemetry data (post-demodulator data) Bit sync (post-demodulator data) Word sync (post-demodulator data) Time code Composite telemetry (pre-demodulator data) Station functions	1947 Tapes of an eventual 2000 (approximate) stored in Operational Document Control (ODC) at the JPL Space Flight Operations Facility
Telemetry-processing-station master record digital tapes	Pre-demodulator data Post-demodulator data Time Station functions	Tapes stored in ODC
Station merge master tapes (in duplicate so that a running master will be available for use)	Continuous and sequential stream of the best telemetry data for each DSIF station	Tapes for Weeks 1-38 completed
Final composite merge master tapes (in duplicate so that a running master will be available for use)	Continuous (except for explained outages) and sequential stream of the best telemetry data for the Mariner IV mission	Tapes for Weeks 1-27 completed
Processing records (microfilmed)		
Telemetry-processing-station records Telemetry-processing-station engineering lister (Programmed Data Processor 4)	Monitor printout of telemetry data being processed by Programmed Data Processor 4	Records microfilmed and stored in ODC
Telemetry-edit program processing records (three sets: pre-demodulator data, post-demodulator data, and processed teletype data)		
Processing log	Printout of all significant reference data plus any data or time anomalies encountered during processing	Records for Weeks 1-41 completed
Bad-data listing	Tabular listing, by time-tagged spacecraft data frame, of all program input data that cannot be synchronized into the output data stream (all data frame counts also listed)	Records for Weeks 1-41 completed
Quality-control log	Listing of telemetry frames with time or frame count anomalies, and a compilation of the statistics on such anomalies by day or by tape number	Records to be run on all telemetry-edit output tapes
Telemetry-re-edit program processing records (three sets: pre-demodulator data, post-demodulator data, and processed teletype data)		
Processing log	Same as that of telemetry-edit program processing log, except that all input control parameters used to correct time are also listed	Records for Weeks 1-41 completed
Bad-data listing	Same as that of telemetry-edit program bad-data listing	Records for Weeks 1-41 completed
Station merge program processing records		
Processing log	Same as that of telemetry-edit program processing log, except that data start and stop times and frame counts are also listed	Records for Weeks 1-38 completed
Engineering lister	Listing of engineering data by frame	Records for Weeks 1-38 completed
Quality-control log	Same as that of telemetry-edit program quality-control log	Records to be run on all station merge output tapes
Station functions listing	Printout of the station functions recorded on each tape	Records to be run on all station merge output tapes

Table 2. Description and status of MDL records (cont'd)

Record	Content	Status
Processing records (cont'd)		
Final composite merge program processing records		
Processing log	Same as that of telemetry-edit program processing log	Records for Weeks 1-27 completed
Science lister	Listing of scientific data	Records for Weeks 1-27 completed
Engineering lister	Same as that of station merge program engineering lister	Records to be run on all final composite merge output tapes
Quality-control log	Same as that of telemetry-edit program quality-control log	Records to be run on all final composite merge output tapes
Comment data (to explain peculiarities and/or anomalies that occur in both the telemetry and tracking data)		
Space flight operations log	_____	_____
DSIF operations logs from each station	_____	_____
Trajectory tables	_____	_____

III. Communications Engineering Developments

A. S-Band Implementation for DSIF: Acquisition Aid for Ascension Island

The Ascension Island (DSIF 72) acquisition aid equipment for the 30-ft antenna has been installed and partially tested; equipment necessary for boresight and final RF measurements is not yet available at the site. Final tests will be made after the station is completed, as all subsystems must be operational before final boresighting, snap-on, and tracking tests are performed.

B. 100-kw S-Band Final Amplifier

Two X3060 klystrons have been delivered to the Venus Station. One has been installed in a transmitter cabinet and has undergone partial acceptance testing. The trans-

mitter cabinet houses, in addition to the klystron itself, the klystron mounting structure, cooling water plumbing and metering, filament supply, reflected power monitoring and arc detector systems and their associated RF switches, remotely driven RF drive attenuators, and various other metering and interlock circuits. By modifying an existing transmitter cabinet, formerly used to house a smaller klystron, a considerable saving was realized, although at some sacrifice in accessibility.

Acceptance testing of the klystron at 2388 Mc (planetary radar frequency) has been completed. The results summarized in Table 1 are in general agreement with those achieved in the manufacturer's acceptance tests (SPS 37-36, Vol. III, p. 31). Fig. 1 is a typical output power versus drive power curve.

The manufacturer achieved 112-kw at a proportionally higher beam power input, but since the purpose of JPL tests was merely to establish the klystron's ability to meet the contract specification (100-kw output power at 35% minimum efficiency with specified gain and bandwidth)

and not to measure the maximum capabilities of the klystron, the results obtained are satisfactory.

Acceptance tests were suspended until early January, 1966 because the only adequate power supply (the 1.0-Mw supply at Venus) is totally committed to the planetary radar program until then. The remaining acceptance tests will consist primarily of investigating the tuning characteristics of the klystron. Upon completion of acceptance tests, the performance of the klystron as a dual carrier amplifier will be investigated.

Table 1. Acceptance test results

Performance	
Power output, kw	105
Efficiency, %	44
Bandwidth (1 db)	15
Gain, db	59.5
Operating conditions	
Beam voltage, kv	35
Collector current, amp	6.6
Filament voltage, v	13
Filament current, amp	5.4
Focus magnet current, amp	18.2
Body current, ma	295
Tuning	High efficiency

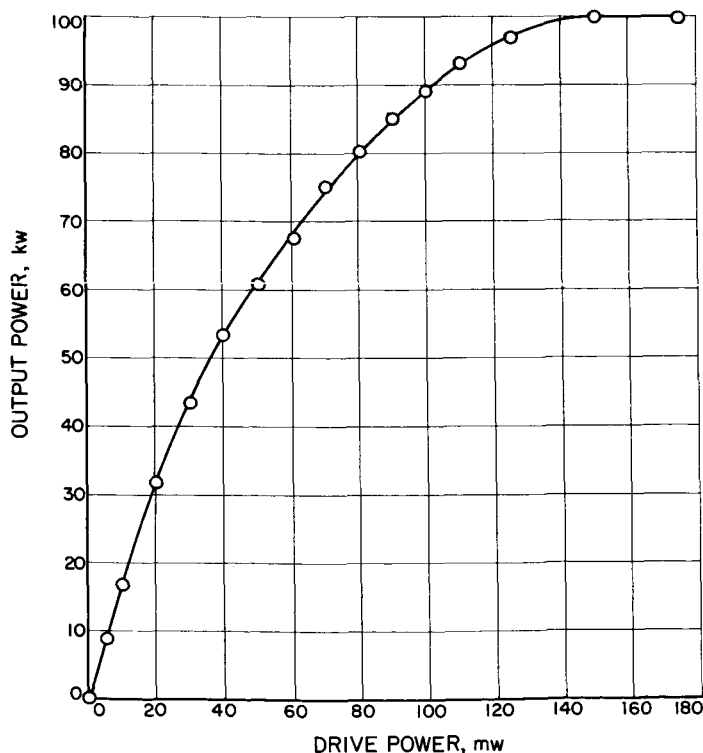


Fig. 1. Output power versus drive power

C. Multiplier Chains (Phase and Amplitude Stability)

1. Summary

Typical multiplier and VHF amplifier units comprising a complete S-band chain have been evaluated individually, and in combination, with respect to phase and amplitude stability versus ambient temperature and RF drive level. In all cases, phase shift measurements were conducted at the output S-band frequency and the phase stability referred to the output of the test chain was recorded. Results of measurements indicate that all units can be expected to perform satisfactorily under service conditions and that the maximum phase shift of a complete S-band $\times 75$ multiplier chain over a 10-hr tracking period can be expected to amount to approximately 800 deg. The evaluation of these multiplier chains, currently in use at the S-band radar site, also establishes typical performance of the X-band system (excepting the final $\times 4$), inasmuch as the design is essentially identical.

2. Test Setup Description

The test setup for the measurement of relative phase shift is shown in Fig. 2. Coherent inputs at 31.84 and 31.44 Mc are applied to two $\times 75$ multiplier chains—one containing the units under test, the other a reference channel. The outputs from each of these channels, after suitable attenuation, are mixed in a balanced mixer, the 30-Mc output of which is amplified and compared in phase with a 30-Mc signal which is phase coherent with each of the test and reference chain signal inputs. Phase shift of the test channel may be read directly from a calibrated phase shifter in series with the coherent 30-Mc signal by nulling the phase detector. It should be noted that this method actually measures the differential phase shift between the test and reference channels so that the results are subject to a tolerance equal in value to the phase stability of the reference channel during a temperature run. A phase shifter is included at the input to the reference channel so that the calibrated shifter may be set to zero at the beginning of a run.

3. Results of Measurements

The variation of phase shift with temperature is shown in Figs. 3-5 for the individual multiplier and amplifier units comprising an S-band transmitter exciter chain and in Fig. 6 for the antenna-mounted VHF amplifier and $\times 15$ multiplier units combined. Since we are primarily concerned with the phase shift variations appearing at

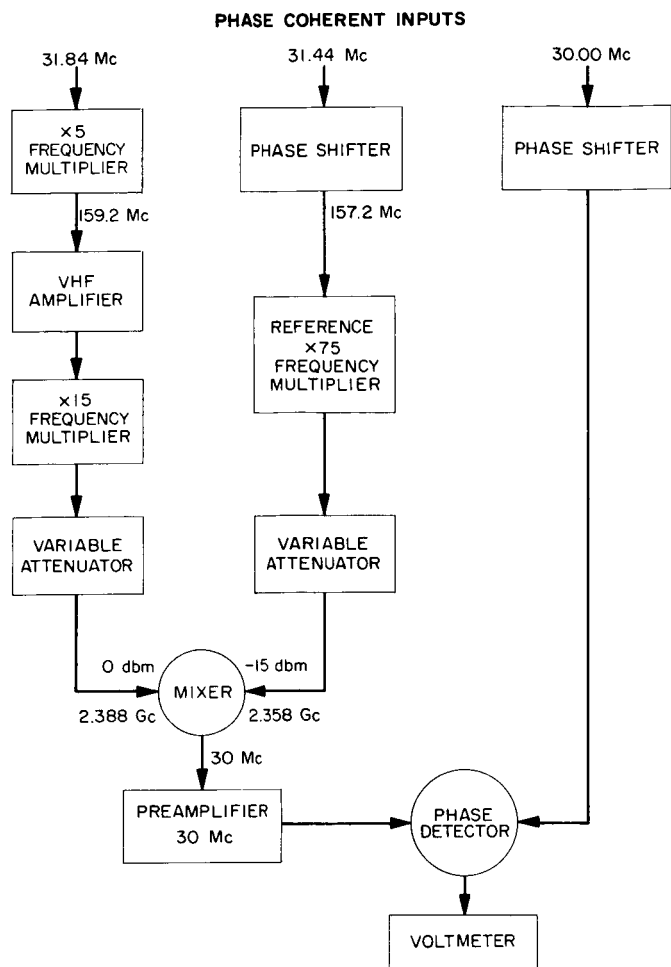


Fig. 2. Test setup block diagram

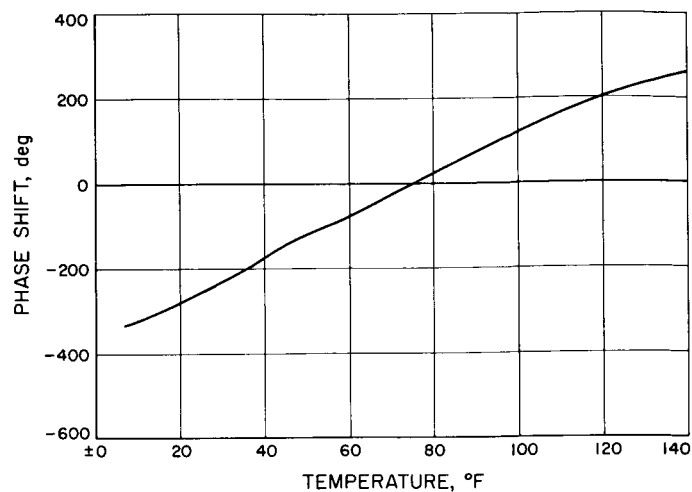
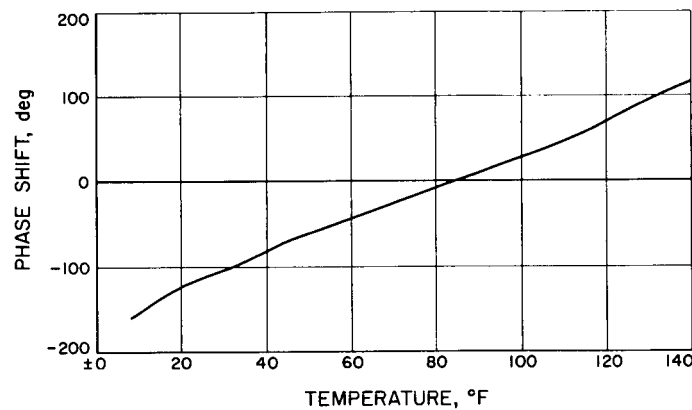
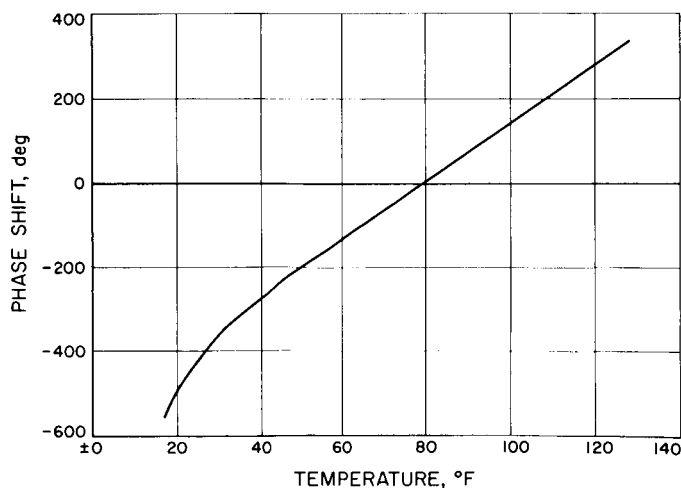
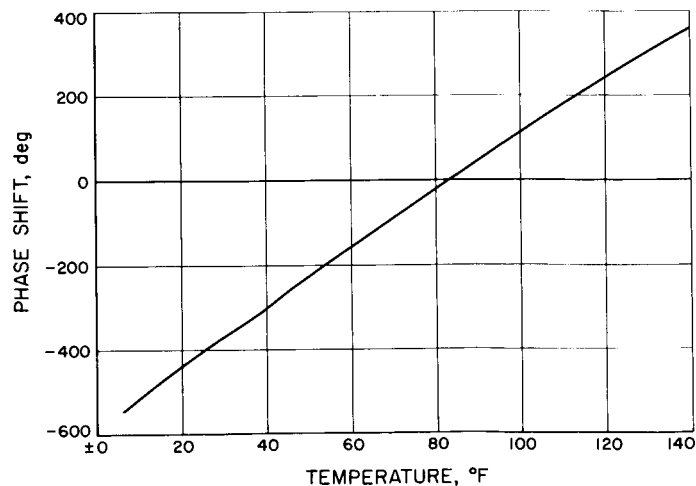


Fig. 4. Phase shift versus temperature, VHF amplifier

Fig. 5. Phase shift versus temperature, $\times 15$ multiplierFig. 3. Phase shift versus temperature,
 $\times 5$ multiplierFig. 6. Phase shift versus temperature, $\times 15$ multiplier
plus VHF amplifier

the output of the test chain, all phase shifts were measured and recorded at this point, so that, in the case of the $\times 5$ multiplier and VHF amplifier units, the phase shift variations shown exceed the intrinsic values of the units by 15 times. The over-all phase shift of the antenna-mounted equipment over the temperature range 14 to 132°F averages 6.8 deg/°F, the major portion (4.75 deg/°F) being contributed by the VHF amplifier. The $\times 5$ multiplier unit, although normally located in the control room, was tested and operated satisfactorily over the full range of temperatures when the phase stability was found to equal 7.1 deg/°F. The amplitude stability with change in temperature is indicated in Figs. 7-9,

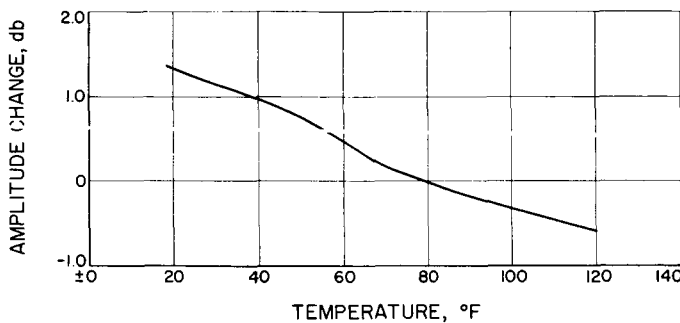


Fig. 7. Amplitude versus temperature, $\times 5$ multiplier

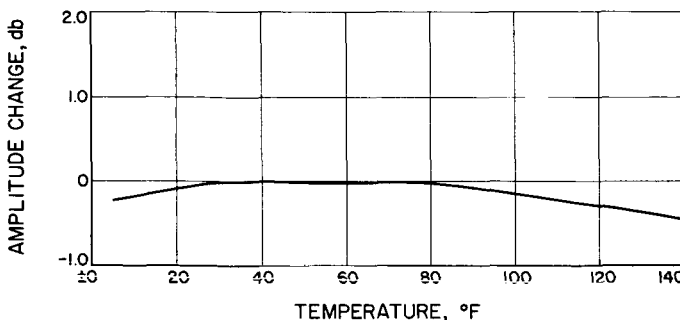


Fig. 8. Amplitude versus temperature, VHF amplifier

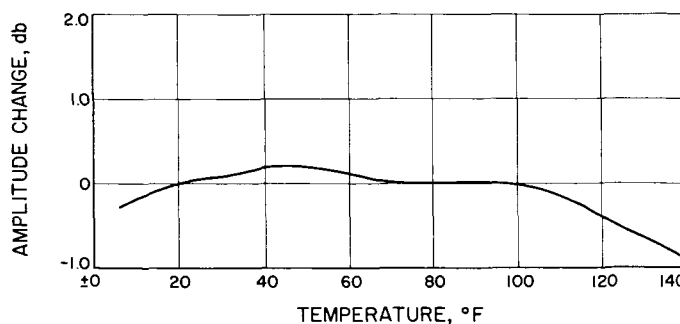


Fig. 9. Amplitude versus temperature, $\times 15$ multiplier plus VHF amplifier

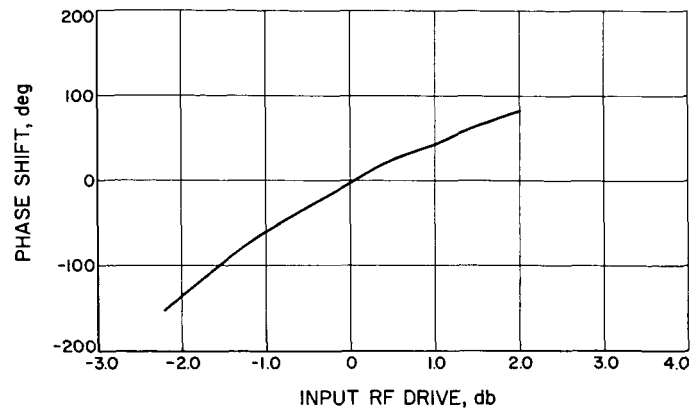


Fig. 10. Phase shift versus RF drive, $\times 75$ multiplier chain

and amounts to ± 1.1 , ± 0.15 , and ± 0.3 db over the full temperature range for the $\times 5$ multiplier, VHF amplifier units and VHF amplifier plus $\times 15$ multiplier combination, respectively. From Fig. 10, the total phase shift of the complete $\times 75$ multiplier chain for a ± 1 -db change in RF input drive amounts to 93 deg and is accompanied by less than 0.1-db change in amplitude of the output signal.

4. Conclusions

All units performed satisfactorily when subjected to the full range of environmental (14 to 132°F) and RF drive (± 1 db) conditions specified for antenna-mounted equipment. However, in assessing the over-all phase shift of a complete $\times 75$ multiplier chain for the purpose of determining the contribution toward tracking error, it will be assumed that the maximum variation in ambient temperature during any 10-hr tracking period (between horizons) will equal 61°F for antenna-mounted equipment, and 22°F for equipment located in the control room, so that a complete $\times 75$ frequency multiplier chain can be expected to contribute a maximum phase shift of approximately 769 deg, made up as follows:

Antenna-mounted equipment (VHF amplifier, $\times 15$ multiplier). Assuming temperature variations during a 10-hr tracking period will not exceed 61°F

$$6.8 \times 61 = 415 \text{ deg}$$

Control room equipment (VHF amplifier, $\times 5$ multiplier). Assuming maximum variations in temperature will not exceed 22°F

$$\begin{array}{rcl}
 (7.1 + 4.75) \times 22 & = & 261 \text{ deg} \\
 \text{RF drive } \pm 1 \text{ db} & & 93 \text{ deg} \\
 \text{Total} & & \underline{769 \text{ deg}}
 \end{array}$$

The total delay in the transmitter exciter and receiver local oscillator chains now being used at S-Band can be expected to contribute a ranging error of:

$$\frac{2 \times 769 \times 3 \times 10^8}{360 \times 2.4 \times 10^9} = 0.54 \text{ m, worst case}$$

This amounts to approximately 30% of the over-all system target figure.

D. Phase Response of the RF Carrier Tracking Loop (CTL) S-Band Transponder Ranging Station

The S-band transponder ranging station (SPS 37-32, Vol. III, p. 62 and SPS 37-20, Vol. III, p. 50) was originally designed to be similar in dynamic characteristics to the DSIF system; however, in a recent evaluation, carrier loop instability became evident.

An initial test on the station indicated that the $2B_{L0} = 152$ cps carrier loop was conditionally unstable. This system (Fig. 11) is unique in two ways: (1) a 7-pole, 2-kc band-pass filter is used in the 455-kc IF amplifier, and (2) a high Q crystal VCO is used; therefore, a detailed investigation was made of all loop time constants.

This report derives a detailed model for this specific loop, applies the model by compensating a previously

unstable loop, and then evaluates loop performance on all three carrier loop bandwidths at both threshold and strong signal conditions.

The loop natural frequency was experimentally measured to determine that there had not been a design error or hardware failure. This measurement was made by adjusting the α potentiometer to a simulated threshold condition, α_0 (where α is the limiter suppression factor and describes the relationship between the S/N and the loop gain),¹ and then shunting the damping resistance in the loop filter (R2 in Fig. 12) with a variable resistor until a sustained oscillation (controlled to be approximately 20 deg, peak-to-peak) was observed at the output of the phase detector. The frequency was measured on a recorder and is the natural frequency. Fig. 13 illustrates that the intersection of the extension of the 40 db/decade slope and the unity gain line is, by definition, the natural frequency. The effect of reducing R2 is to increase ω_2 until it approaches ω_n and causes the loop to oscillate at the natural frequency.

¹Rechlin, E., "Design of Phase-Lock Oscillator Circuits," JPL Section Report No. 8-566, February 7, 1957.

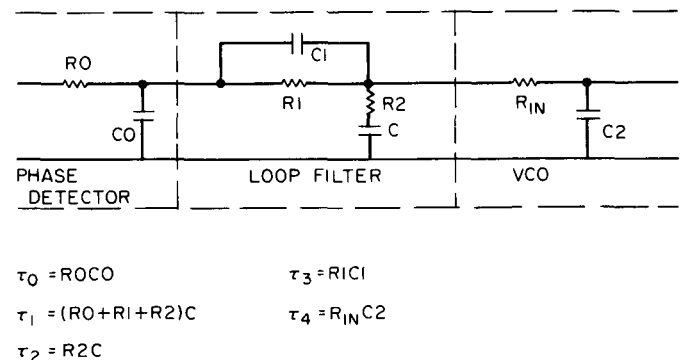


Fig. 12. Carrier tracking loop filter schematic

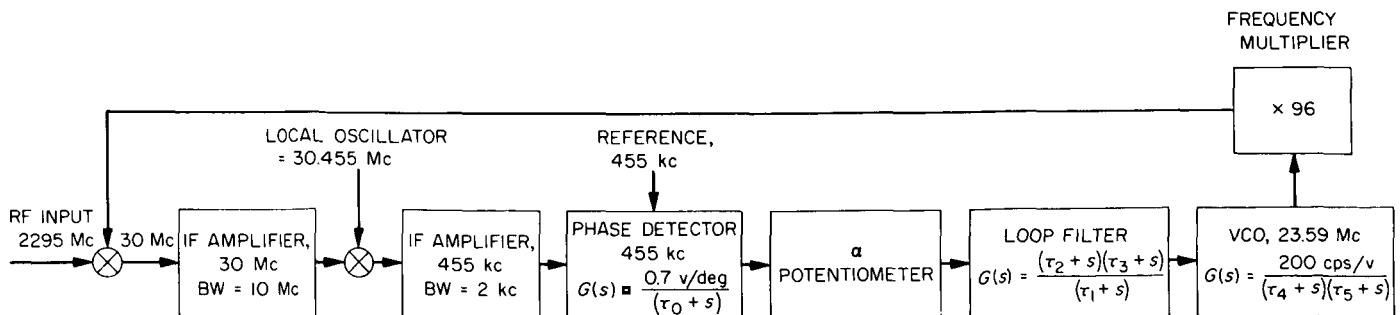


Fig. 11. Carrier tracking loop

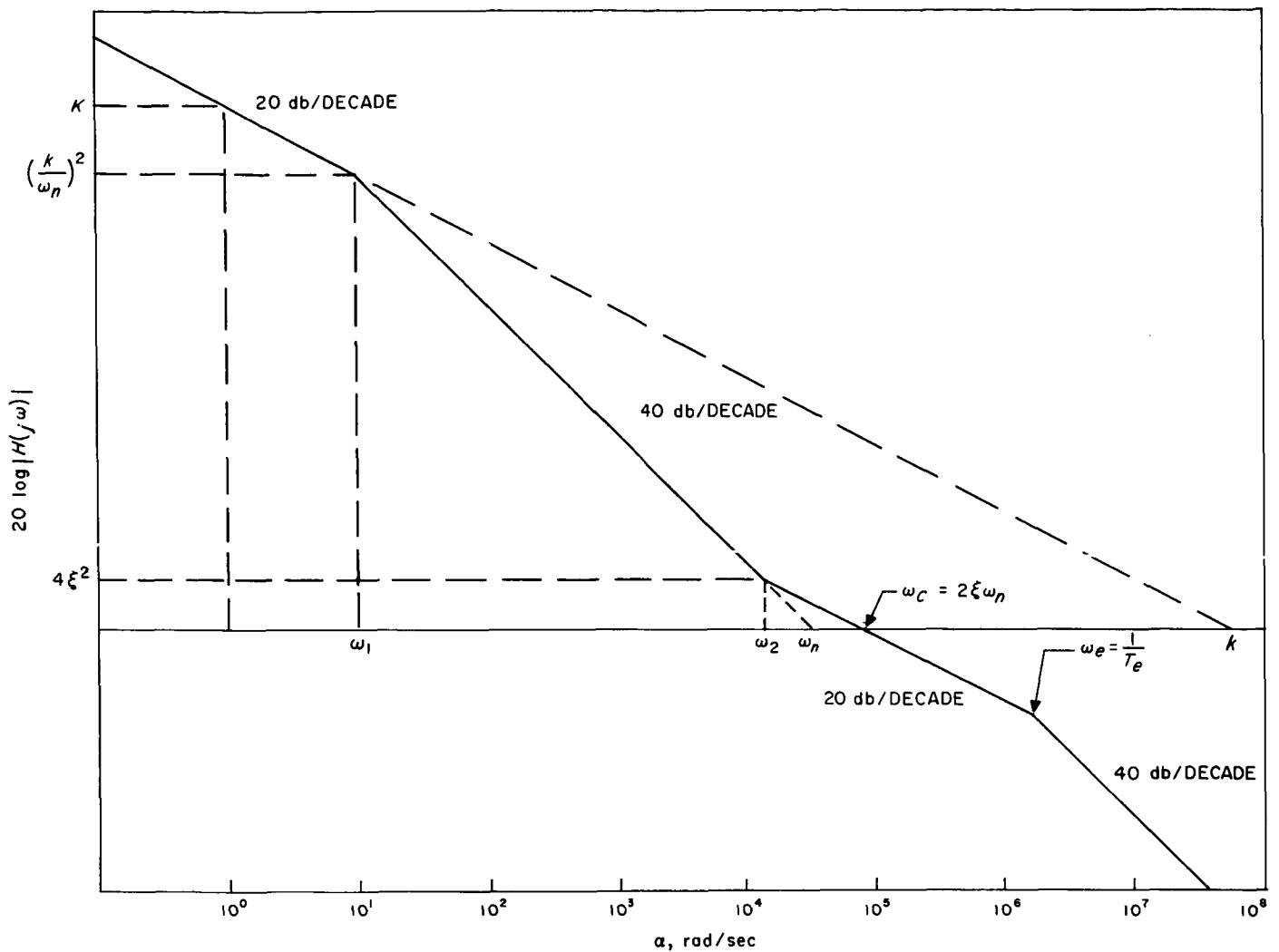


Fig. 13. Generalized open loop frequency response with a single extra time constant

The results of this test (Table 2) indicated that the loop gain was approximately 10% low. However, the loop behaved essentially as designed.

When the $2B_{L0} = 152$ cps was evaluated for α greater than α_0 , the carrier tracking loop oscillated α for ≥ 0.94 . This indicated a gain margin of 12.8 db at threshold, while the ideal linear model indicated a gain margin of 24 db.

Since the ideal linear model was not adequate, further investigation was required.

No adequate analytical equivalent model could be derived for the 7-pole filter because of its complex pole-zero characteristic so a phase measurement was made (Figs. 14 and 15). Since there is not perfect symmetry in the phase response, it was decided to use the average phase response in the analysis model.

Table 2. Loop bandwidth measurement

Design $2B_{L0}$	Nominal f_n , cps	Measured f_n , cps
12	1.8	1.69
48	7.2	7.0
152	22.6	22.1

The VCO crystal was investigated with the theory that the high Q crystal acted as a low-pass filter for the low frequency modulation about its center frequency. The crystal Q was measured and its 3-db (double-sided) bandwidth determined ($Q = 2.3 \times 10^5$ and $BW_3 = 157$ cps). The phase response of the VCO was measured by two

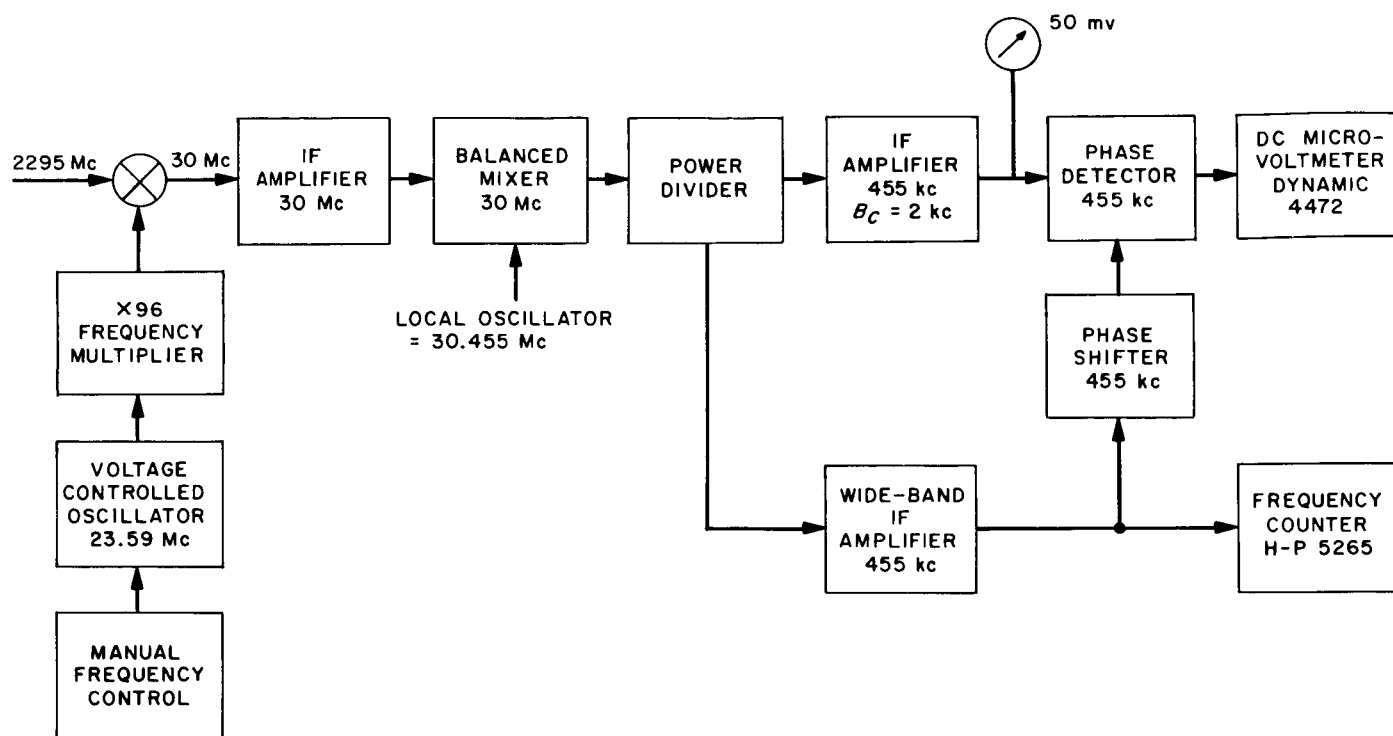
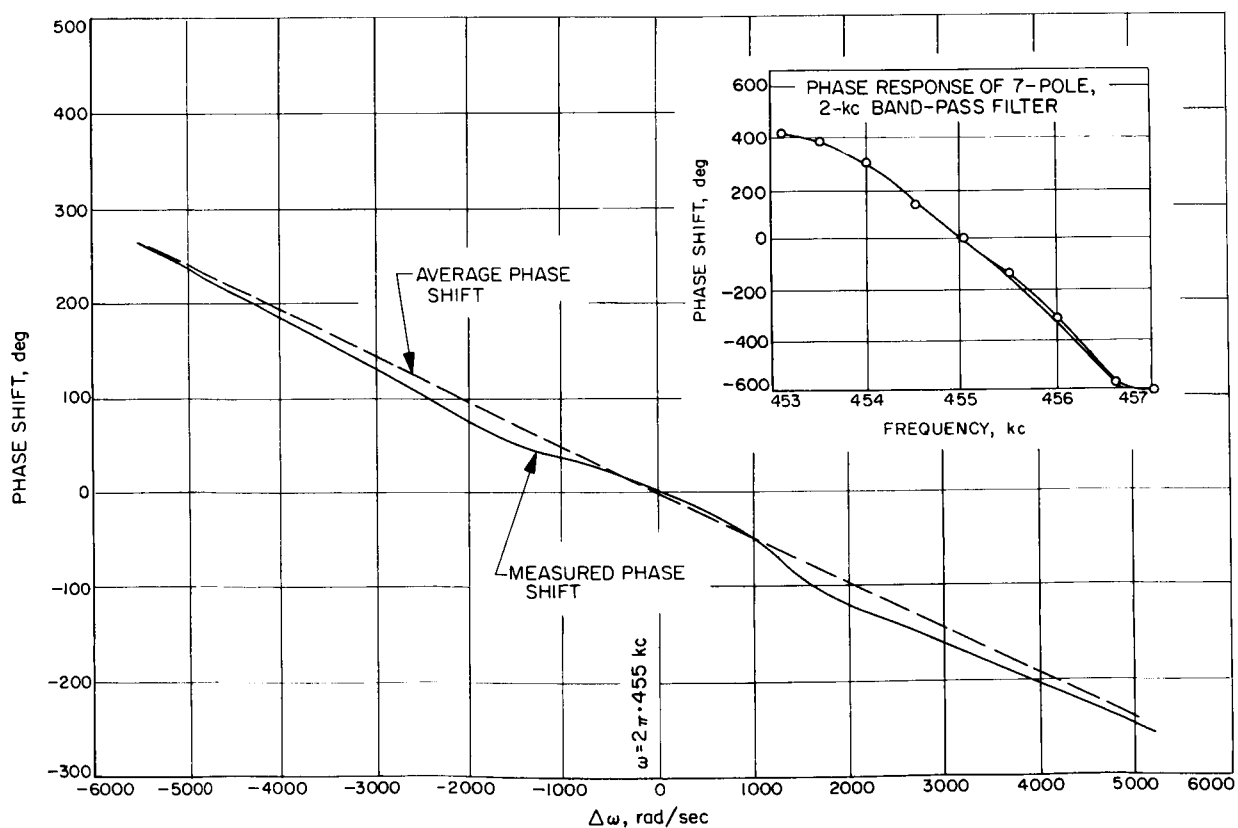
Fig. 14. Test setup to measure band-pass filter (B_c) phase response

Fig. 15. Phase response of 7-pole, 2-kc band-pass filter expanded approximately 455 kc

methods, illustrated in Figs. 16 and 17. The FM discriminator method gave good low frequency response up to approximately 200 cps, while the Marconi frequency deviation meter gave a valid response from 40 cps to greater than 1 kc. The Marconi test setup was evaluated by substituting the H-P 5100 frequency synthesizer in lieu of the VCO and was found to have a reasonably flat phase response over the range of 40 cps to 1 kc.

Since no single measuring device could be found to cover the frequency range of dc to 1 kc with a flat phase

response, the measured phase response was derived by using data from the FM discriminator for the low frequency data (dc to 200 cps) and data from the Marconi setup for the high frequency data.

The results of this test indicate that the VCO crystal can be represented by a low-pass filter whose corner frequency is the same as the measured crystal 3-db double-sided bandwidth. Fig. 17 shows the favorable comparison of the model to the measured phase response, provided the low-pass filter model is restricted to frequencies that are not higher than an octave above the corner frequency. No satisfactory explanation was found for the lead in the VCO phase characteristics. The parallel resonance of the crystal was measured and found to be 37 kc from the series resonance frequency and is not considered pertinent in this model.

An analysis was performed using the known loop filter time constants, the average value of the measured 2-kc band-pass filter phase response, the phase detector output circuit time constant, and the low-pass filter equivalent of the VCO crystal (Fig. 18).

This analysis shows a gain margin of 13 db (measured value was 12.8 db) and a loop phase response of 180 deg at 920 rad/sec (which was experimentally observed since the loop oscillated at this frequency).

The model appeared to be adequate and the 152-cps carrier loop was compensated by adding a lead in the loop filter ($C1 = 180$ pf in parallel with the measured stray capacitance across the filter of 30 pf) such that the compensation canceled the apparent VCO crystal corner.

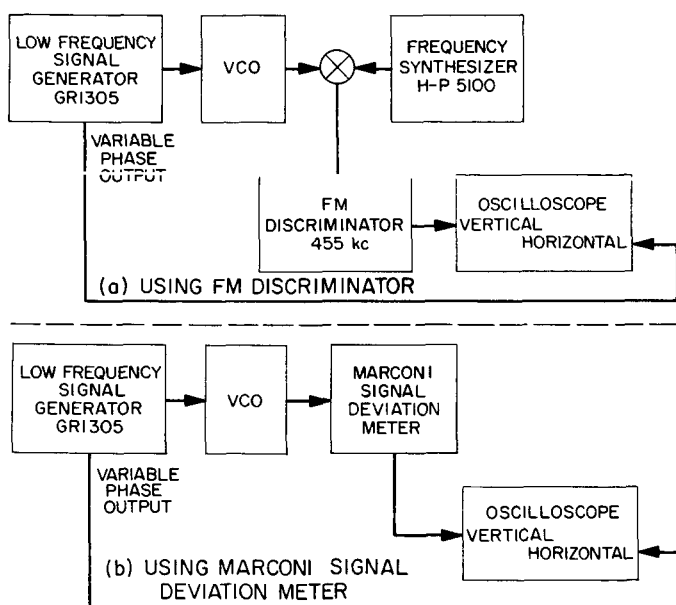


Fig. 16. Test setup to measure phase response of VCO

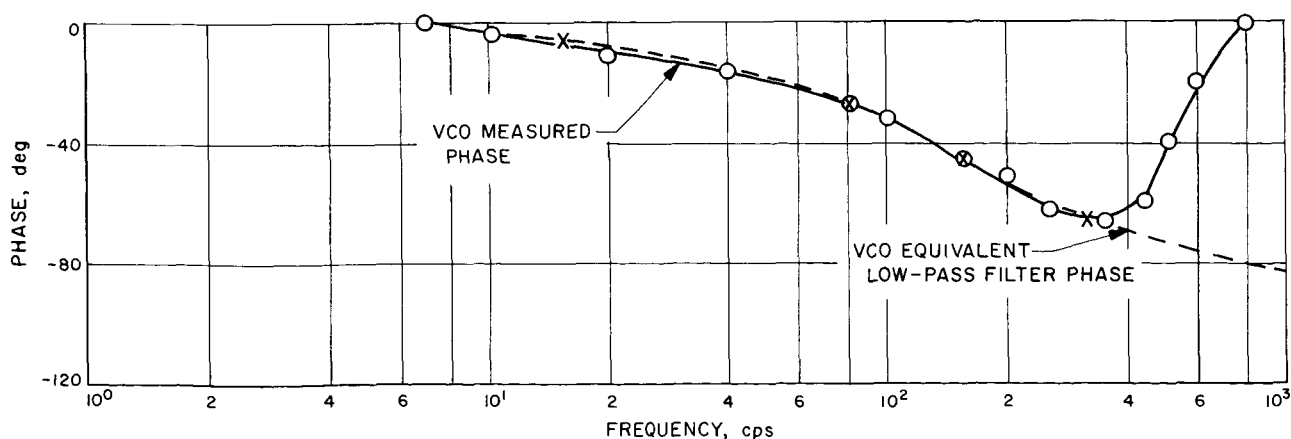


Fig. 17. VCO phase response

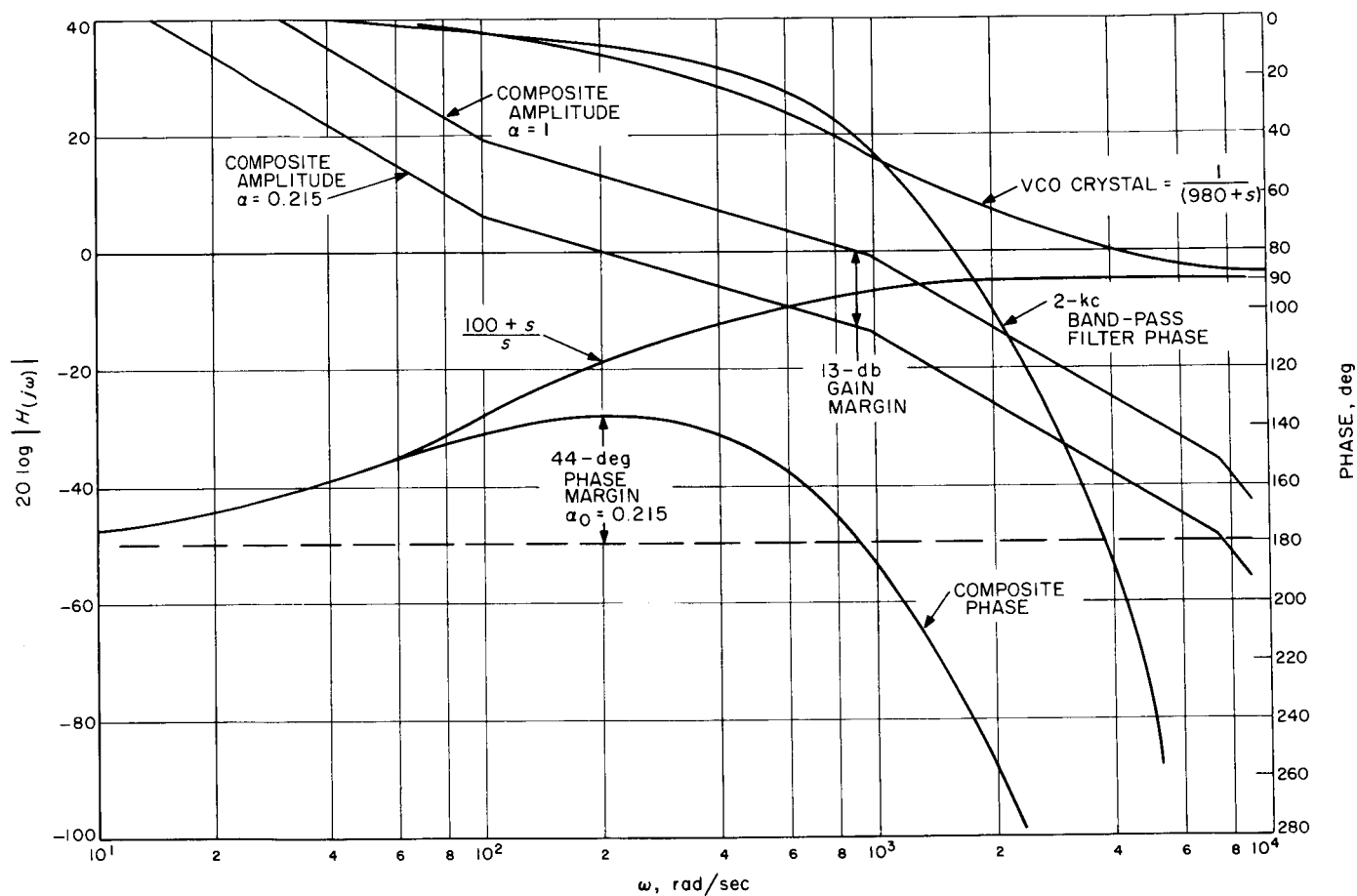


Fig. 18. Open loop frequency characteristic for uncompensated CTL, $2B_{L0} = 152$ cps

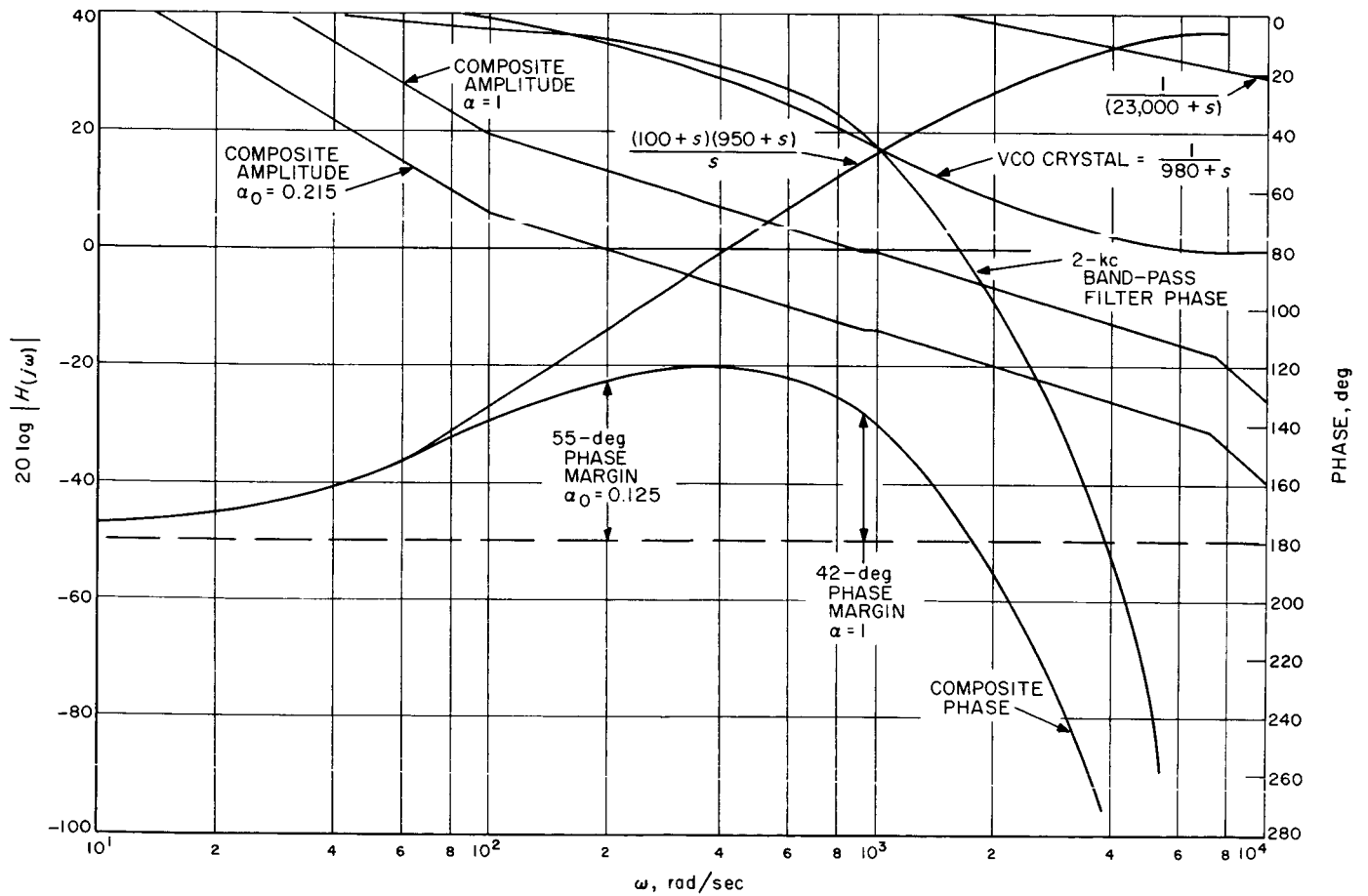


Fig. 19. Open loop frequency characteristic, $2B_{L0} = 152$ cps

The new model was used to analyze the compensated response (Fig. 19). The phase margin was determined to be 42 deg when $\alpha = 1$. It was assumed that the loop transfer function could be approximated (in the area of ω_c , the crossover frequency) by a quadratic function, such that a phase margin of 42 deg could be related to a damping factor of 0.39 (Fig. 20 and Ref. 1). The damping factor can now be interpreted as overshoot in the closed loop frequency response (Fig. 21 and Ref. 2). The predicted overshoot was 5.0 db while the measured overshoot was 4.8 db.

A similar analysis was performed on both the $2B_{L0} = 12$ cps and 48 cps loop bandwidths. Figs. 22 and 23 are the open loop frequency characteristics of these

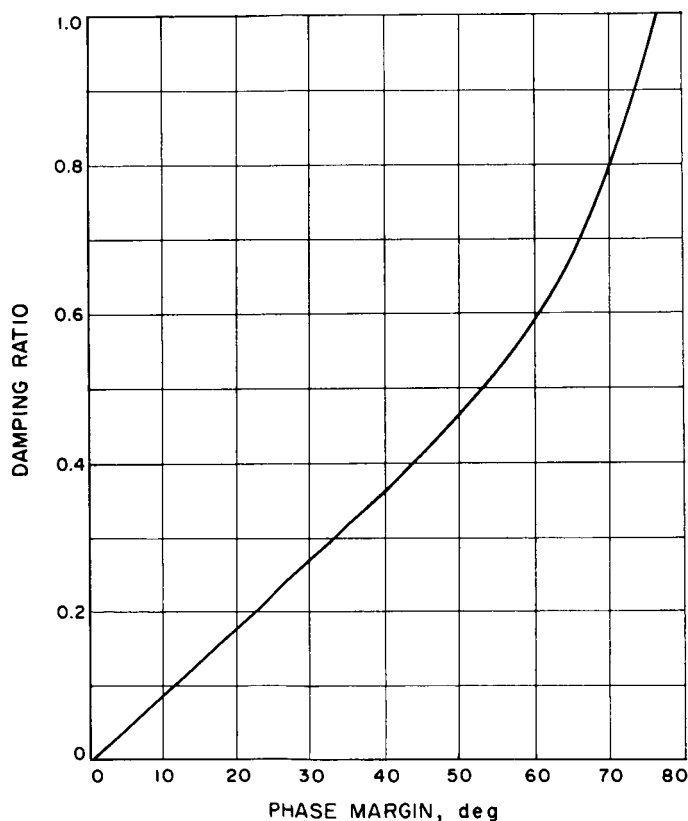


Fig. 20. Phase margin versus damping ratio

Table 3. Comparison of nominal $H_{(j\omega)}$ versus measured loop characteristics using the new loop model

$2B_{L0}$, cps	$\alpha = \alpha_0$					$\alpha = 1$				
	Phase margin, deg	ζ	Predicted overshoot	Measured overshoot	Discrepancy, %	Phase margin, deg	ζ	Predicted overshoot	Measured overshoot	Discrepancy, %
12	+63	0.707	2.0	2.0	0	+75	0.96	0	0	0
48	+62	0.7	2.0	2.0	0	+50	0.47	3.1	2.9	6
152	+55	0.53	2.0	2.3	15	+42	0.39	4.5	4.8	6

loops. No compensation is required in the $2B_{L0} = 12$ cps. The $2B_{L0} = 48$ cps was not compensated at this time. However, cancellation compensation could be employed by letting $C1 = 390$ pf. This should change the phase margin to 71 deg and cause the closed loop frequency response to have a 1.5-db overshoot for $\alpha = 1$.

Fig. 24 indicates the test setup used to determine the closed loop frequency response $|H_{(j\omega)}|$ while Fig. 25 indicates the test setup used to determine the error response $|1 - H_{(j\omega)}|$.

Figs. 26-31 are the closed loop frequency responses and the error responses for all loop bandwidths at both α_0 and $\alpha = 1$. The "new model" nominal was derived by using the open loop frequency response $[G(s)]$ from the Bode plot] to synthesize the closed loop frequency response $H(s)$ since:

$$H(s) = \frac{G(s)}{1 + G(s)}$$

The error response was easily obtained from $H(s)$ since:

$$\text{Error response} = 1 - H(s).$$

Table 3 shows the nominal versus measured $H(s)$ response for all loop bandwidths at both α_0 and $\alpha = 1$.

It may be concluded:

(1) The low-pass filter equivalent of the VCO crystal is valid if not used a frequency higher than an octave above the corner frequency. This model will be useful as narrower IF bandwidth and higher Q crystal VCO's are utilized to advance the state of the art.

(2) The assumption that the loop behaved as a quadratic in the area of ω_c appears to be valid, since the predicted overshoot (obtained by relating phase margin to damping factor and then determining overshoot) agrees with both the measured data and the predicted overshoot derived from using the open loop response to synthesize the closed loop response $H(s)$.

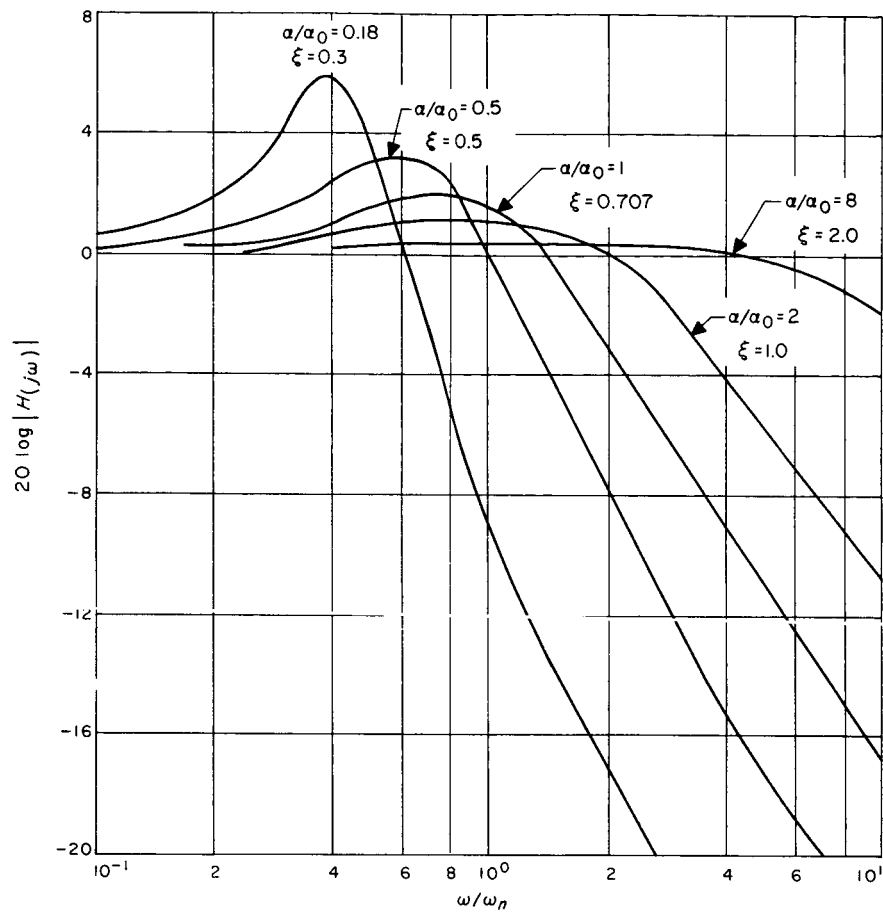


Fig. 21. Frequency response in decibels versus ω/ω_n for various α/α_0

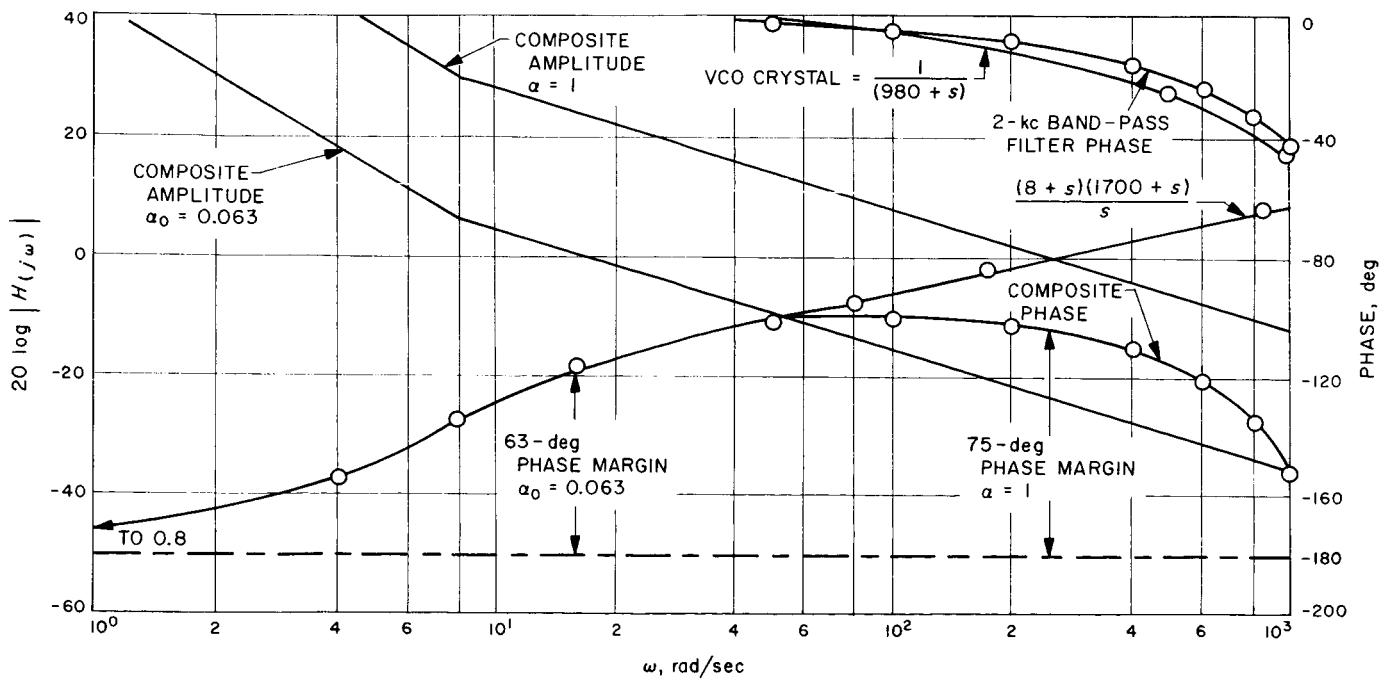


Fig. 22. Open loop frequency characteristics, $2B_{L0} = 12$ cps

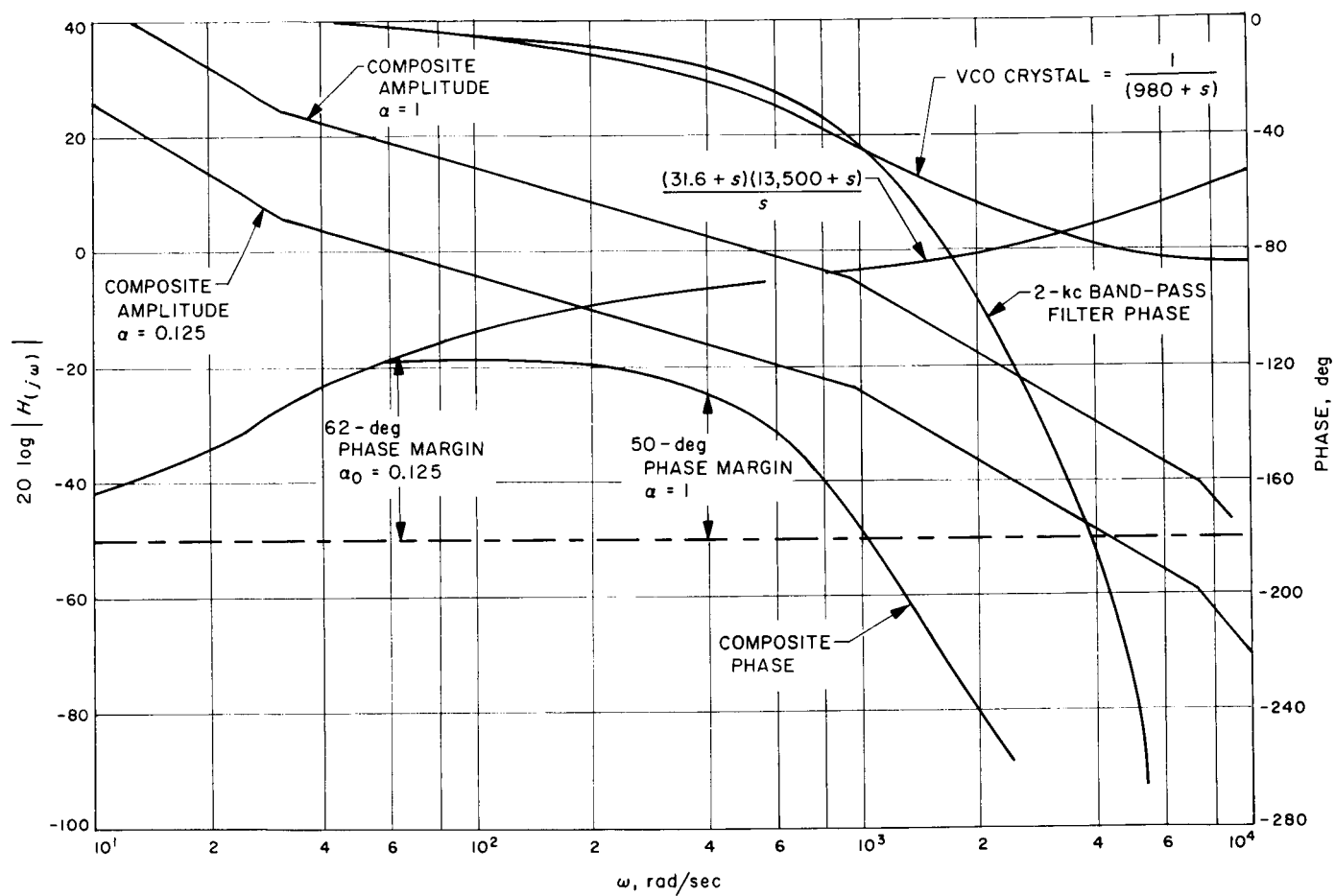


Fig. 23. Open loop frequency characteristic, $2B_{L0} = 48$ cps

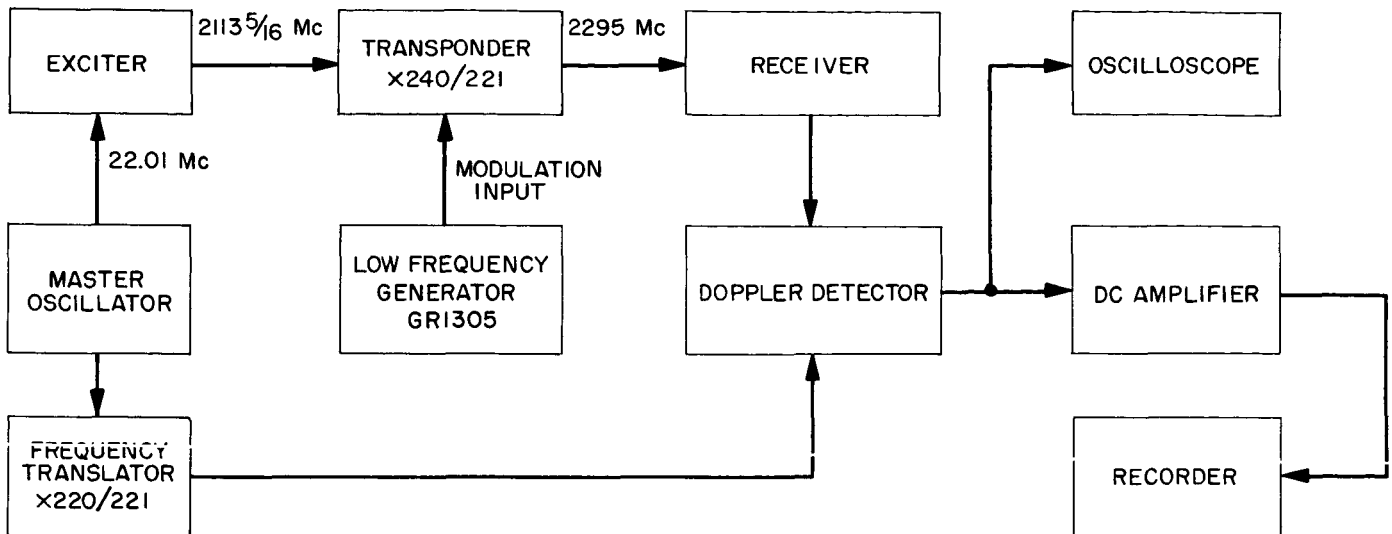


Fig. 24. Test setup to measure closed loop frequency response $H(j\omega)$

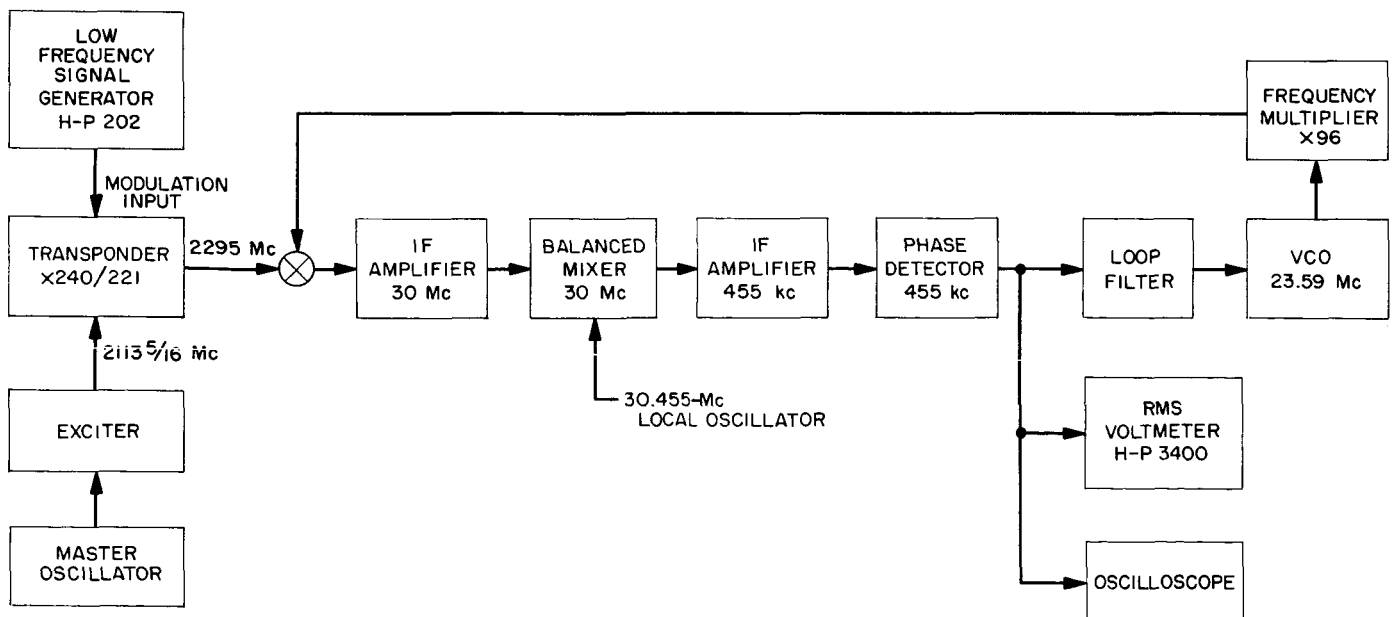


Fig. 25. Test setup to measure closed loop error response $1 - H(j\omega)$

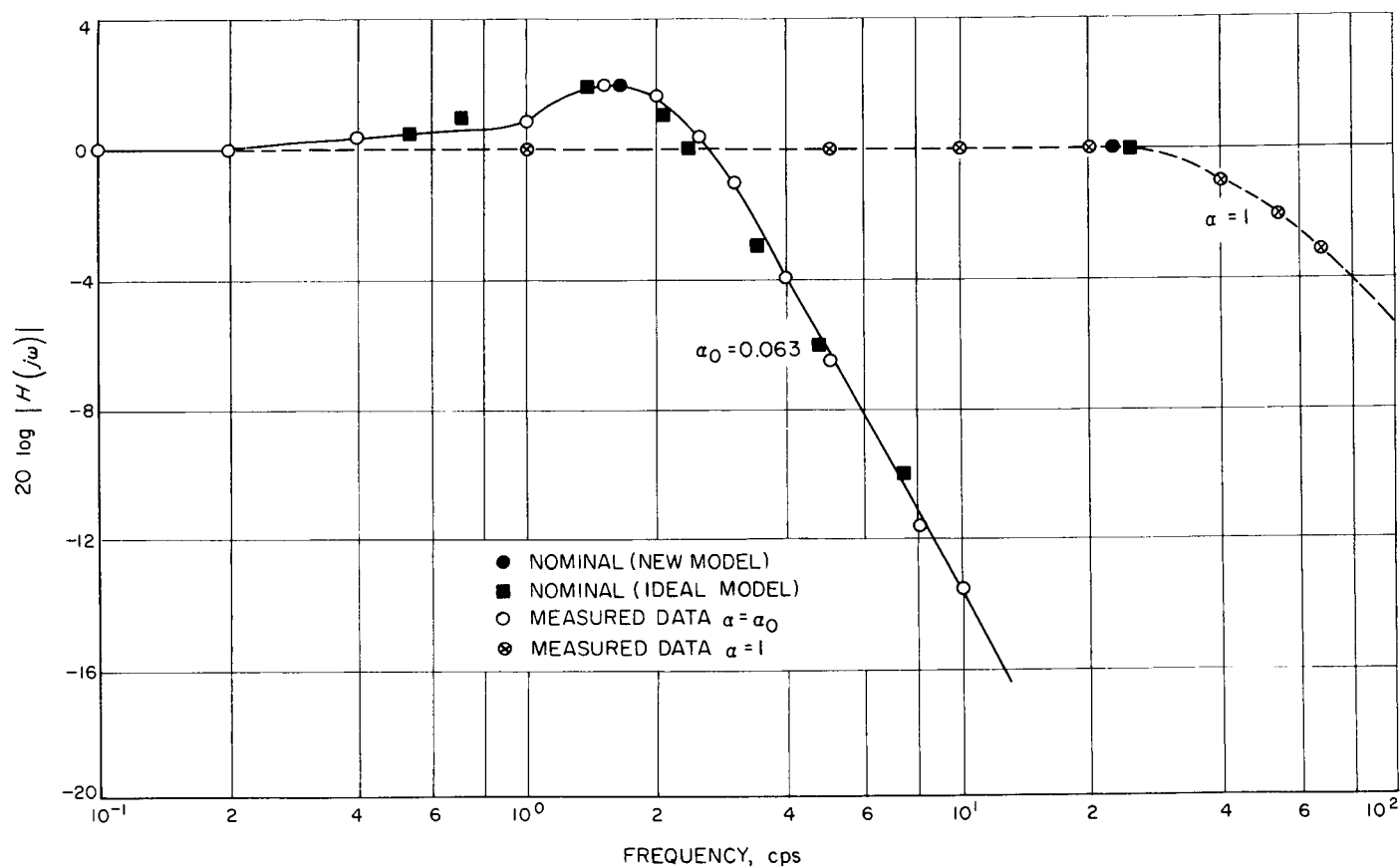


Fig. 26. $H(j\omega)$ for CTL, $2B_{L0} = 12$ cps

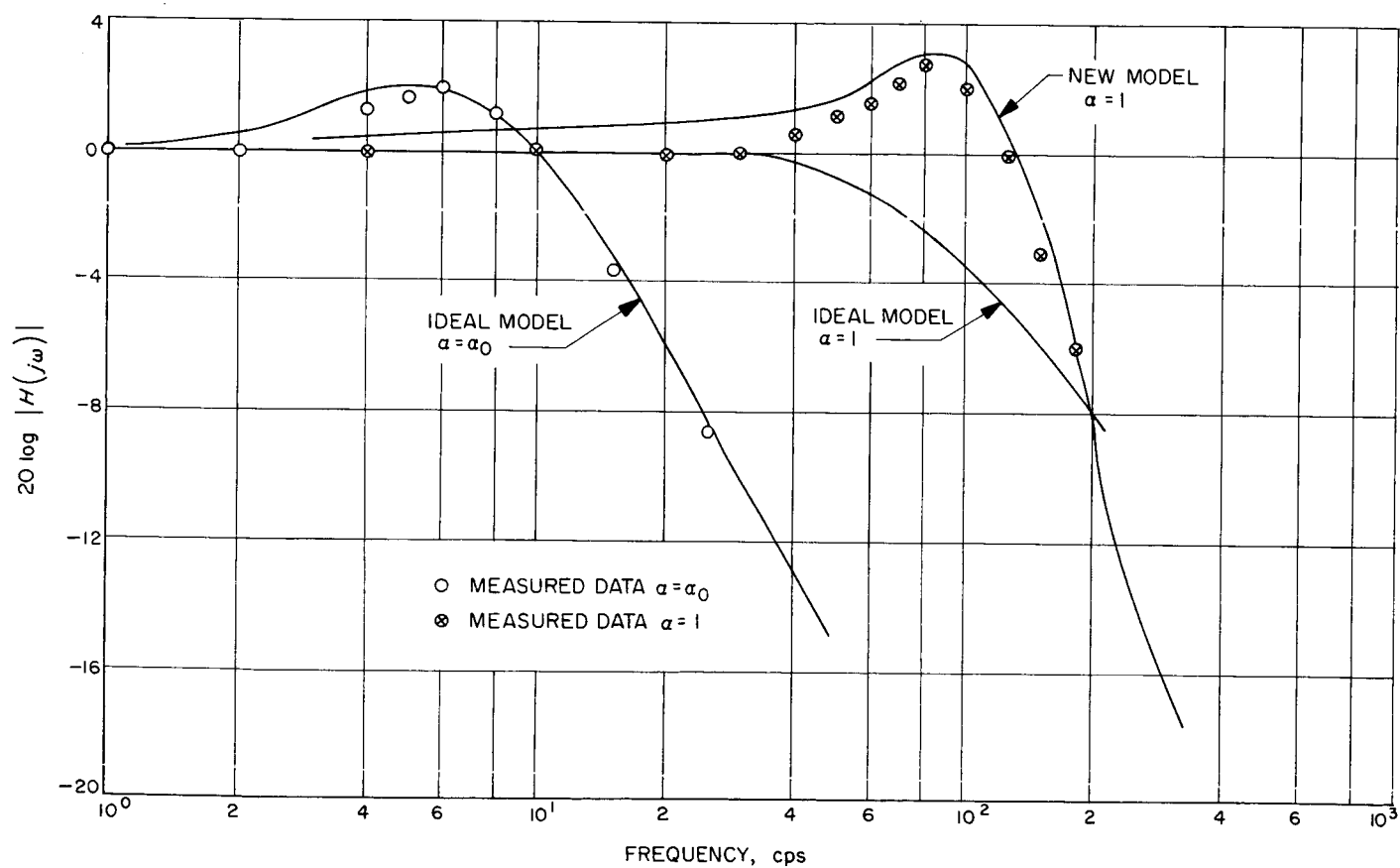


Fig. 27. $H(j\omega)$ for CTL, $2B_{L0} = 48$ cps

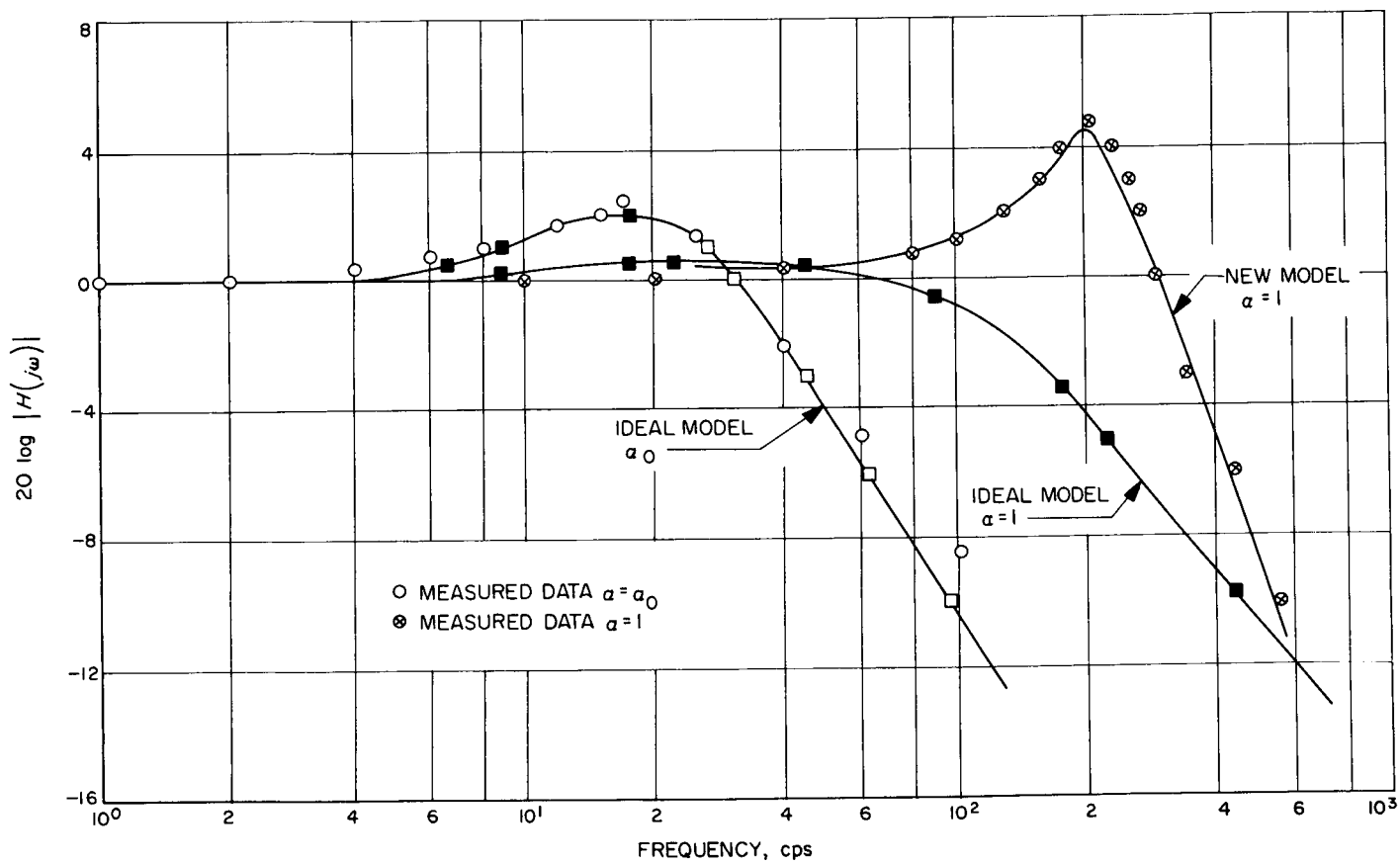


Fig. 28. $H(j\omega)$ for CTL, $2B_{L0} = 152$ cps

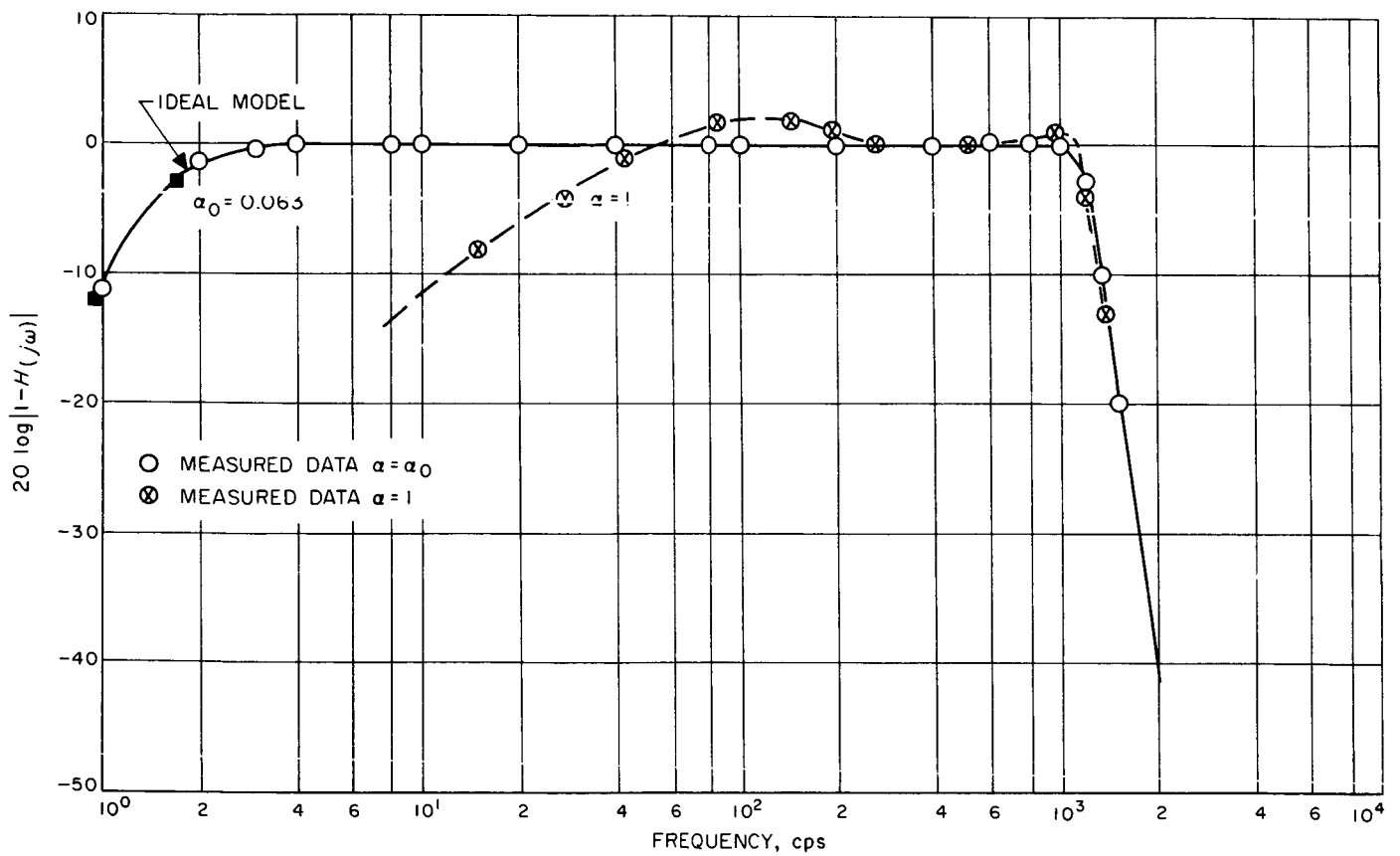
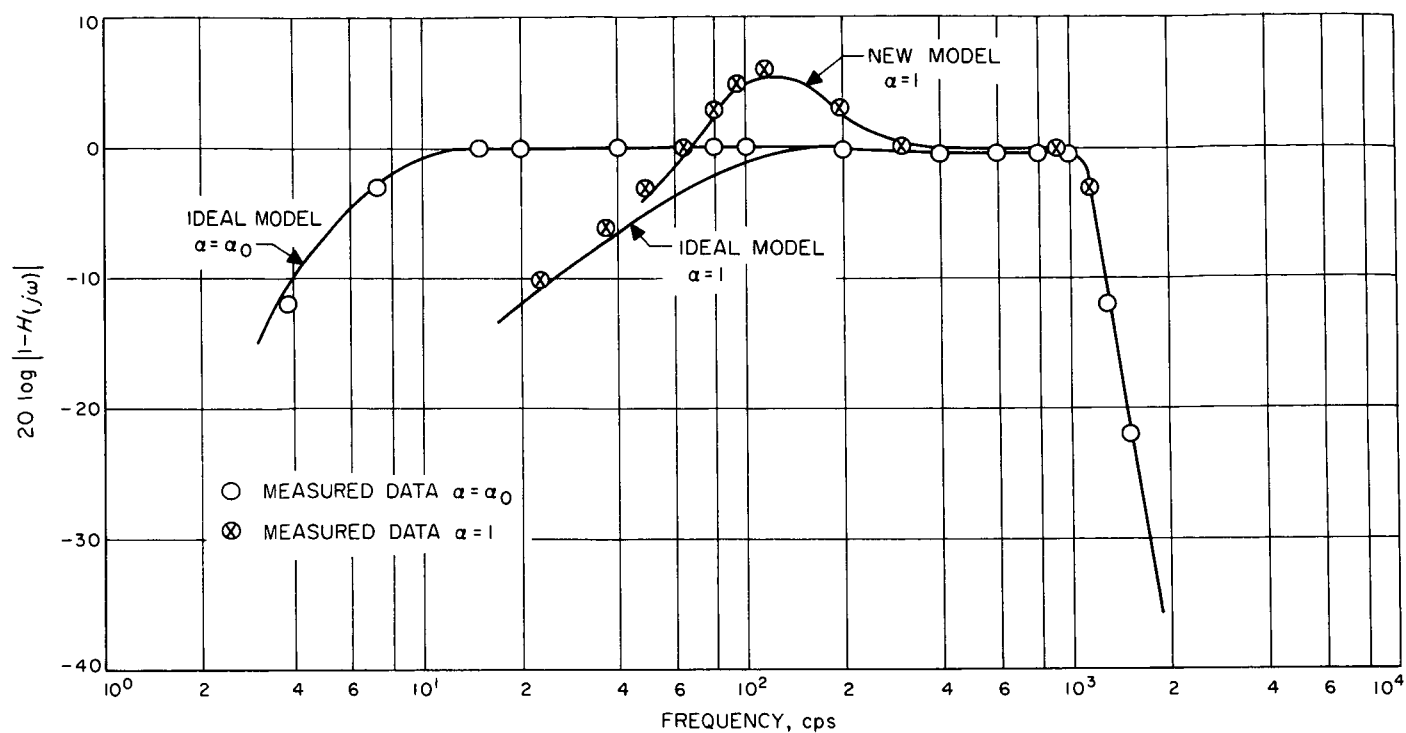
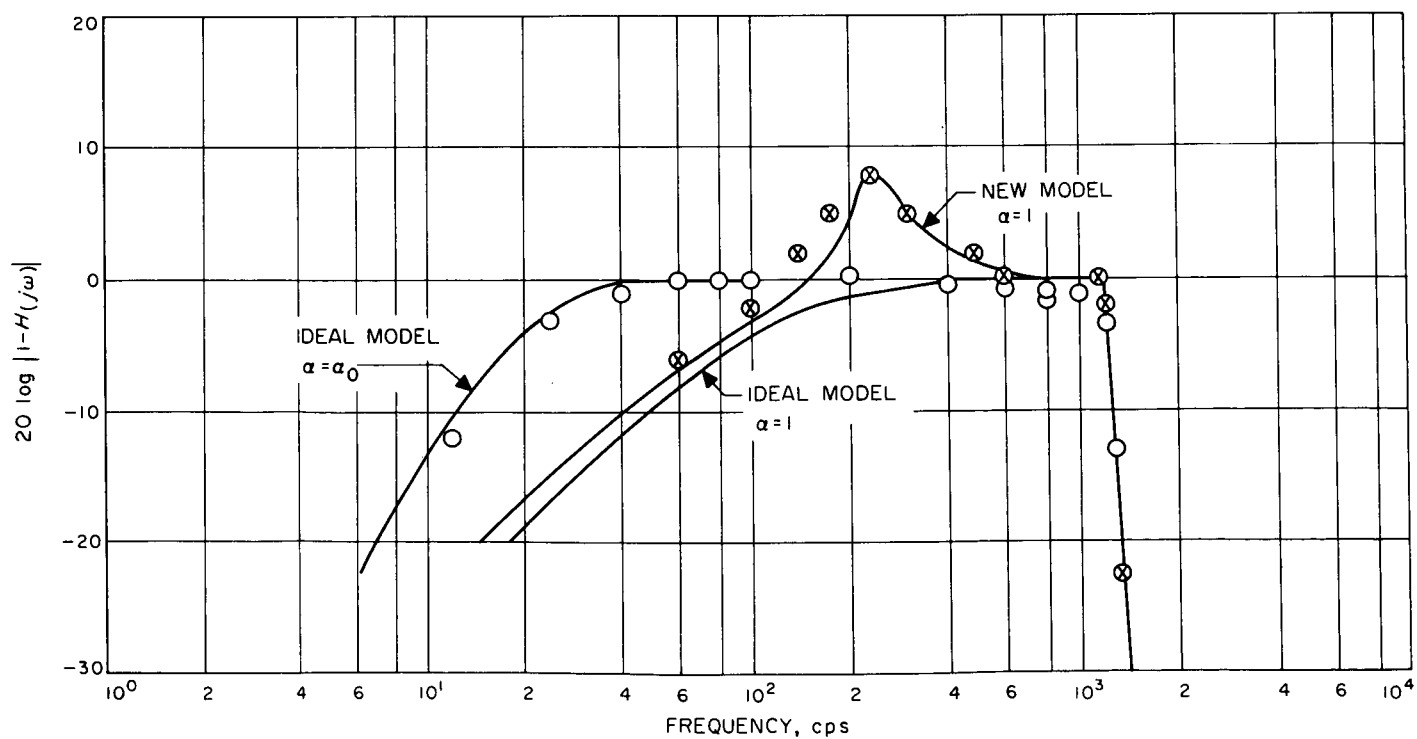


Fig. 29. $1 - H_c(j\omega)$ for CTL, $2B_{L0} = 12$ cps

Fig. 30. $1 - H(j\omega)$ for CTL, $2B_{L0} = 48$ cpsFig. 31. $1 - H(j\omega)$ for CTL, $2B_{L0} = 152$ cps

E. Amplitude Stabilized Signal Source

A description of an amplitude stabilized signal source, to be used during antenna gain measurements, is given in SPS 37-35, Vol. III, p. 52. This report describes the performance obtained during final testing of the package.

Fig. 32 shows the control panel which is mounted in a carrying case. The antenna-mounted assembly with the cover open and the insulation removed to expose the temperature control assembly is shown in Fig. 33.

As indicated in the previous SPS, the stability design goal was ± 0.05 db over a reasonable temperature range and line voltage variation. The tests were:

Line voltage. When the complete system was subjected to a line voltage variation of $\pm 10\%$, there was no measurable variation in the output. For the test, the resolution of the output measuring system was approximately 0.005 db.

Temperature. Output stability tests were run for 48 hr and covered a temperature range of 40 to 120°F. The change in output during this period was ± 0.03 db centered at 80°F.

Signal generator and traveling wave tube (TWT) level changes. As long as the TWT is not saturated, the system will accommodate any combination of signal generator level changes and TWT gain drifts over a ± 7 -db range. Laboratory tests were conducted to evaluate the effect of various combinations of signal generator levels and TWT gains on output power levels. Over a ± 7 -db range, the output variation was less than 0.01 db peak-to-peak.

The final specifications are:

Line voltage	117 v ac $\pm 10\%$, 60 cps
Output power adjustable range	1-10 w 2285 ± 15 Mc
Output frequencies	2110 ± 10 Mc
Stability	
Long term (24 hr)	± 0.05 db
Short term (10 min)	± 0.01 db
Noise	< 0.01 db rms

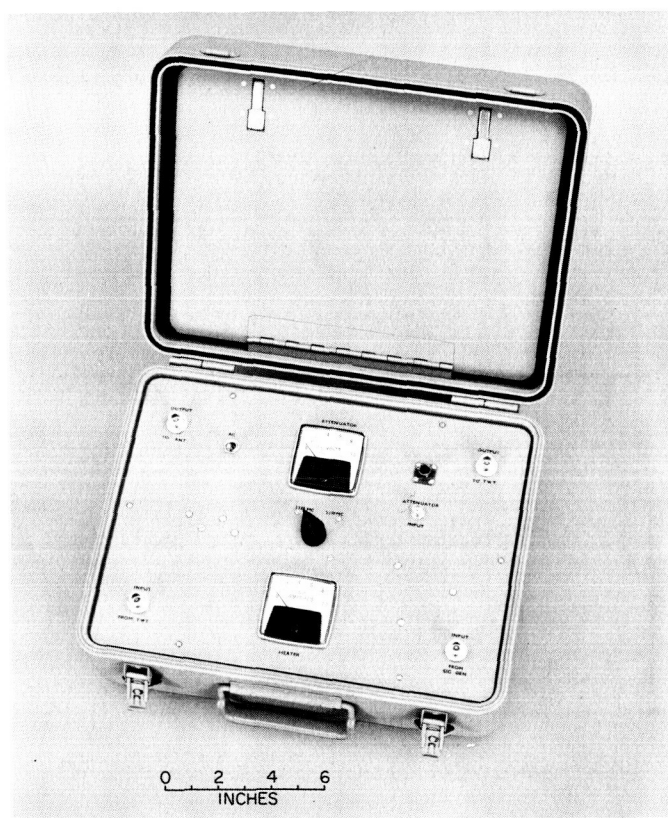


Fig. 32. Stable source control panel

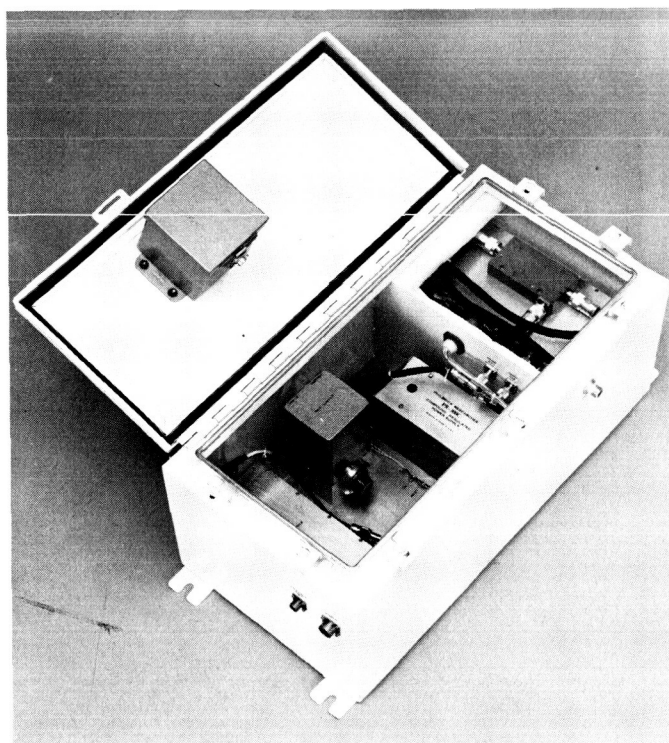


Fig. 33. Antenna-mounted assembly

Temperature range	40-120°F
Dynamic range of voltage controlled attenuator	± 7 db
VSWR at output jack (all frequencies)	1.1:1 (max)

The stable source has been completed and tested. Temperature control of some of the components is necessary, as determined in tests on the individual component. The operation of the temperature control module has proved satisfactory and the fully assembled system meets the design goals set forth previously. Over-all performance indicates that the stable source will be a useful device in both the lab and field.

References

1. Ahrendt, W. R., and Savant, C. J., "Servo Mechanism Practice," Second Edition, p. 555, McGraw-Hill Book Company, Inc., New York, 1960.
2. Hoffman, L. A., "Receiver Design and the Phase Lock Loop," prepared for the Electronics and Space Exploration Technical Lecture Series sponsored by the IEEE, Aerospace Corp., El Segundo, California, 1964.

IV. Communications Research and Development

A. Experimental Closed Cycle Refrigerator for Masers

Testing of the prototype machine is in progress at JPL and Goldstone. Concurrently some effort is being made to simplify the instrumentation required to monitor system performance. In SPS 37-36 Vol. III, p. 43, a simplified solution to the measurement of rate of flow of helium gas was described. Similarly, a new technique has been derived for the measurement of cryogenic temperatures.

The principal innovation over the DSIF configuration has been the elimination of a reference power source (mercury battery) and a dc amplifier. This is achieved by using a thermocouple for a constant voltage source and a microammeter in series with a thermistor to monitor the cryogenic temperature. Fig. 1 shows the physical configuration schematically. T_a is the ambient temperature and T_c is the cryogenic temperature to be measured. The volt-

age generated by the gold + 2.11 atomic % cobalt thermocouple is substantially independent of T_c in the region of 4 to 20°K. Moreover, T_a is sufficiently well regulated so that the current through the thermistor (a 1/8-w carbon resistor) is a direct measure of its resistance, which in turn is a function of T_c .

Since the microammeter may be used to read thermocouple currents directly at higher temperatures, a complete instrumentation for the closed cycle refrigerator is readily achieved.

Fig. 2 shows the complete schematic as applied to a cryogenic refrigerator. Table 1 describes the various functions corresponding to the switch positions.

The resistor R1 is a sensitivity adjustment when reading the thermocouples directly and is generally set for a full-scale reading on switch position 3 when the machine is down to operating temperatures. The thermocouples

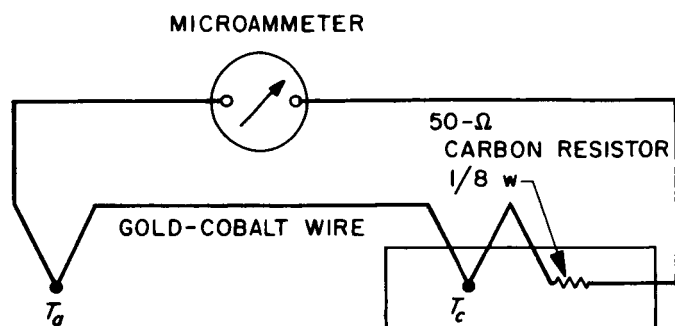


Fig. 1. Simple cryogenic temperature indicator schematic diagram

are used to monitor the machine performance during cool-down and no attempt has been made to calibrate them for accuracy.

However, the thermistor-thermocouple combination provides an accurate measurement capability in a difficult region. A typical calibration curve for the range from 4.2 to 20.4°K is shown in Fig. 3. A hydrogen vapor pressure gage provided the 16.5°K reference point, and a helium vapor pressure gage provided the 4.2°K point. The elec-

Table 1. Switch functions

Switch position	Microammeter connected to:
1	Self for zero adjust
2	Thermocouple on 70°K station
3	Thermocouple on 15°K station
4	Thermocouple on 4.4°K station
5	Thermistor-thermocouple on 15°K station
6	Thermistor-thermocouple on 4.4°K station

tronic gain of a traveling wave maser attached to the 4.2°K station provided the other points on the curve as the machine warmed after shutdown. The assumption used for electronic gain as a function of temperature was: electronic gain in decibels = constant/absolute temperature. The curve shows that an accuracy of approximately $\pm 0.1^\circ\text{K}$ is realizable.

A helium vapor pressure gage requires a careful balance between the amount of gas and the relative volumes at the low temperature and ambient (gage) temperature. Inconsistent readings have been observed in the 5 to 6°K region and further experimental studies are planned.

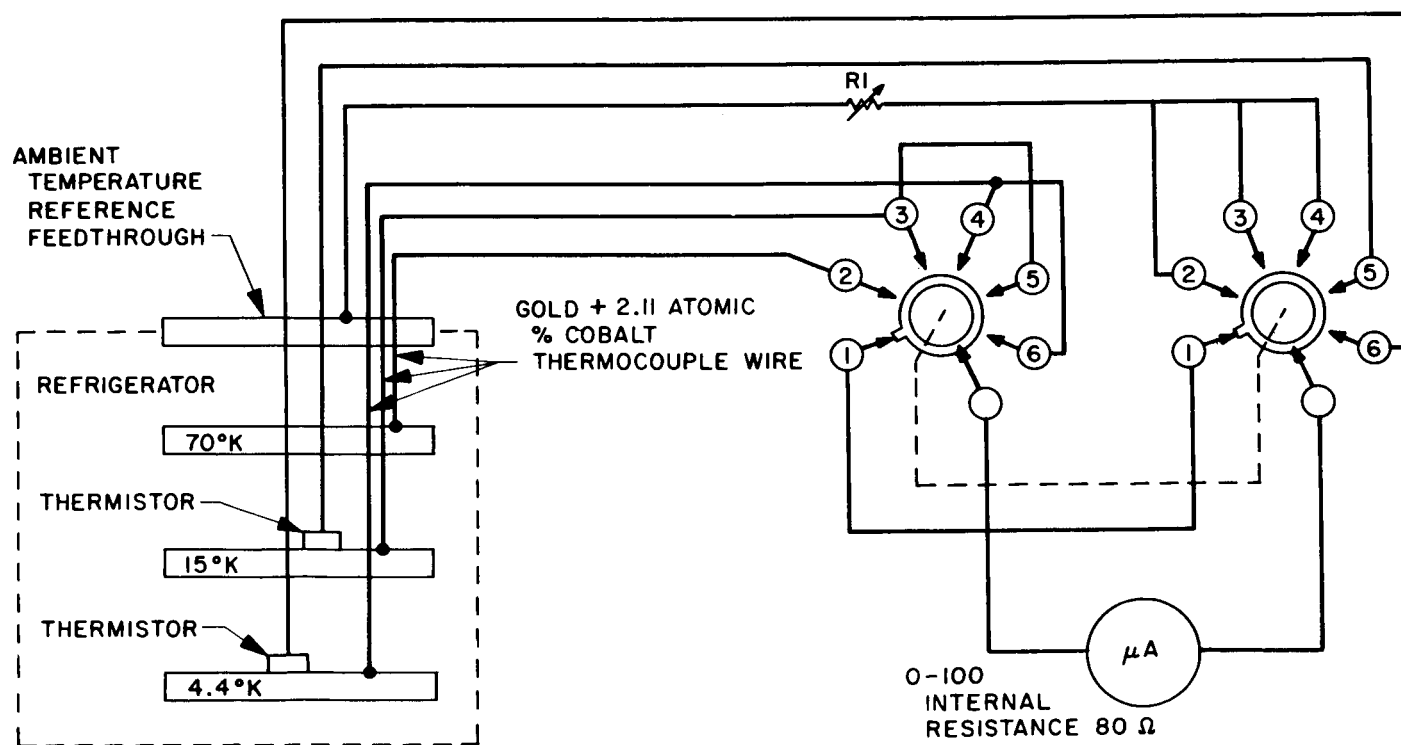


Fig. 2. Schematic diagram of complete instrumentation as applied to a cryogenic refrigerator

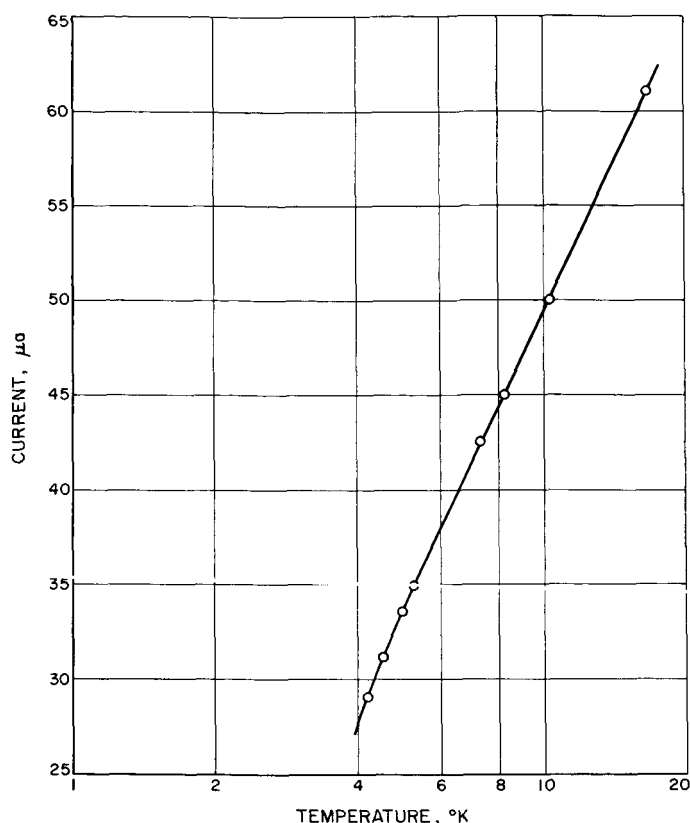


Fig. 3. Calibration curve for a thermistor-thermocouple temperature sensor

B. Continuous Wave (CW) Signal Power Calibration With Thermal Noise Standards

1. Introduction

An attempt to improve the accuracy of the calibration of the CW received signal power in the DSN is presently under way. A convenient measure of a spacecraft received power level is the receiver AGC voltage, which is calibrated for absolute received power, defined at the receiver input, with a calibrated test transmitter. The theory, method of data acquisition, and equipment have been discussed previously (SPS 37-35, Vol. III, p. 58). Simultaneous measurements of the *Mariner IV* spacecraft were made at the Echo, Pioneer, and Venus Stations at Goldstone for several weeks. This report presents the preliminary

computed results from the Echo Station for July 5-23, 1965. These results are presented in the form

- (1) nominal CW received power
- (2) calibrated CW received power
- (3) calibrated CW received power, normalized for 100% antenna efficiency

2. Antenna Efficiency

As discussed in SPS 37-35, Vol. III, p. 62, the antenna efficiency of each station was measured using radio star tracks over an extended period, typically 3 or 4 wk. A Y-factor method of evaluating radio source temperatures was chosen because a simple, quick test was required, a test which would not interrupt normal station operation to any great extent and which could be carried out by station personnel. Each station tracked a radio source and the antenna efficiency was derived from Eq. (14), SPS 37-36, Vol. IV, p. 272:

$$\eta = \frac{\text{measured source temperature}}{\text{theoretical source temperature}} = \frac{T_o + T_R}{T_{st}} \left\{ \frac{1}{Y_1} - \frac{1}{Y_2} \right\} \quad (1)$$

where

T_{st} = theoretical source temperature, °K

T_R = receiver temperature, °K

T_o = temperature of ambient load, °K

Y_1 = Y-factor, switching between ambient load and antenna on the radio source (ratio)

Y_2 = Y-factor, switching between ambient load and antenna off the radio source (ratio).

Two radio sources, Omega and Taurus A,¹ were chosen and each station tracked these almost nightly, for several weeks. Fig. 4 shows the form used to record the information at each station. Data taken by the DSIF 12 (Echo) Station August 13, 1965, on Omega is presented. Eq. (1) gives the antenna efficiency defined at the maser input. In order to refer this measurement to the antenna input, it would be necessary to measure and account for the transmission line losses between the antenna and the maser input. However, for our purposes, where the spacecraft power is also measured and defined at the maser input, Eq. (1) results in the proper antenna efficiency for transforming the spacecraft power measurements to the

¹Antenna Acceptance Test, JPL Procedure No. DZM-1074-TP, p. 38, April 29, 1965.

RADIO SOURCE MEASUREMENTS

STATION: 12

DATE: 13 AUGUST 1965

1. Track source: OMEGA
2. Boresight
3. While tracking source switch between ambient load and antenna:
 Y_1 (on source): 1. 4.65 db 2. 4.64 db 3. 4.65 db 4. 4.64 db 5. 4.64 db
4. Antenna off source about 3 deg. Switch between ambient load and antenna:
 Y_2 (off source): 6. 7.86 db 7. 7.86 db 8. 7.87 db 9. 7.86 db 10. 7.85 db
5. Temperature on ambient load = 27.8°C
- 6.

ON SOURCE				OFF SOURCE			
Data point	Time, GMT	Hour angle	Declination	Data point	Time, GMT	Hour angle	Declination
1	074308	045.744	343.848	6	074629	043.574	343.848
2	074340	045.878	343.848	7	074702	043.708	343.848
3	074407	045.990	343.848	8	074729	043.820	343.848
4	074431	046.094	343.848	9	074753	043.918	343.848
5	074500	046.214	343.848	10	074829	044.068	343.848

$$Y_1 \text{ average} = 4.644 \text{ db} = 2.9134 \text{ ratio}$$

$$Y_2 \text{ average} = 7.860 \text{ db} = 6.1094 \text{ ratio}$$

$$\eta = \frac{273.18 + 27.8 + 11}{99} \left\{ \frac{1}{2.9134} - \frac{1}{6.1094} \right\} = 56.59\%$$

Fig. 4. Radio source measurements data sheet

antenna input. When this is done for each station there will be a common basis for comparison.

Other DSIF station antenna efficiencies are reported in SPS 37-33, Vol. III, p. 48.

Fig. 4 shows that if the theoretical source temperature for Omega is taken as 99°K,¹ then the measured antenna efficiency for that night was 56.59%.

The average of 21 measurements on Omega and Taurus A, made from July 10 to August 30, 1965, gave the relative efficiency of the Echo antenna as 54.84% with a probable error of 0.25% which arises only from random measurement errors and does not include bias errors. The probable error, from random measurement errors, of the individual data points is 0.98% and this number must be compared with the corresponding predicted value of 0.69% from the error analysis (SPS 37-36, Vol. IV, p. 272).

3. CW Power Calibration, Echo Station

The data reduction method previously discussed (SPS 37-35, Vol. III, p. 58) has been modified slightly into a form suitable for computerized calculation. Fig. 5 shows the IBM 1620 computer output format for the Echo Station for July 23, 1965. System temperature, pre- and post-calibration references, and received signal AGC voltage were discussed in SPS 37-35, Vol. III, p. 58. The term *GFSK* is the product $g(f_s) \cdot k$

where

$g(f_s)$ = normalized gain at the signal frequency, f_s

k = Boltzmann's constant

BWR is the computed bandwidth, in cps, of the narrow-band filter, also discussed in SPS 37-35; α is the diode's noise versus CW sensitivity correction factor (SPS 37-36, Vol. III, p. 44) which has been considered zero for all results in this report. The possible inclusion of α , as a refinement to the present results, will be investigated when further data on this correction factor have been obtained. The columns in the figure are similar to those of data in Table 2, SPS 37-35, Vol. III, p. 60, except that here the nominal signal power level has been corrected to take into account the calibration of the step attenuator in the test transmitter.

Previously, the data reduction method proceeded from this point by a graphical technique. The computerized

method now uses a more accurate statistical analysis. The best second-order curve

$$y = a + bx + cx^2 \quad (2)$$

is fitted to the 11 pairs (in the example of Fig. 5) of data points where

x = corrected nominal signal power level, dbm

y = AGC voltage, v

a, b, c = constants of the second order curve Eq. (2)

The results of this analysis are printed in Fig. 5 below the subheading "Nominal AGC curve." Numerical values for the constants a , b , and c have been found and these define the best second-order curve to fit the entire nominal AGC curve. Numerical values for the probable errors of the constants have been found and are also printed below the subheading.

The best second-order curve

$$y = ac + bcx' + ccx'^2 \quad (3)$$

is then fitted to the five calibrated power level data points, where

x' = calibrated signal power level, dbm

y = AGC voltage, v

ac, bc, cc = constants of the second-order curve Eq. (3).

The results of this analysis, which are printed out below the subheading "Calibrated AGC curve," define the best second-order curve to fit the calibrated AGC curve.

Eqs. (2) and (3) are solved by the computer for proper values of x and x' for the first five AGC voltage values of y . The average difference between these solutions for x and x' yields the best value for the correction factor which is defined as the average difference, in db, between the nominal and calibrated AGC curves over the calibration range. The correction factor is printed out below the constants of Eqs. (2) and (3).

The receiver AGC voltage, -2.22 v in Fig. 5 when the antenna is locked on the spacecraft, is substituted into

CW POWER CALIBRATION

STATION 12

DATE 22-7-1979

SYSTEM TEMPERATURE 44.75 DEGREES PRE-CAL REFERENCE 25.00 DB POST-CAL REFERENCE 24.89 DB
 RECEIVED SIGNAL AGC -2.22 VOLTS GFSK= -198.61 BWR= 10279.475 ALP (M)=1.000
 ANTENNA EFFICIENCY 54.24 PERCENT

DATA POINT	AGC VOLTS	SIGNAL POWER DBM	NOMINAL POWER DBM	ATTENUATOR DBM	CAL-POWER DBM
1	-6.340	-110.0	-110.000	55.800	-111.130928
2	-5.940	-115.0	-115.000	50.530	-114.409379
3	-5.560	-120.0	-120.000	45.750	-121.213592
4	-5.140	-125.0	-125.000	40.680	-117.264999
5	-4.700	-130.0	-130.000	36.130	-111.141235
6	-2.870	-149.0	-148.950		
7	-2.440	-153.0	-153.150		
8	-2.080	-157.0	-157.150		
9	-1.700	-161.0	-161.150		
10	-1.300	-165.0	-165.150		
11	-1.200	-166.0	-166.150		

NOMINAL AGC CURVE

A=-.12870037E+02 PEA= .51167917E+00
 B=-.37039279E-01 PEB= .74952421E-02
 C= .20069243E-03 PEC= .26926613E-04

CALIBRATED AGC CURVE

AC=-.82487171E+01 PEAC= .95603333E+00
 BC= .37360537E-01 PEBC= .15821734E-01
 CC= .49096737E-03 PECC= .65277026E-04

CORRECTION FACTOR= -1.353604 DBM

RECEIVED SPACECRAFT POWER LEVEL =-155.89378 DBM NOMINAL

RECEIVED SPACECRAFT POWER LEVEL =-157.24739 DBM CALIBRATED

RECEIVED SPACECRAFT POWER LEVEL =-154.63936 DBM NORMALIZED FOR 100 PERCENT ANT. EFF.

Fig. 5. Computer output: CW power calibration

Eq. (2) which is also solved by the computer for the received spacecraft power level (nominal value). The corresponding calibrated value is found by the computer by applying the correction factor. The received spacecraft power level normalized for 100% antenna efficiency is calculated using the average value for antenna efficiency found above.

The three values for received spacecraft power level (nominal, calibrated, and normalized) for each day that measurements were made at the Echo Station, have been plotted in Fig. 6 as a function of time. Also shown in this figure is the best second-order curve fitted to each set of data. These curves were calculated, ignoring all data on July 6 and 7. These bad data points probably result from a "personnel learning period."

It is interesting to note that the standard deviation of the nominal and calibrated data points, excluding July 6 and 7, are 0.37 and 0.22 db, respectively. The calibration process has thus smoothed or reduced the spread of the data. The standard deviations of the calibrated and the normalized data are identical, as expected.

A possible bias error could be the effect of a drop in maser gain from the time of maser tune-up during the pre-calibration routine and the acquisition and measurement of the spacecraft. This will be investigated at the three stations where calibration measurements were carried out and may lead to a further refinement of the data.

C. Simultaneous Lobing Radiometric Tracking System

The S-band system modes of operation for the 210-ft-diameter antenna will involve use of a simultaneous lobing angle tracking feed system. A radiometer, which could be used in conjunction with the tracking feed, would be useful for angle pointing and gain calibrations of the antenna system, using radio star sources. This technique is especially important for the 210-ft-diameter antenna which does not have a collimation tower capability.

A prototype of such a radiometer is currently being evaluated using the Echo Station 85-ft-diameter antenna. Results to date indicate that such a device is indeed feasible.

On September 17, 1965, tracking data were taken on the radio source Omega Nebula when it was at a declination very close to that of *Mariner IV* and at a sidereal hour angle approximately 3 hr behind *Mariner IV*. This source therefore provided not only repeatability data and tracking jitter data, but also provided a comparison against the *Mariner* tracking data taken on the same day. These data have now been reduced and are presented in Fig. 7. Though the tracking of *Mariner IV* appears

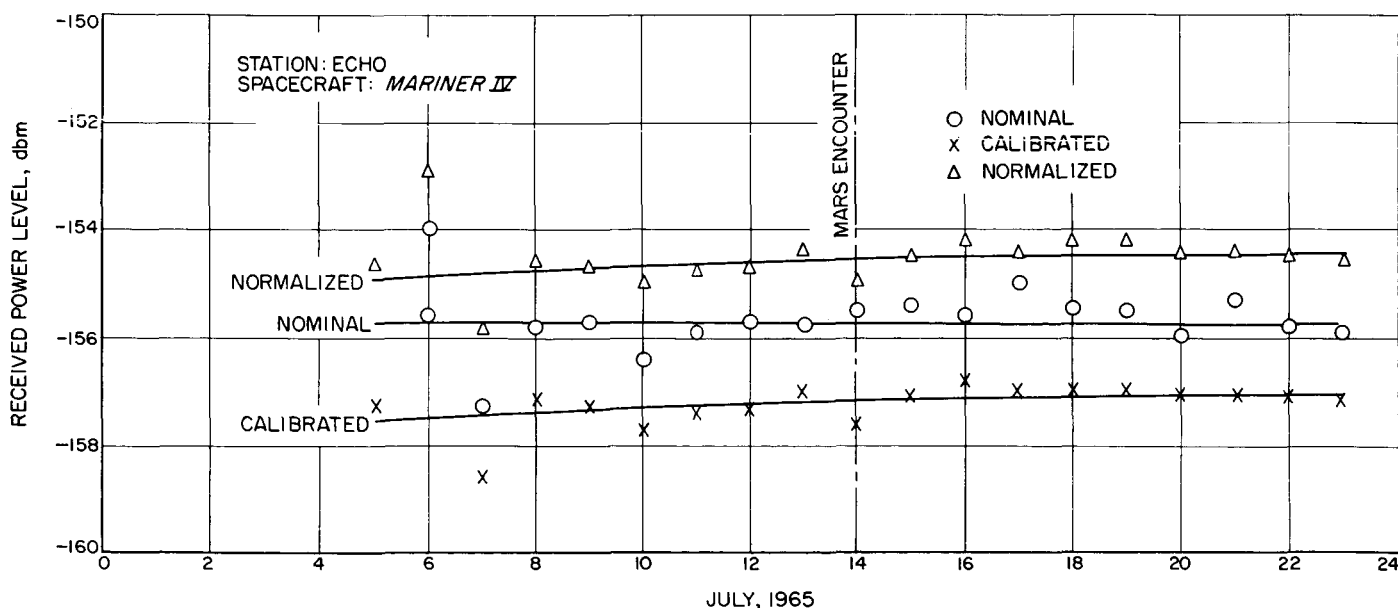


Fig. 6. Nominal and calibrated received power level

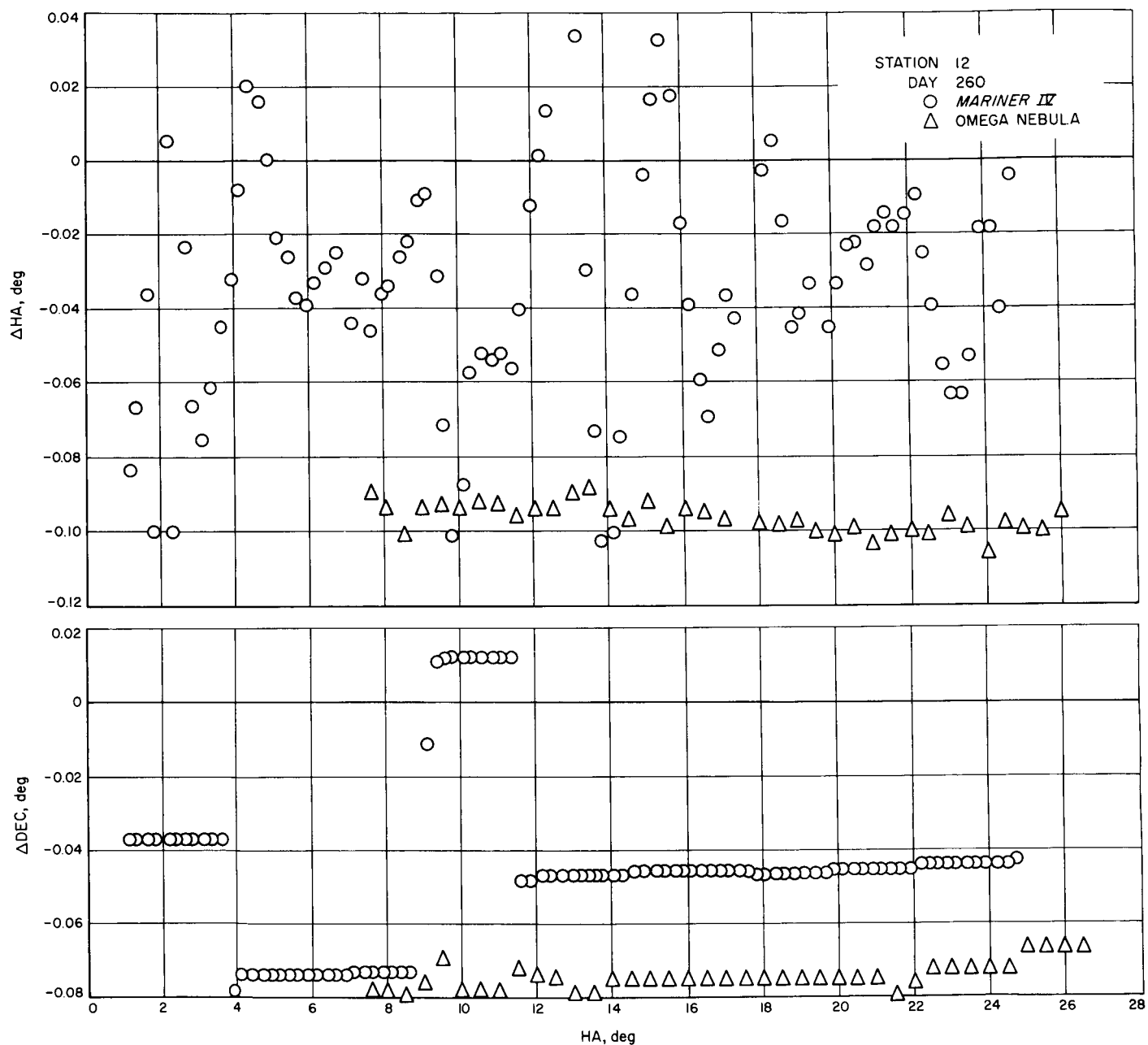


Fig. 7. Hour angle and declination pointing error versus hour angle

relatively rough, the mean of the tracking data can be compared to that taken on Omega Nebula. This comparison yields a difference, or apparent boresight shift, of approximately 0.065 deg in HA. At present, the reason for the apparent boresight shift is unknown but is probably due to the uncertainty in the position of the radio center of Omega Nebula; this is being investigated.

As stated in SPS 37-36, Vol. III, the system has been operated in an experiment designed to eliminate the necessity of a collimation tower when phasing the receiver for automatic tracking of a spacecraft. It was also stated that the average difference between receiver angle channel phase shifter settings obtained from the collimation tower and the radio source was approximately 25 deg. A subsequent test run against the collimation tower indicates that the null depth of the angle error feed (HA axis) is great enough to cause no boresight shift, within the resolution of the encoders, for this amount of phase misalignment. It can therefore be stated that the primary effect of this amount of phase misalignment will be an increase in tracking jitter which, on a theoretical basis, is approximately 10% for a phase mis-

alignment of 25 deg. It would be desirable to verify this result using a far-field moving source (i.e., a spacecraft). Tracking commitments permitting, this will be done soon.

Another question that arose involves the effect of the electromechanical dynamics of the antenna-servo system on the tracking of the source. That is, do the dynamics of the system cause the antenna to lag the source? This was answered by connecting a strip chart recorder to record the error voltages being sent from the simultaneous lobing radiometer to the servo system. First, the input to the recorder was terminated so that a base line could be established (Fig. 8). The antenna was then moved ahead of the source in HA and the brakes were locked. The source was then allowed to drift through the beam of the antenna (Fig. 9) while the recorder was used to record the HA error voltage, thereby calibrating the chart in terms of angular degrees. The antenna was then allowed to automatically track the source (Crab Nebula) in HA while error voltage recordings were taken (Fig. 10). This figure clearly shows that the mean electromechanical dynamical errors of the antenna-servo system are less than 0.002 deg.

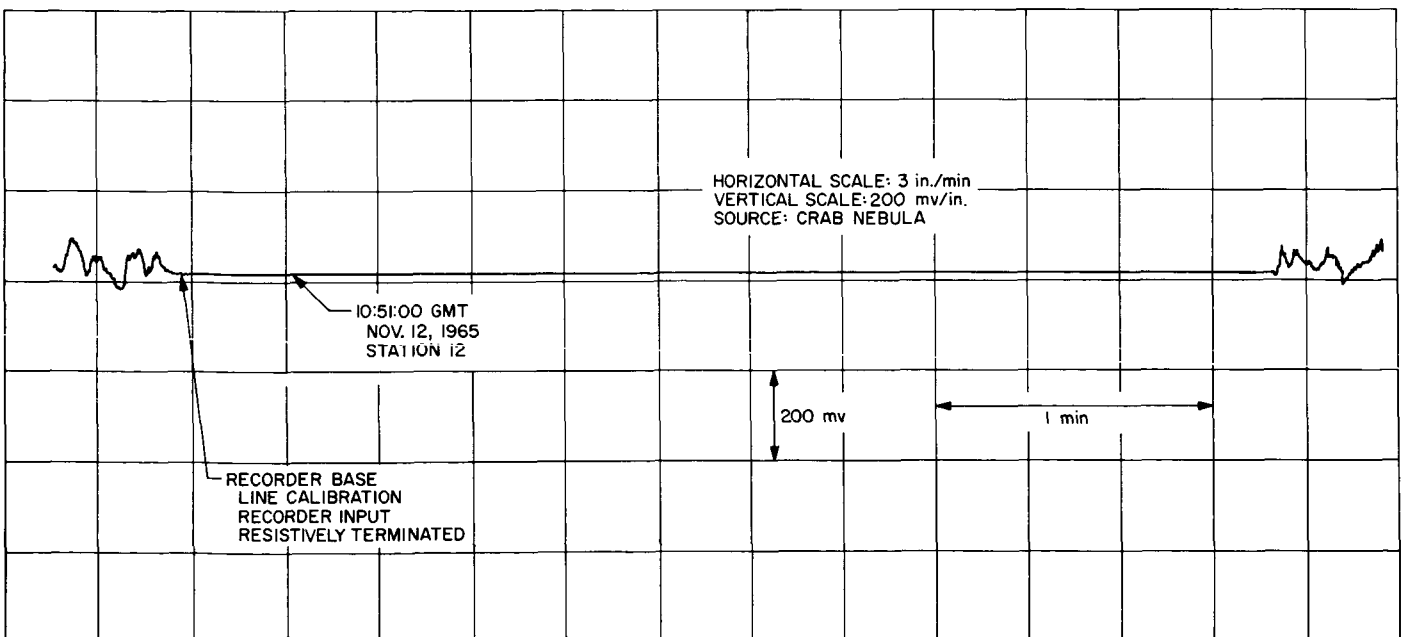


Fig. 8. Calibration of recorder base line

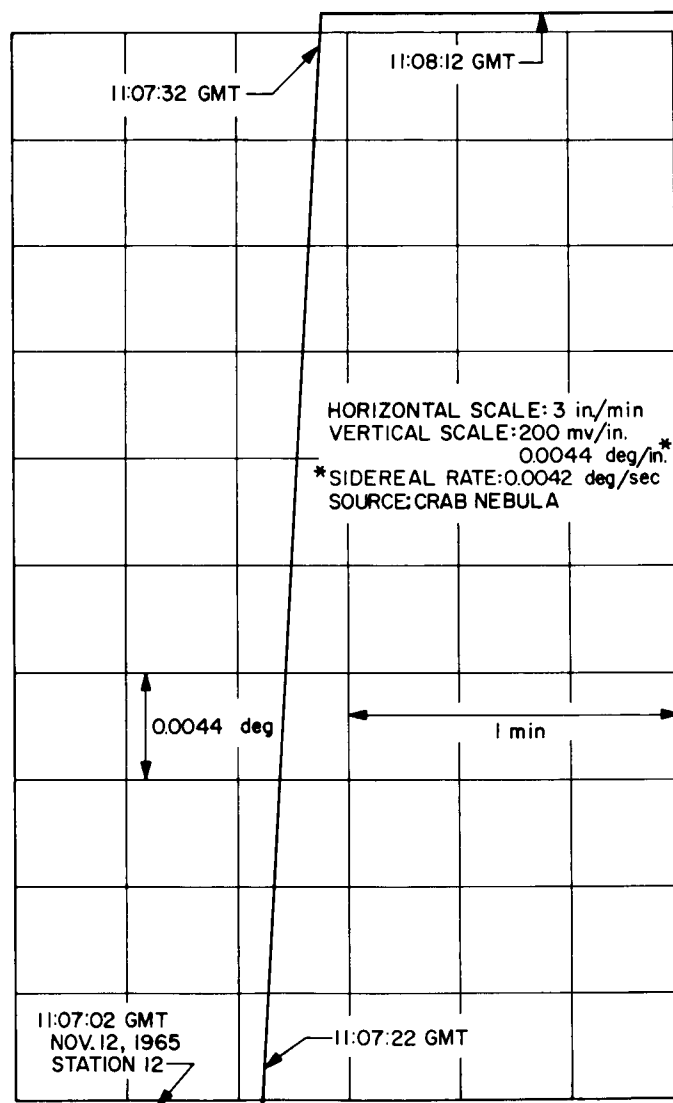


Fig. 9. Calibration of servo error voltage, deg

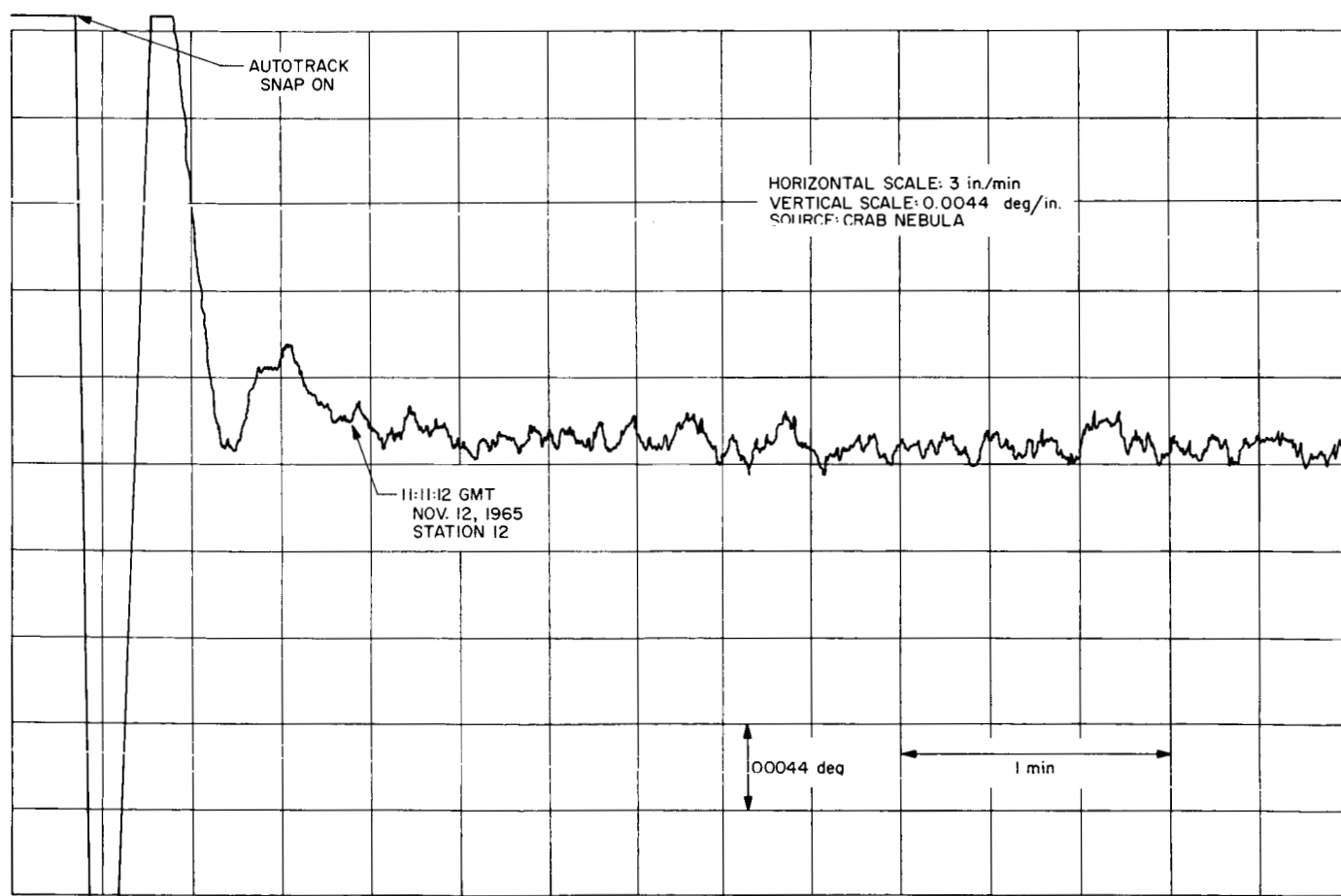


Fig. 10. Angle error recording of automatic tracking of Crab Nebula (hour angle axis)

D. Microwave Maser Development

The development of techniques which improve the performance of masers has resulted in a traveling wave maser (TWM) structure which can be fabricated from a solid piece of copper. The TWM structure has no joints which might result in loss of microwave signal power, or which might restrict the transfer of heat from the maser material to the cooled flange of the TWM. The new structure and a test setup for evaluation of its electrical length are described in this Report.

1. Improved TWM Structure

A one-piece comb-type maser structure is shown in Fig. 11. The cover (with tuning screws), a typical ruby slab, an isolator strip, and a temperature sensor are also shown. The sensor is a carbon resistor, held between two copper discs which mount on the TWM. Tests con-

ducted with resistive heat loading, and with the application of pump power, indicate adequate heat transfer through the solid copper structure.

Fabrication of the TWM shown in Fig. 11 involved conventional machining techniques. Difficulty was encountered in holding uniform dimensions in the comb area and tuning screws for the resonant fingers were used to compensate for the lack of machining precision. Successful machining techniques were subsequently developed by the JPL machine shop, resulting in a practical and accurate process for TWM fabrication. The use of a shaper, a machine which removes metal with a scraping process, has produced an excellent surface finish and uniformity of 0.0001 in. in the most critical area of the comb structure.

More recently, the use of electric discharge machining for metal removal between the fingers of the comb has

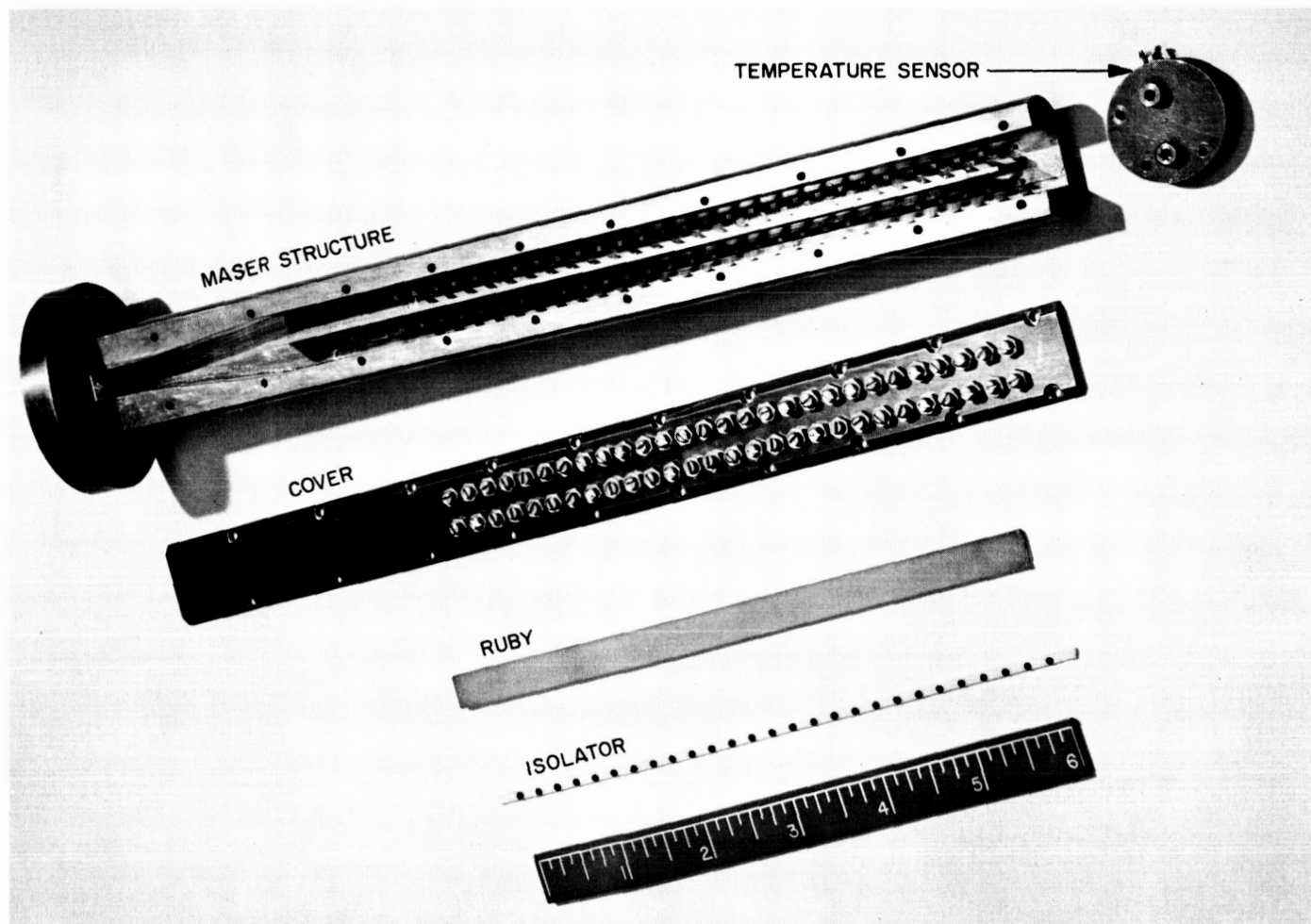


Fig. 11. One-piece copper maser comb structure fabricated with conventional machining techniques

enabled the fabrication of structures with close interval and long finger length. Fig. 12 shows a product of the improved fabrication process. The TWM is shown prior to the installation of rubies, isolators, and coaxial input and output lines. Tuning screws are required only at the ends of the comb, where the last fingers encounter end effects.

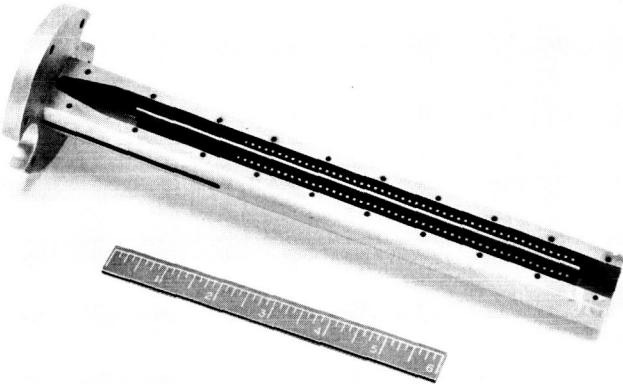


Fig. 12. One-piece copper maser comb structure fabricated with improved process

2. Setup for Measurement of Electrical Length

Resistive losses in the comb structure at the signal frequency have received primary consideration in structure designs. Usable net gain, effective noise temperature, bandwidth, and gain stability are degraded by excessive loss. Resonant slowing provides the electrical length necessary for high gain. Since the attenuation of signal power due to resistive losses is proportional (in db) to the electrical length, the attenuation and length must be compared during structure evaluation. Fig. 13 is a block diagram of the test equipment used for measuring the electrical length of a TWM.

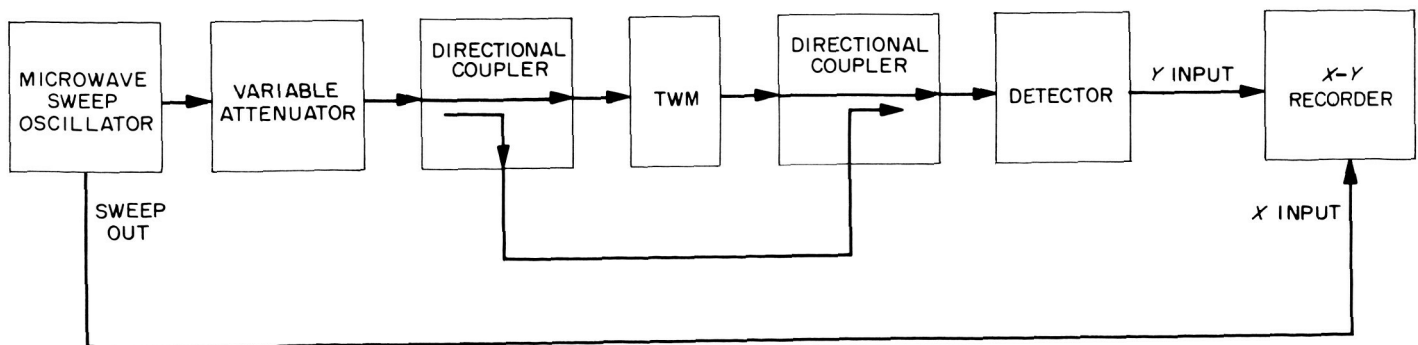


Fig. 13. Method for measurement of TWM electrical length

The pattern which results on the X-Y recorder is shown in Fig. 14. In-phase and out-of-phase signal voltage addition causes peaks and nulls to occur. The difference in frequency between two adjacent peaks or nulls is inversely proportional to the difference in electrical length of the two signal paths between the directional couplers. The electrical length L_e of the TWM is given by the expression

$$L_e = \frac{c}{\Delta f} = \frac{300 \text{ m}}{\Delta f} \quad (1)$$

where

c = velocity of light

and

$\Delta f = \Delta\omega/2\pi$ = the frequency difference in Mc between two adjacent peaks or nulls

The slowing factor S is given by

$$S = L_e/L_o$$

where

L_o = physical length of the TWM

Alternatively, it is possible to solve for S in the usual terminology as follows:

$$S = c/v_g = c/(\Delta\omega/\Delta\beta)$$

where

$v_g = \Delta\omega/\Delta\beta$ = group velocity

and

β = phase change coefficient

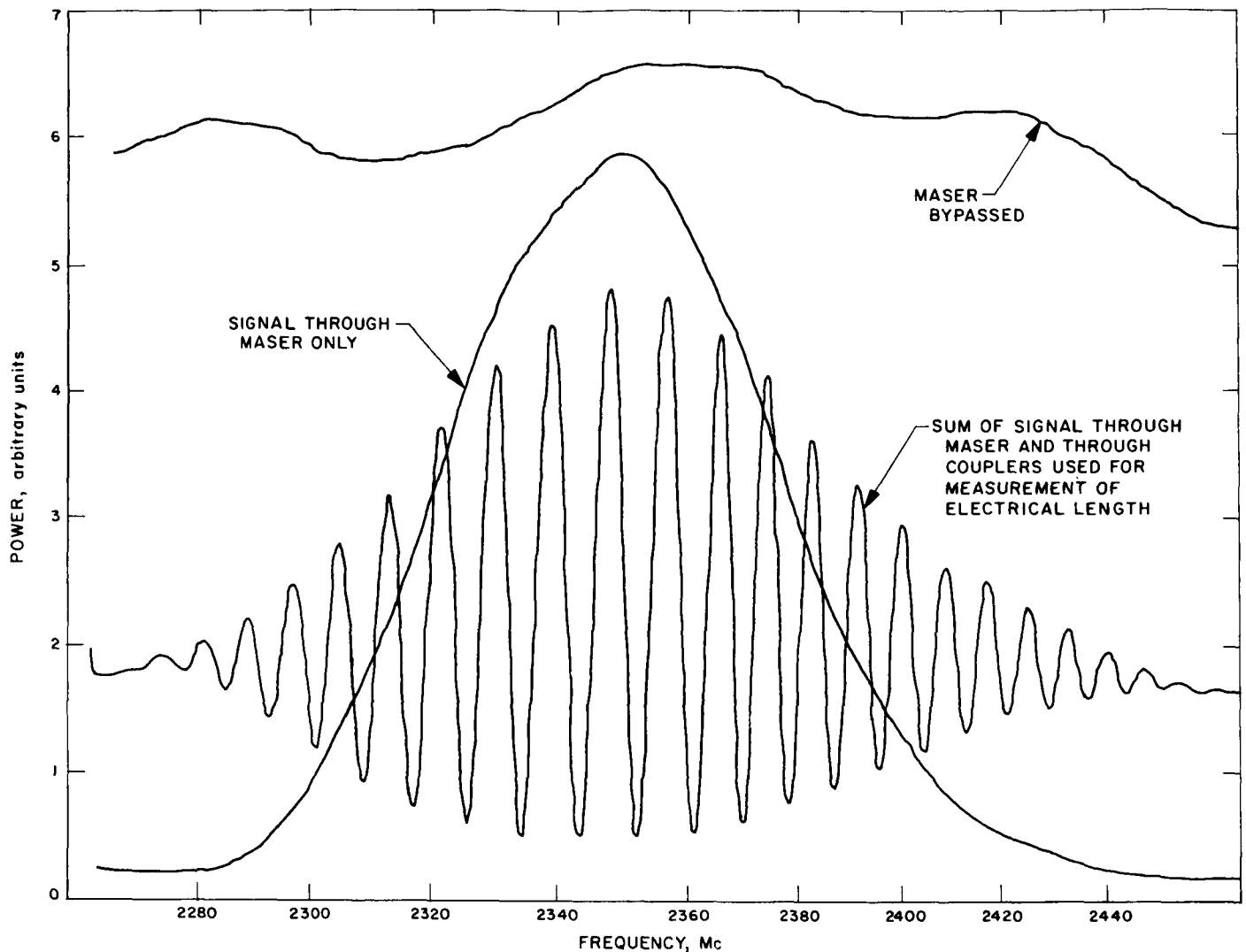


Fig. 14. X-Y recording of TWM band pass and electrical length

Hence, if $\Delta\omega_n$ is measured between the $(n+1)^{\text{th}}$ and n^{th} maxima (or minima) then:

$$\Delta\beta = \beta_{n+1} - \beta_n$$

$$\Delta\beta = \left(\beta_o + \frac{2(n+1)\pi}{L_o} \right) - \left(\beta_o + \frac{2n\pi}{L_o} \right)$$

or

$$\Delta\beta = 2\pi/L_o$$

Therefore,

$$S = \frac{2\pi c}{\Delta\omega L_o} = \frac{c}{\Delta f L_o}$$

in agreement with the previous result. It should be noted that β_o above is undetermined in this method; however, the quantity β_o is of little importance in the design of TWM's. If ω_n is plotted as function of $(\beta_n - \beta_o)$ it is possible to obtain the $\omega - \beta$ curve for the structure. This curve, whose slope is equal to the group velocity v_g , is of great importance in determining the useful bandwidth of the maser structure. A large frequency range with constant v_g is required for a distortion-free amplifier.

The curves in Fig. 14, marked "maser bypassed" and "signal through maser only," illustrate the TWM band pass in comparison to the measurement of electrical length. The variable attenuator setting has been changed to give a convenient scale factor for each curve. The

variable attenuator may be used to measure the insertion loss of the TWM.

The one-piece comb structure has reduced copper losses at the signal frequency to a practical minimum. Other details of the TWM will be described in future reporting.

E. Frequency Generation and Control: S/X-Band Central Frequency Synthesizer

Three modular frequency synthesizers have been fabricated by a local vendor to satisfy the frequency requirements of the 455- and 520-kc subsystems, and the 1.44-Mc synthesizer (SPS 37-33, Vol. III, p. 92).

The synthesizers are very similar in design and structure to the 35.2-Mc frequency synthesizer (SPS 37-34, Vol. III, p. 63). All three synthesizers employ frequency conversions as per the simplified block diagram (Fig. 15).

All RF modules have met stringent requirements prior to acceptance. Performance data are given in Table 2.

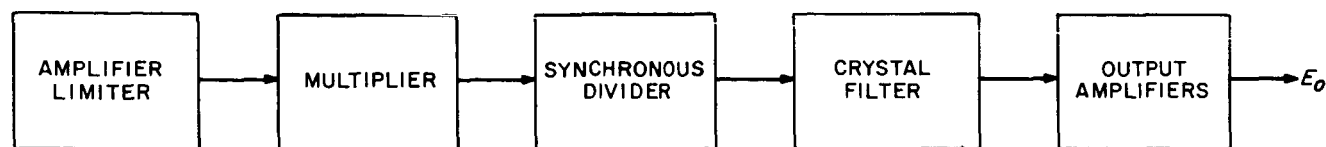


Fig. 15. Synthesizer block diagram

Table 2. Performance data for synthesizers

Module	Input VSWR at +13 dbm, ± 3 dbm	Output level into 50 Ω , + dbm	Isolation from input to output, db	Dynamic range of Input for constant output, db	Harmonic distortion, %	RF leakage, all frequencies, μ v	Spurious signals, μ v	Power supply variations of 13 % versus output, db	Output noise with input terminated, μ v	Bandwidth of output at 3 db, cps	Temperature versus output from 0–50°C, db/°C
455 kc	<1.10	13.8	> 70	40	2.5	<1.0	0.0	–1.2	130	469	0.008
520 kc	<1.10	13.2	> 70	30	0.04	<1.0	0.0	–1.1	10	6751	0.062
1.44 Mc	<1.10	14.3	> 120	40	0.05	<1.0	0.0	–0.8	52	59	0.008

F. Information Processing

1. Punctured Cyclic Coder–Decoder

The punctured cyclic coder, introduced by Solomon and Stiffler (SPS 37-23, Vol. IV, pp. 149–151), whose design was described in SPS 37-27, Vol. III, pp. 97–103, is a device for encoding and decoding a fixed number k of binary data symbols into any nontrivial (n, k) ($n \leq 2^k - 1$) linear code which exists for that k . Thus, one simple machine has the capability of using the code which best satisfies the varying physical constraints of a particular communication system. The code can be readily changed as those constraints change. The encoder–decoder is only slightly more complex than one designed for the full-length $(2^k - 1, k)$ code alone. This is a report on the completion of the basic encoder–decoder system for $k = 6$ information bits.

a. Background. The basic idea of this coder is to have an encoding and decoding procedure for a parent $(2^k - 1, k)$ maximal length shift register code, which procedure is modified slightly for codes of smaller length n by a so-called *puncturing program* which deletes, or punctures, fixed check bits of the parent code.

To encode, a shift register acts upon k information bits and generates words of length $2^k - 1$, all of which have $2^{k-1} - 1$ ones (except for the all-zero word). For codes of length n smaller than $2^k - 1$, a “puncture program” with ones in each of the coordinates to be deleted, and with zeros elsewhere, circulates synchronously with the

shift register sequence. Ones of the puncture sequence are used to control a high-frequency clock that shifts undesired coordinates away before they are transmitted.

b. Decoding procedure. The decoding procedure will now be reviewed. Let a be the received word. For b any fixed non-zero of the parent code word, let $T^i b$ denote the code word which results from the puncturing of the i th cyclic shift of b , $0 \leq i \leq 2^k - 2$. The machine then computes the weight (number of ones) $w(T^i b \oplus a)$ of $T^i b \oplus a$ as i varies from 0 to $2^k - 2$, and also computes the weight of a , $W(a)$. The machine then chooses the word corresponding to the minimum weight as the transmitted word, unless $W(a)$ itself is the lowest, in which case the all-zero word is assumed transmitted.

c. Puncturing methods. Puncturing of the parent 2^{k-1} code is accomplished by different methods in the encoder and decoder. As is well known, the maximal length shift register code of length $2^k - 1$ bits is easily generated from a shift register of length k with the proper linear feedback. The encoder uses such a shift register with a variable clock. When no puncturing is desired, the shift register is clocked with the bit clock. When some of the bits are to be punctured, a high-speed clock is switched in to shift the undesired bits away. One buffer flip-flop on the output removes the undesired bits from the transmitted sequence. The puncture or high-speed clock is 2^k times the rate of the bit clock so that any number of bits may be punctured between two bit clocks.

In the decoder, the puncturing is accommodated by the calculation of the $(T^i b)_l$, the l th bit of $T^i b$. If there were no puncturing involved, the calculation of $T^i b$ would be simple. A shift register yielding the maximal length sequence could run along in synchronism with the received word, generating $(T^i b)_l$, as l varies from 0 to n , the length of the nonpunctured word. A shift of this register with respect to the received word would then allow i to vary from 0 to $2^k - 1$, and thus finish the decoding process. When puncturing is involved, however, this technique has to be changed. It would be possible to use a decoding scheme similar to the puncturing of the encoder, i.e., to shift the punctured bits of the maximal length sequence away while holding the data word fixed. This method, while economical from the hardware point of view, is extravagant in that the time used to decode a punctured word is exactly the same as for an unpunctured word. The method to be used in the constructed device uses hardware rather than time to calculate the $(T^i b)_l$. This trade off results in a decoding time which is directly proportional to the length of the punctured word.

d. The trade off. When a code word a of length $n < 2^k - 1$ is circulating in the input register, it is necessary to match the i th component of a with the $\phi(i)$ th component of the parent word, where $\phi(i)$ is a function which will be known for each puncturing. For example, in a certain (60,6) code, the 7th, 8th and 13th components of the (63,6) code have been punctured so that the $i = 7$ th component of the punctured word is the $\phi(i) = 9$ th component of the unpunctured code word. This same reasoning applies to every word in the dictionary. That is, no matter what the puncturing is, there are still $2^k - 1 = 63$ words in the dictionary, and each is simply the mapping of the (63,6) dictionary onto the $(n,6)$ dictionary by a deletion of exactly the same coordinates of the parent code word.

The parent (63,6) code is generated with a 6-bit K-register with a modulo 2 feedback of its last two positions. Thus, the recursion relation for terms in this sequence is $b_n = b_{n-5} \oplus b_{n-6}$ (for example, $b_{12} = b_7 \oplus b_6$). But since $b_7 = b_2 \oplus b_1$ and $b_6 = b_1 \oplus b_0$, the recursion implies $b_{12} = b_7 \oplus b_6 = b_2 \oplus b_1 \oplus b_1 \oplus b_0 = b_2 \oplus b_0$. This last step is possible because $b_1 \oplus b_1 = 0$. Similarly, every term in the sequence can be written as a linear combination of the six generators b_0 through b_5 . Thus

$$b_n = c_0^{(n)} b_0 \oplus c_1^{(n)} b_1 \oplus c_2^{(n)} b_2 \oplus c_3^{(n)} b_3 \oplus c_4^{(n)} b_4 \oplus c_5^{(n)} b_5 \\ = C^{(n)} \cdot B$$

say, for all n and some set of constants c_i . The conclusion is that any b_n can be calculated using the same set of six generators b_i , $0 \leq i \leq 5$, anding them with the proper $c_i^{(n)}$, and then sending the result to a circuit which generates the modulo 2 sum of six variables.

These $c_i^{(n)}$'s are very easy to calculate, for it can be proved (SPS 37-20, Vol. IV, pp. 104-105) that the $c_i^{(n)}$, i fixed, obey the same recursion formula as do the terms in the original maximal length sequence, i.e.,

$$c_i^{(n)} = c_i^{(n-5)} \oplus c_i^{(n-6)}, \quad 0 \leq i \leq 5.$$

The problem of generating the $\phi(i)$ th component of $T^i b$ is now seen to reduce to the problem of generating the set of $C[\phi(i)]$ in the proper order. These are generated by the program counter, an easily programmed device that will count through any specified sequence of vectors.

e. Completion of the basic system. The basic coder-decoder has been completed and checked out in this reporting period. The maximum usable system clock is

approximately 1.5 Mc rather than the anticipated 2 Mc. The discrepancy can be traced to a race condition in the programmable counter (which uses five levels of logic) due to a low threshold value at the *nand* gate input. This problem has been corrected in the new design of the Division 33 standard modules.

Since very little is known about the correct decoding of messages which contain more than the guaranteed number of correctable errors, the machine has already proved itself useful. While the (63,6) code is guaranteed to correct all patterns of 15 errors, the machine has demonstrated that most random error patterns of up to 22 errors are capable of being corrected.

G. Combinatorial Communication Research

1. Character and Synchronization Correction for DSN Teletype

In previous issues of SPS the necessary steps involved in developing a reliable communications system for transmission of teletype messages over existing circuits have been discussed. The first step is to determine the error characteristics of the circuits to be used. Described in SPS 37-31, Vol. III, pp. 76-78; 37-34, Vol. III, pp. 64-68; and 37-36, Vol. III, p. 66, were the tests that were performed on the circuits to yield such information as bit and symbol error rates, burst error statistics and synchronization error rates. With these data, the implementation of a code for reliable communication is in order. This report will discuss the format of the code, its error correction capacities, and plans for implementation.

a. Code for reliable transmission of teletype characters. Data gathered in tests of the NASCOM circuits gave the information necessary for the selection of a code. The most important worst-case statistics (10^{-2} character error rate; 10^{-4} synchronization error rate; absences of burst character errors) led to a modified Reed-Solomon code which was a (15,9) code (over a 16-symbol alphabet consisting of the 16-element field) having 9 information symbols and 6 check symbols. This code was modified in three ways. First, the code was shortened to a (14,8) code and an extra symbol attached at the front of every code word to act as a synchronization symbol to determine word-by-word synchronization in a message sequence; this guards against insertion and deletion errors.

Second, since the Reed-Solomon code was only 4 levels of the 5-level capability of the teletype character, the remaining level was chosen to act as an (even) parity check on the other 4 levels. (Even parity is required so that teletype machines at foreign relay points will have proper "carriage return" and "line feed".) Third, as a further guard against mistaken identity between code words in the event of a synchronization (insertion or deletion) error, a permutation of the symbols of the encoded word is performed, which moves the synchronization symbol to the center of the code word. Why this permutation is necessary and its effect will be discussed in the section on code evaluation.

b. Encoding of the code word. The first 4 levels of the synchronization symbol *s*, and the 8 (4-bit) information symbols are elements of the field of 2^4 elements, $[GF(2^4)]$. By the use of a polynomial of degree 9, the information symbols are used to compute the next 6 symbols of the code word. These symbols are checks on the first 9 symbols and together with the first 9 symbols form a word length 15 in a certain cyclic code. Each of these 15 symbols is composed of 4 binary bits. A fifth even parity bit is added to each of the symbols. Then before transmission the permutation (81234567) is performed, thereby placing the sync symbol, which had been the first symbol, into the middle position of the code word. The word is then ready for transmission. This encoding is to be performed on a SDS-910 computer in less than 3 msec.

c. Decoding of the code word. The decoding procedure is partially the inverse of encoding, and in the absence of error the inverse can be taken directly. The presence of errors corrupting the code word makes the encoding of symbols necessary and the decoding of the message sequence difficult. However, the decoding is possible in real time, making use of a stored program in the SDS-910 communications processor machine. The decoding operation requires on the order of 0.05 sec. This is small in comparison with the 2.5-sec transmission time of a code word. Thus, real time decoding is feasible.

Actual operation of the decoder proceeds in the following way: Upon receipt of a message word, a first test for synchronization is made. If any synchronization errors have taken place, a request for retransmission of the message word is activated on a return channel. The system will continue in this mode until synchronization has been reestablished. If no synchronization error has occurred, the permutation (23456781) cycles the synchronization symbol around to the beginning and then

the actual algebraic decoding procedure (outlined in SPS 37-26, Vol. IV, pp. 223-225; 37-27, Vol. IV, pp. 190-193) takes place. If more errors occur than the program will correct, a request for retransmission of the word is activated.

d. Evaluation of code performance. The code chosen for transmission has a minimum distance 7. Thus, in the absence of a synchronization error, the code could correct all triple errors. However, for reasons of low error probability, as well as for decoding simplicity, only single errors will be corrected. Then all combinations of up to five errors are detected and retransmission requested.

The necessity of having the permutation to place the sync symbol in the middle of the word will be discussed. If the sync symbol is placed at the beginning of the word and is deleted, then all symbols from that point to the end of the word will be in error unless for the i th position the transmitted symbol $S_i = S_{i+1}$. Therefore, a single sync error could result in up to 14 symbol errors. There is only distance 7 between code words, so a sync error of this type would not necessarily be detected. If the sync symbol is positioned in the middle of the word, the greatest number of symbols that could be affected by a deletion is 7. This greatly enhances the chances for correct transmission. Hence the choice of the middle position for the sync symbol.

H. Venus Station Operations

1. Experimental Activities

The major activities (summarized in Table 3) at Venus Station during this reporting period were S-band planetary radar experiments and *Mariner Mars 1964* experimental tracking.

a. Planetary radar. Experiments carried out with the S-band planetary radar system were open-loop ranging and total spectrum on Venus and total spectrum on Jupiter. The ranging data indicate that the actual round trip range to Venus was less than predicted, although moving into agreement with the prediction. For example, on December 13, 1965, the planet was 5.567 msec closer in round trip range than the prediction, compared with approximately 6.6 msec 6 wk earlier.

Table 3. Summary of Venus Station experimental activity (October 14-December 12, 1965)

Activity	Hours	Percent
Primary experiment		
Planetary radar (Venus)	373	25.9
Planetary radar (Jupiter)	131	9.0
Mariner experiment		
Transmission, reception, and testing (includes time required to change Cassegrain feed cones)	81	5.6
Testing, calibration, construction, scheduled maintenance, and nontarget time	808	56.2
Holidays and scheduled nonoperating time	48	3.3
Total	1440	100.0

b. Mariner Mars 1964. October 31, 1965, the R&D Cassegrain feed cone was removed from the 85-ft antenna and the *Mariner Mars 1964* cone was installed. November 1, an attempt was made to receive the signals still being radiated by *Mariner IV* via its omnidirectional antenna. Since the expected signal strengths were below the threshold of the S-band receiver, the 9-channel auto-correlator and other signal processing equipment normally used for planetary radar work were employed. Initially, no signals were received within the 480 Hz bandwidth being examined. The programmed local oscillator was then offset 342.2 Hz (at S-band) and the spacecraft carrier and two sidebands were received. Fig. 16 is the resulting plot of signal power versus frequency, with the nominal carrier frequency in the center of the plot; although, as can be seen, the carrier is not centered on the spectrum plot. This noncentering is a result of the programmed local oscillator not being offset far enough. Analysis indicates that the carrier frequency radiated by the spacecraft was actually 350 ± 0.5 Hz different from the predicted frequency. Total signal power within the spectrum slot being scanned was measured to be -175.83 dbm while the carrier power was measured to be -178.05 dbm. November 1, the *Mariner* cone was removed from the 85-ft antenna and

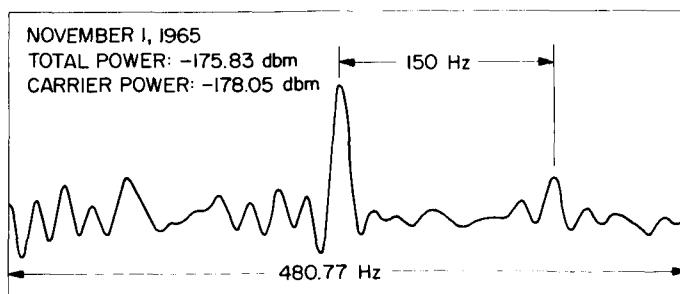


Fig. 16. Power spectrum from Mariner IV

the R&D cone reinstalled in time to track Venus again on November 2.

This process was repeated at the end of November, with *Mariner IV* again being successfully received December 1, with similar results, although the total received signal power was measured to be only -178.10 dbm. (The spacecraft was approximately 343,000,000 km away at the time.)

c. Radio star coordinates. Discrete radio sources are frequently used when checking antennas for pointing accuracy. In the past, determination of the coordinates of desired radio sources involved tedious and laborious hand calculations. In addition, published data on the basic coordinates of these sources revealed appreciable differences between various investigators. Accordingly, a long-term program has been initiated to determine the optimum coordinates for a group of suitable sources in terms of the Venus 85-ft diameter antenna.

Since Venus Station time is devoted primarily to equipment development and planetary radar experiments, many months will necessarily elapse before any meaningful results are obtained. However, the program will have the following objectives:

- (1) Acquire information on basic radio source coordinates as obtained by various investigators.
- (2) Determine which of these coordinates are most accurate in terms of the Venus Station antennas by using them to star track and by comparing results.
- (3) Keep a central file of star tracking data on standard forms for future reference.
- (4) Make radio source coordinates available for use by other DSIF stations.

There are now in existence at the Venus Station two computer programs (based on different methods) which permit the calculation of source coordinates, thereby eliminating the former laborious hand calculations. The first of these programs produces radio source coordinates for the first of every month for a full year; the second program produces coordinates for any particular date desired. The second program, however, requires a greater input of information and is therefore most difficult to work with. It is hoped that these efforts will eventually result in data useful to the DSIF stations, as well as to others.

2. Subsystem Performance

a. 100-kw transmitter (operation). During this reporting period, the R&D transmitter was being reworked to accommodate the new 100-kw klystron and magnet. This amplifier is now being used for acceptance testing of the new klystron tubes. A total of 50.6 filament hr and 15.0 beam hr has been accumulated on the first of the new tubes.

Mariner amplifier 1 was installed in the R&D cone with R&D S/N 3 VA858 klystron and has operated for a total of 820.8 filament hr and 499.5 beam hr.

The total off time due to failures was 12 hr, 25 min for the R&D transmitter and associated system. The major portion of this lost time was due to a failure of the high-voltage vacuum switch in the input to the high-voltage rectifier transformer; other contributors were relay failures, high-voltage cable breakdown, and reflected power coupler variations.

b. *Mariner* 100-kw transmitter. The *Mariner* transmitter amplifier 2 has operated, for testing purposes, 47.7 filament hr and 23.7 beam hr with no failures.

c. Mod IV receiver. Operation of the Mod IV receiver has been normal with no lost time due to equipment failure. The modification to permit closed-loop operation at 2388 MHz has been completed. This modification allows operation with a 2-Hz loop bandwidth and a further choice of 4- and 8-Hz bandwidths. The receiver has been used in this mode in a recent closed-loop experiment with the planet Venus. Appropriate receiver outputs have been provided for doppler recording. The Mod IV receiver, in conjunction with the *Mariner* subsystem equipment, was also used in the successful reception of signals from *Mariner IV*. The receiver open-loop mode was utilized in this operation. More modifications to the receiver are under way to simplify operation and improve performance.

X-band portion. The X-band receiver was used during this period for the calibration and leakage measurement of the X-band signal generator. The AM and ranging channels of the X-band receiver are being used in the S-band planetary experiments. This is accomplished by cross-cabling the 30-MHz signal input from the S-band system into the X-band system.

S-band portion. The Resdel signal generator has been reinstalled in the R&D cone and checked for proper operation. The "top hat" meter panel on the receiver was removed and returned to JPL for modification. A temporary

instrument panel, monitoring crystal current, dynamic phase error, and the receiver in-lock indication are now in use. The main VCO acquisition power supply has been mounted in the receiver control cabinet to facilitate receiver operation in the closed-loop mode.

d. Programmed local oscillator (PLO).

Digital portion. Three failures occurred, one of which involved a digital card malfunction. All failures have been repaired, and the system operation is normal.

Radio frequency portion. The divide-by-75 module was found to lack sufficient bandwidth to operate at both the frequency required for the Venus experiments and for *Mariner* track, PLO assisted mode. A new divide-by-75 module is under development at JPL. A prototype of this unit was used successfully during the last *Mariner* track.

e. Central frequency synthesizer (CFS). Installation of the rubidium frequency standard standby batteries has been completed. The batteries, a lead-acid type, were installed in a protective housing outside the station control room for proper ventilation. Evaluation of the charging requirement and the discharge capacity is under way. The 35.2-MHz synthesizer module was returned to JPL for modification. Removal of this module affects the system operation only at X-band frequencies.

3. System Improvements

a. R&D transmitter. A new R&D exciter (2388 MHz) was installed in the cone, and new modules were installed on the cold plate in the control room portion of the exciter. The system was checked out and is now in operation. The filter capacitors in the crowbar for the high-voltage (50 kv) power supply were changed from six 30-kv units to a single 60-kv unit.

b. Digital equipment

Mod III stored program controller (SPC).

Mod III SPC has been overhauled and updated. During a short shutdown prior to the start of Venus tracking, several harness and cabling assemblies were replaced and terminal blocks relocated. This substantially reduced chafing and strain on taper pin blocks, and snagging of cables during withdrawal of computer mainframes. This project is approximately 25% complete; work will continue as schedules permit.

An extensive rework of input-output (I/O) structure was initiated. Major recabling and logic reallocation were

accomplished during shutdown; detailed wiring and logic work were carried forward as tracking permitted and are now complete.

New high-speed pseudonoise (PN) coders of extended code length were installed as a subsystem in Mod III SPC, and necessary logical and electrical interfaces were fabricated and installed. The resulting composite slow-fast PN coders now available for programming are described on p. 53. As a facet of this installation, new logical gating was wired in to permit software selection of various output modes from the composite coders. This will be necessary soon for the selective excitation of analog-digital modulators in receivers-transmitters for S- and X-band. This work is substantially complete. In addition, similar selective logic is being assembled for the sync-and-shift drive to the new composite 9-15 channel correlators.

During the shutdown period, power was removed from Mod III SPC logic for approximately 24 hr, the longest off-line period in more than a year. Upon repowering, logic card failures occurred in excessive numbers and continued for 2 wk.

Mod III stored program controller I/O revision.

Mod III SPC was originally installed at Venus Station as a close duplicate of its predecessor, Mod II SPC (SPS 37-21, Vol. III, pp. 63-76). Predictably, differences in application and usage have created differences in machine structure. The most recent change involved a moderate reworking of the input-output subframe of Mod III.

Both input and output systems were originally formed to incorporate three categories: words, internal signals, and external signals. Sufficient numbers of each were provided to cover expected needs. More than 2 yr of field application have resulted in the following usage ratios:

Input words	12%
Input internal signals	50%
Input external signals	0%
Output words	85%
Output internal signals	93%
Output external signals	30%

Since the mainframe of Mod III is tightly packed and has no room for expansion, input capacity was cut down to provide the increase in output capability. Table 4 provides before-and-after comparisons.

Table 4. Mod III SPC I/O specifications

Category	Before	After	Current octal address range
Input			
(1) Words	128	64	20200-20277
(2) Internal signals	128	128	21000-21177
(3) External signals	64	64	21200-21277
Output			
(1) Words	32	48	22200-22257
(2) Internal signals	64	96	23000-23137
(3) External signals	64	64	23200-23277
(4) Heavy relays	—	16	23300-23317

It was found that a need existed for category (4) outputs (Table 4), which accordingly were implemented. These relays have their own selection logic with a new class of address; the relays handle 125 v at 10 amp per contact; the DPDT contacts are wired to fan-out barrier strips to provide quick on-demand connections. Care was taken to isolate grounds and to separate logic signals; there has been no adverse effect on computer operation at this time.

Octal address ranges are now listed in Table 4. I/O address assignments are kept current; copies of "Mod III Address Book" are available from the Goldstone Venus Station.

High-speed ranging coder subsystem

Planetary ranging and range-gated mapping experiments have been carried on at Venus Station by means of a PN code subsystem installed within Mod III stored program controller (SPC). For the lunar target, this had been supplemented by a simple subsystem fabricated on-site, having a fixed digit period of 1 μ sec and a code length of 16,383 bits from a shift register coder of 14 stages. The latter has just been replaced by a new subsystem with flexibility comparable to the planetary coders and with speed and code length equivalent to that of the lunar coders. Digit period length can now be varied smoothly from 0.5 to 125 μ sec, comfortably overlapping the planetary coder minimum of 50 μ sec.

The two coders are linked not alone by common control from, and housing within, Mod III SPC but also by sharing a common unit shift register (USR) and number-controlled oscillator (NCO). Consequently, together they form a composite coder capable of slow or fast, long or short, PN code generation as needed. Since their intended uses are no longer specific, they hereafter will be referred to as the "slow coders" and the "fast coders."

Coder operation. Fig. 17 is a simple block diagram (sufficient for an applications understanding) of the fast coders. Previous publications covering Mod III SPC (SPS 37-21, Vol. III, pp. 63-76) and planetary coder subsystem (SPS 37-27, Vol. III, pp. 70-79) explain the interfaces shown.

The Mod III SPC internal clock (1 MHz) is multiplied, shaped, and delayed to provide coherent 8-MHz clocking to the fast coders. Divided by 4, this clock gives the coder its minimum digit period of 0.5 μ sec, shiftable in either direction in increments of 0.125 μ sec. This is accomplished by storing a true (right shift) or a 2's complement (left shift) number in address 22230, precisely as is done in the case of the slow coders. Operation of the range rate number-controlled oscillator also proceeds as for the slow coders. The basic unit shift for the slow coders is a μ sec increment; for the fast coders, the basic unit shift is a 0.125- μ sec increment.

By storing a positive number of up to 8 binary bits in address 22234 the basic digit period is forced to count down the contents of the digit period counters until the payoff puts a shift pulse into the coder shift registers. If the digit period register contains a zero the payoff occurs each 0.5 μ sec; if a one, each 1.0 μ sec; if a two, each 1.5 μ sec; etc.

By storing a sign-and-magnitude number of up to 15 binary bits (plus sign bit) in address 22237, the receiver coder can be forced either left or right an amount in digit periods equal to the number stored. This occurs each time the displacement register is dumped into the displacement counter. Note that this offset happens only on the command PSE 23032 and that different numbers may be loaded into 22237 before each command, if desired.

SYNC, RESET and HOLD, and START coder commands are executed exactly as for the slow coders. When 23037 is SET, outputs are inhibited and coder shift registers are emptied; RSE 23037 holds them in this state until PSE 23036 is given, when both coder shift registers start together and in phase.

The coder shift registers are of 15 stages, generate a code 32,767 digit periods in length. Drive to the appropriate modulators is taken from stage 6, again exactly as in the slow coders.

Counter. Fast coder offset may be counted in the slow coder counter, to a least-bit accuracy of 1 μ sec, exactly

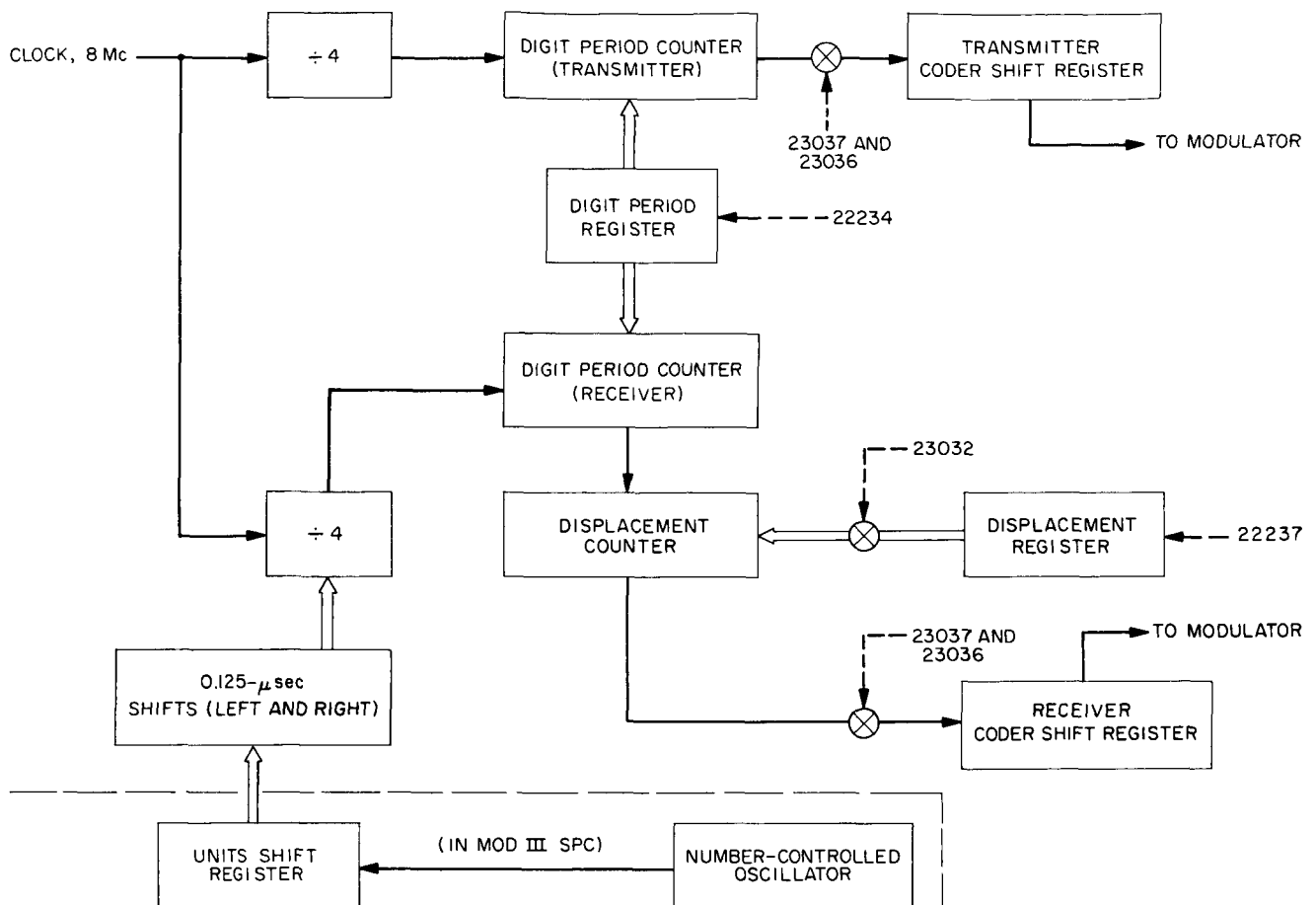


Fig. 17. Block diagram of fast coders

as for the slow coders, providing that the input gating is selected properly. To prepare the counter to count fast coder offset, the following command sequence is used:

- (1) RSE 23033, 23034, 23035
- (2) SET 23033
- (3) PSE 23034
- (4) RSE 23033

Mod III instructions. To select slow coders for use, SET 23037; to select fast coders, RSE 23037. This addressing insures that only one set of coders can be enabled at one time.

Equipment. The fast coders described are composed of three logic frames of Decisional Control Associates, Inc., "Versalogic" digital modules. The module types employed (GA-34, FF-32, FF-34, and PA-34) use germanium solid-state devices and operate at speeds up to 8-MHz.

4. Station Improvements

Larger cone weights require shorter crane operating radii if continued use is to be made of the existing Goldstone crane (a 35-ton rated, P&H-555-TC). A series of aerial photographs of the 85-ft antenna and vicinity indicates that to obtain shorter radii the present crane pad will have to be extended by approximately 15 ft. Plant Services has been requested to design and arrange for the fabrication of this extension.

V. Tracking Stations Engineering and Operations

A. Goldstone Operations

The *Pioneer PN-6* spacecraft was launched from Cape Kennedy in the early morning of December 16, 1965. Echo Station first acquired the spacecraft at 20:03:20 GMT the same day. Concurrently, the rescheduling of the *Surveyor* Project enabled personnel at the Pioneer Station to move the S-band system from the annex building into a permanent location in the east wing of the control building.

1. Pioneer PN-6 Project

Through November and until the *Pioneer* launch on December 16, 1965, Echo Station personnel were engaged in final testing of all interfaces between the *Pioneer* ground operational equipment and the Station S-band system. Preparation for the *Pioneer* mission was continuous since April 1965 (SPS 37-33, Vol. III, p. 7 through SPS 37-36, Vol. III, p. 9).

Prior to the launch, Echo Station personnel participated in three operational readiness tests with the space flight operations facility at JPL. The Station was operationally ready for the start of the mission.

Forty-eight hours prior to the launch, the closed cycle refrigerator of the traveling wave maser equipment gave

indications of low capacity. As backup protection, the Pioneer Station maser refrigerator was brought to the Echo Station, cooled down, and held in readiness. In addition, the antenna mounted parametric amplifier, and the Echo Station spare, were tuned and readied. The Echo Station maser refrigerator was removed from the antenna, cleaned of any possible contaminants and a new refrigerator crosshead was then installed. After replacing the maser refrigerator on the antenna, it was cooled down, given a stability test, and accepted. There was no further difficulty.

The first view period began with acquisition of the spacecraft at 20:03:20 GMT, December 16, 1965, and ended at 06:52:50 GMT, December 17, 1965. Eleven commands were successfully transmitted to the spacecraft from the Echo Station. A practice transfer was made with DSIF-42, Tidbinbilla, Australia, at 03:00:14 GMT, and from Tidbinbilla to the Echo Station at 04:46:50 GMT. No difficulty was experienced in either transfer procedure.

The second view period began with the spacecraft acquisition at 20:08:10 GMT, December 17, 1965, and ended at 07:04:12 GMT, December 18, 1965. The Type II orientation was performed during this period to align the spacecraft high gain antenna with the Earth. Prior to command transmissions, spacecraft control was transferred

from JPL to the Echo Station at 21:20:00 GMT. A total of 198 commands were transmitted from the Echo Station to the spacecraft between 21:28:00 and 04:18:00 GMT. Spacecraft control was retransferred to JPL at 04:24:20.

After successfully completing the spacecraft orientation, the Echo Station began a daily tracking schedule.

2. Lunar Orbiter

Concurrent with preparation for, and subsequent tracking of, the *Pioneer* spacecraft, Echo Station personnel continued operational testing and interface testing of the *Lunar Orbiter* ground equipment. As the prime station at Goldstone for both *Lunar Orbiter* and the *Pioneer* space probes, the Echo Station is being readied to provide simultaneous coverage for both missions. This is being accomplished by a transfer rack assembly enabling a rapid changeover between the S-band system and either the *Lunar Orbiter* or the *Pioneer* ground equipment.

On December 14, 1965, the *Lunar Orbiter* test model spacecraft was delivered to Goldstone and installed in the spacecraft test facility shieldroom (Fig. 1). Using microwave link antennas mounted on the roof of the shieldroom, and passive reflector antennas mounted on a hill west of the Echo Station and in the view range of the 85-ft antenna, full system operational tests will be performed. These tests will exercise the normal operation compatibility between the spacecraft electronics and the ground environment at simulated space distances.

3. Surveyor Project

With the rescheduling of the *Surveyor* launch, personnel of the Hughes Aircraft Company are continuing with subsystem tests and assisting in S-band interface and compatibility testing with the S-band system.

During the last week in October and the first week in November, the *Pioneer* Station S-band system was removed from the annex and moved into the east wing of the control building. Originally installed in the annex for testing (SPS 37-27, Vol. III, pp. 5-11), the S-band system remained there for the launch and subsequent tracking of *Mariner IV*.

The installation in its permanent location (Fig. 2) enables the S-band system to assume a standard DSIF configuration. As with the other DSIF installation, a full basement under the control room provides for easy

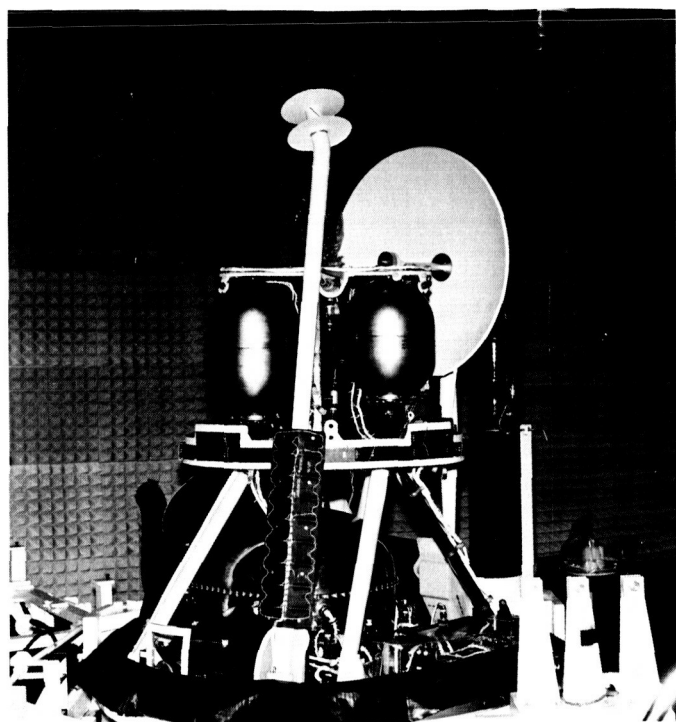


Fig. 1. *Lunar Orbiter* test model in spacecraft test facility shieldroom

access to all rack interconnecting cables, and use of the cable tunnel for control, signal, and power cables to the hydro-mechanical building and the 85-ft antenna.

The permanent location of the S-band system is adjacent to the room containing the *Surveyor* ground control equipment, an arrangement that materially reduces the former long cable runs between the two equipments, and also provides for a higher order of equipment compatibility and easier coordination among personnel.

Currently, system compatibility tests are being performed as a postlude to the S-band move and reinstallation. Full operational and net integration testing is scheduled for early 1966.

4. Mars Station Activities

Digital instrumentation equipment was installed in the control room on the second floor of the pedestal (Fig. 3) of the 210-ft antenna at the Mars Station, DSIF-14. Operational and program testing is in progress. The frequency and timing subsystem was also installed and is in operation. DSIF-14 operations personnel are continuing servo training and maintenance training on the 210-ft antenna, conducted by Rohr Corporation personnel.



Fig. 2. Pioneer Station S-band permanent installation

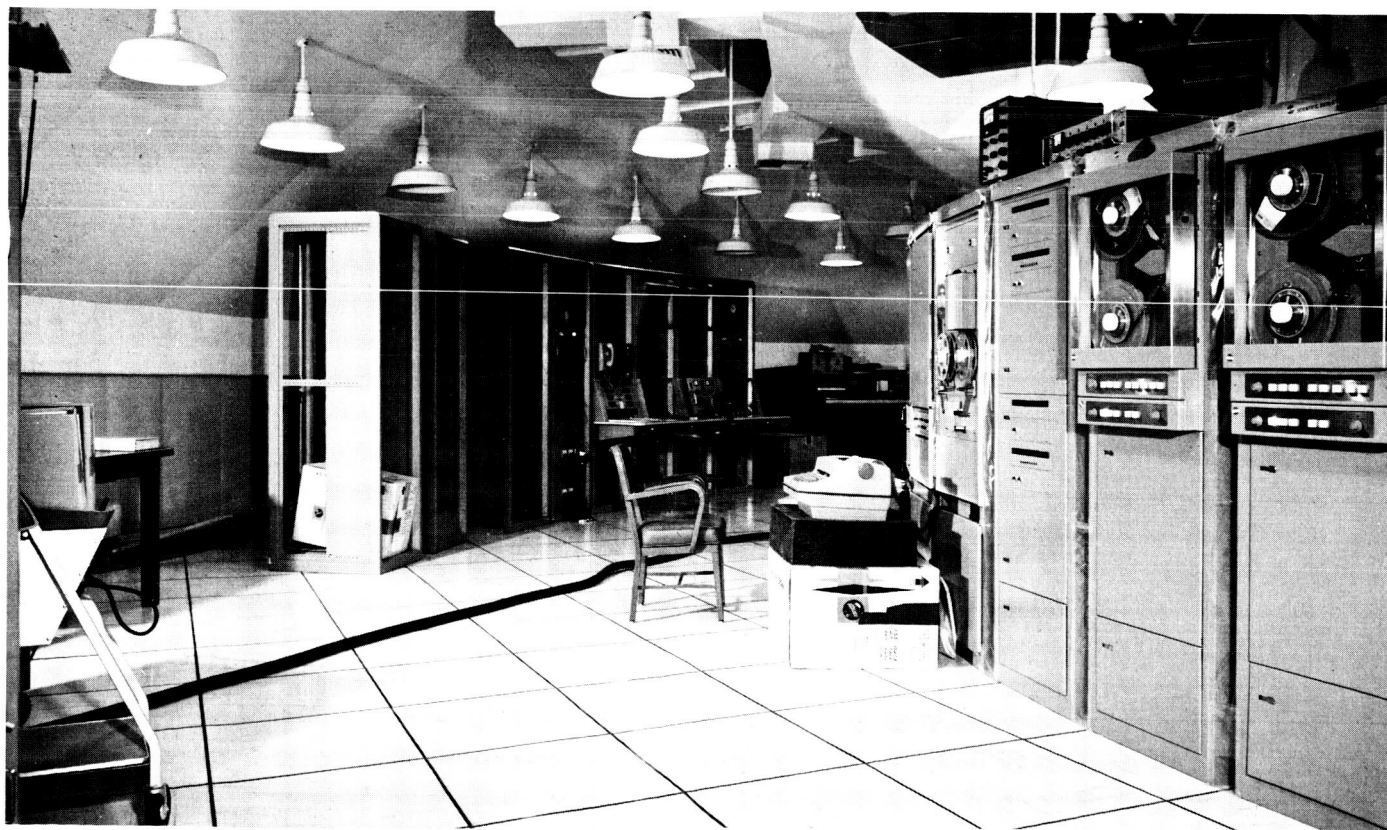


Fig. 3. Mars Station digital instrumentation equipment installation

5. Construction

a. Spacecraft Test Facility. The shieldroom wall and ceiling have been covered with impregnated styrofoam, anechoic material, and the floor with a smooth sectional floor covering of a similar meshing material. Approximately 40-db attenuation of wall-reflected RF is provided by the covering. Fig. 1, illustrating the *Lunar Orbiter* test spacecraft, also illustrates the floor and wall covering.

b. Mars Station. The two wing-additions to the generator building are completed and are ready for additional generator units.



Fig. 4. Example of 25, 50 and 70% porosity aluminum reflector sheets. (Technician is removing mesh screws)

B. Antenna Dish Resurfacing at Woomera

The original reflector surface of the 85-ft tracking antenna at Woomera, Australia, was recently removed

and replaced with one of better performance. The expanded aluminum mesh of the original surface had a porosity of about 70% (that is, the fraction of surface

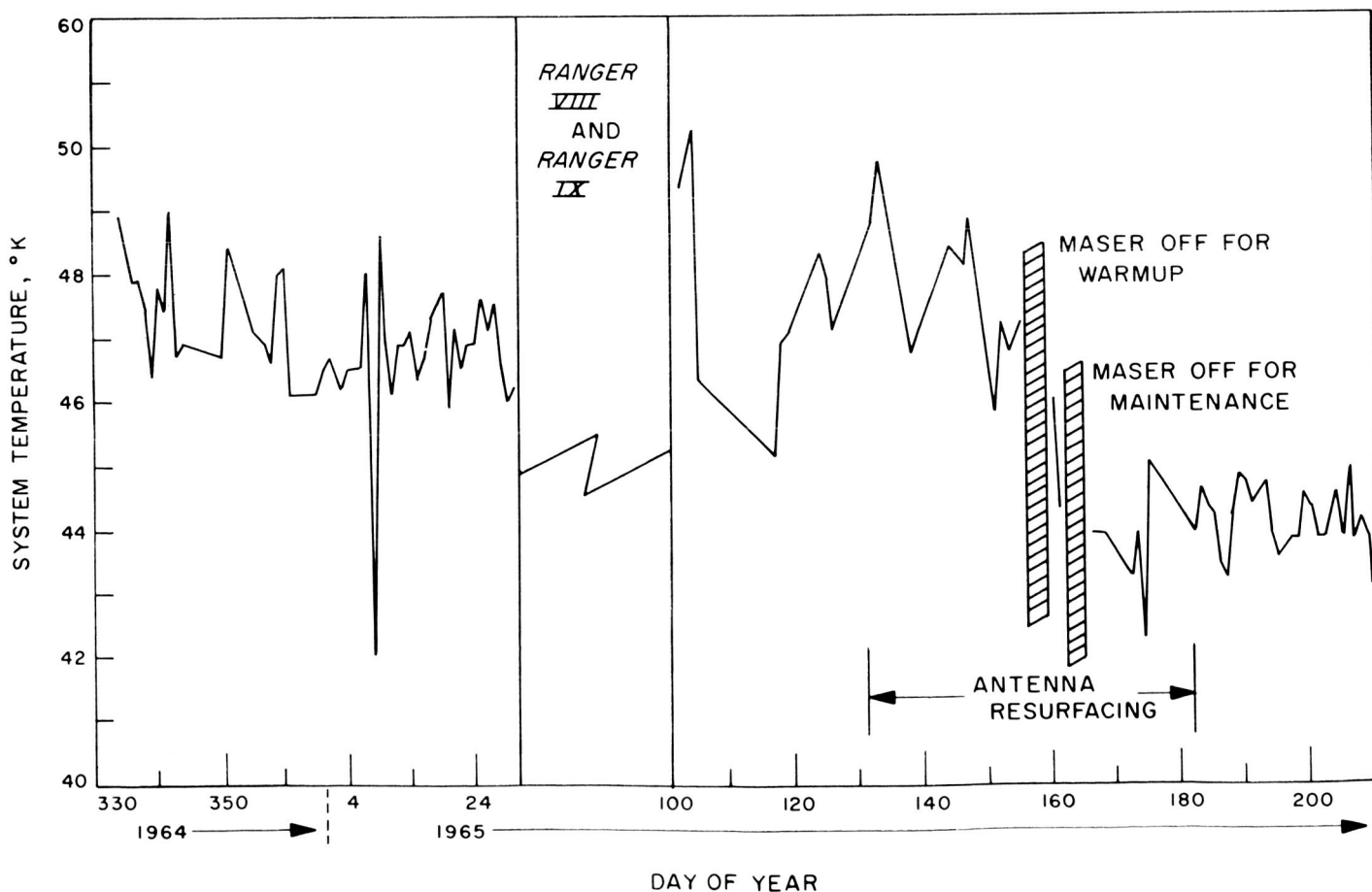


Fig. 5. System temperature vs day of year

not covered by metal). The new surface consists of aluminum sheets having 25% porosity, 0.080-in. thick, for the inner two-thirds of the area, and 50% porosity, 0.080-in. thick, for the two outer "rings". Examples of the three types of sheets may be seen in Fig. 4.

Work was performed by all available personnel during nontracking periods. (At this time about half of the Station personnel were at Goldstone for S-band equipment checkout.) The screws holding the mesh were loosened with long-handled screwdrivers, or with screwdrivers and ratchet attachments, and then removed with power tools or chisels. The replacement sheets were secured with self-tapping screws at about 6-in. centers, inserted by hand and tightened with power tools. About 35,000 screws were removed and 17,000 screws were inserted to secure the 224 new panels.

The improvement in system performance is first shown by a decrease in system temperature (Fig. 5) of about 4°K, and then by an increase in gain of approximately 0.6 db. This can be clearly seen in the "before" and "after" scans through the radio sources in Cygnus A and the Omega Nebula (Figs. 6 and 7) where, although the cold sky reading is colder, the peak of the radio source observation (representing a constant source plus the cold sky value) is higher. The total system temperature is now about 44°K, and aperture efficiency is 0.65.

C. Systems Engineering and Integration at Ascension Island

Following the initial integration of the Ascension Island Station (DSIF-72) system components at Goldstone, the equipment was dismantled and packed for overseas shipment. The equipment was transported to Ascension Island in mid-October via two chartered cargo aircraft.

Installation of the equipment and system integration at Ascension Island is progressing; however, several major problems have been encountered. One major problem is that buildings, power, roads, air conditioning, and other facilities were not completed and available for use before equipment installation and testing were attempted. In particular, the building air conditioning system, being not quite completed, prevented the electronic subsystems from being activated for any length of time.

Rusting of practically all outdoor equipment of steel construction, i.e., antenna structures, acquisition aid collimation tower, is another major problem area. Continuous maintenance will be required to prevent equipment deterioration. Samples of dirt from the antenna pedestal and the operations building cooling plenums were sent to JPL for salt content analysis with the resultant values of 0.32% for the antenna sample and 0.15% for the plenum sample. These values of salt concentration are more than sufficient to cause rapid rusting of any unprotected iron or steel at the Station, and its presence is due to the consistent 30-mph winds which carry the salt-laden ocean spray from the coast 1800 ft below.

Similarly, the physical location of the Station on the island creates a unique environmental condition. Clouds,

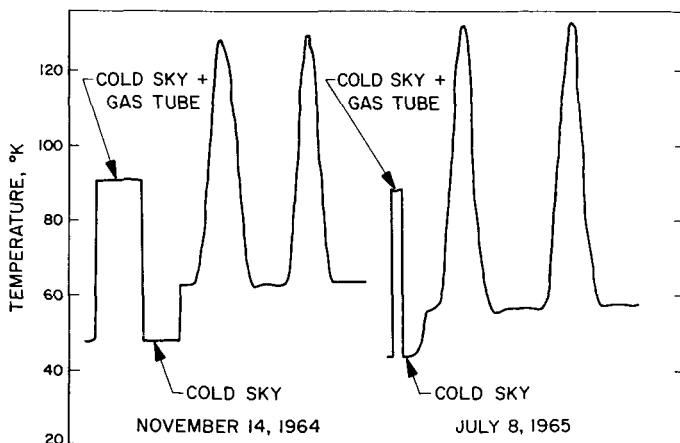


Fig. 6. Cygnus A scans

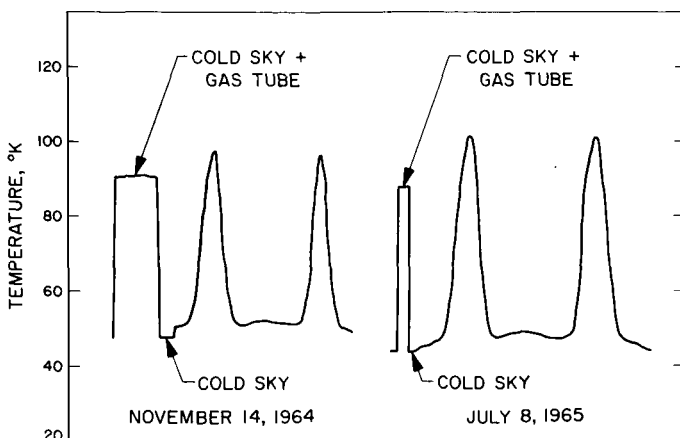


Fig. 7. Omega Nebula scans

at or below the Station elevation, are raised by the winds over the 3000-ft mountain located behind the Station, and swept across the Station itself. This results in dense fog 30 to 40% of the time. Furthermore, clouds above the Station level are cooled by this action and bring rain to the area several times a day.

D. Aircraft Masking Exercise at Tidbinbilla

1. Introduction

An aircraft masking exercise has been conducted at Tidbinbilla DSIF-42 to determine the effect on spacecraft communications caused by aircraft flying through the line-of-sight beam between the Station tracking antenna and the spacecraft. The purpose of the exercise was to provide quantitative measurements of such effects, if any.

During the July encounter of the *Mariner IV* spacecraft with Mars, precautions were taken to reduce the risk of possible RF interference with spacecraft communications. These precautions included the diversion of flights of the Royal Australian Air Force (RAAF) and civilian aircraft from the near vicinity of the Station during tracking operations. It was believed that aircraft flying near the line-of-sight beam extending between the 85-ft tracking antenna and the spacecraft might cause the loss of valuable telemetry, especially when signal strength would be at a very low level. Only by measuring spacecraft doppler and error signals, using aircraft in controlled flight patterns, was it possible to determine if such interference precautions would be required during future spacecraft tracking missions.

2. Aircraft and Equipment

The aircraft used in the exercise was an RAAF DC3, provided by 34 Squadron, Fairbairn. It was flown by RAAF personnel. The aircraft carried a DSIF-42 transponder/transmitter, tuned to the *Surveyor* spacecraft frequency and operated by a Station technician. Voice communication between the aircraft and the Station was established by means of an RAAF very high frequency (VHF) transmitter/receiver installed in the DSIF-42 communications center.

3. Antenna Alignment Marking

Alignment of the aircraft with the antenna was a critical requirement of the exercise. In order to improve the sighting capabilities of the pilot, the cone of the antenna was fitted with a black "collar" of ¼-in. soft cardboard, shown mounted on the antenna in Fig. 8.

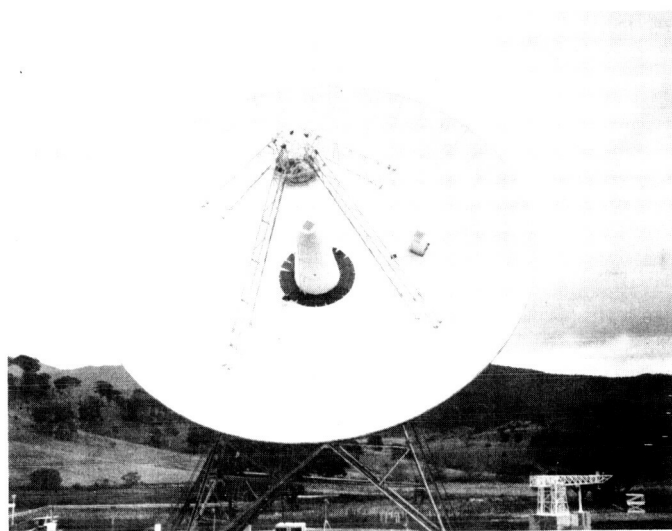


Fig. 8. Antenna with marking collar installed

4. Method

The exercise was designed so that as DSIF-42 tracked *Mariner IV* the aircraft would fly directly towards the antenna and through the center of the beam. This was to be achieved by the pilot's optically aligning the airplane with the black collar and the quadripod tip. When so aligned, the aircraft would then be in a vertical plane containing the antenna and the beam and would pass through the beam during its approach run.

The closeness of the aircraft to the beam was to be measured by error signals generated by the DSIF-42 receiver tuned in to the airborne *Surveyor* transponder frequency. The quality of the run would be checked through use of the optical tracking aid (OTA) and its TV monitor.

5. Exercise Operations

The exercise was originally scheduled for September 7, 1965 but was postponed because of poor weather conditions (low clouds and rain) until September 9th. On this day the weather was still cloudy, but not enough to delay the exercise. Throughout this period DSIF-42 had no commitment to NASA to track *Mariner IV*.

Station equipment was counted down on the evening preceding the exercise in preparation for a normal *Mariner IV* tracking pass. On September 9 the signal from *Mariner IV* was acquired as soon as the spacecraft rose over the eastern horizon, and it was tracked continuously throughout the exercise. The analog and digital instrumentation equipments were also calibrated. Thus, the Station was operationally ready and waiting for the exercise to proceed.

As soon as weather conditions permitted, the DC3 aircraft took off from Fairbairn airfield and flew to the vicinity of Tidbinbilla, where VHF voice communication was established. The transponder on board the aircraft was turned on so that it was transmitting at full power. The aircraft began a series of runs at constant altitude directly approaching and overflying the antenna, with the pilot attempting optically to align the quadripod tip vertically above the black collar surrounding the antenna cone.

During the exercise the aircraft made two series of runs, the first consisting of 11 runs from an easterly direction in the morning, and the second consisting of 13 runs from a northerly direction in the afternoon. The aircraft altitude during any one run was constant, but runs were made during the exercise at heights varying between 1,000 and 3,000 ft above ground level. The afternoon runs were more difficult, from a navigation aspect, than the morning runs. In the afternoon runs the nose of the aircraft obscured the pilot's view of the antenna earlier in the run, because of the higher antenna elevation.

In order to determine the "angle of miss" of the aircraft to the beam, two methods were used. The most direct, although largely qualitative, method was to view the OTA TV screen, which presented a narrow angle view along the optical axis of the antenna. On most runs at least part of the aircraft was sighted, affording an immediate appraisal of the quality of the run.

The second method was to record the signal strength and the hour angle (HA) and the declination (Dec) error channels from Receiver (rcvr) 1, which was tuned to receive the *Surveyor* frequency transmitted by the airborne transponder. This technique prevented the normal error signals from Receiver 2 (tuned to *Mariner* frequency) being available for antenna autotracking of *Mariner*, and the antenna servo system was operated in the aided track mode, using predicted angles.

The Receiver 1 angle error signals (filtered by a 2½-sec lag) were recorded by the analog instrumentation

assembly (AIS) Sanborn pen recorder, as also were the filtered AGC from both receivers and the dynamic AGC from Receiver 2 (through a 0.2-sec filter). From these records it was possible to detect the time at which the airborne transponder passed through the beam (contact) and the minimum angle by which it missed the center of the beam (RF boresight). At the same time, the effect of the aircraft upon Receiver 2 dynamic AGC, filtered AGC, and in/out lock indicator was also determined.

The Station also recorded tracking data handling (TDH) subsystem doppler data and telemetry data as part of its normal *Mariner IV* tracking operation, as well as ½-sec samples by the digital instrumentation assembly (DIS) computer of Receiver 2 dynamic AGC.

The aircraft made 24 runs towards the antenna, 11 of the runs being made in the morning with the antenna azimuth between 085 and 075 deg, and 13 of the runs being made in the afternoon with the antenna azimuth between 358 and 323 deg.

6. Results

Of the 11 morning runs the whole aircraft was sighted in the middle of the TV screen on 2 runs, the aircraft wing was sighted on TV on 2 runs, and the wing tip only was sighted on 2 runs.

Of the 13 afternoon runs the whole aircraft was sighted on the TV screen on 1 run, the aircraft wing was sighted on 5 runs, and the wing tip only was sighted on 3 runs.

Representative analog results for the period of contact during runs on which alignment was sufficient to obtain valid test data (runs 3, 5, 8, 9, 14, 16, 17, 18, 21, and 23) are shown in Fig. 9. Runs on which the aircraft was not in sufficient alignment for valid test evaluation were not recorded. In general, whenever the aircraft was sighted on the OTA TV screen the AIS record of Receiver 1 signal level showed a large increase of about 40 db within a period of about ½ sec. This resulted from the airborne transponder passing close to the center of the beam. At the same time, the Receiver 2 dynamic AGC (*Mariner* signal) indicated a drop in signal strength of up to 5 db (± 1 db), although the Receiver 2 filtered signal level showed no detectable variation to within 1 db. The equivalent Receiver 1 angle errors were small (less than 0.040 deg) whenever the TV screen showed a good run.

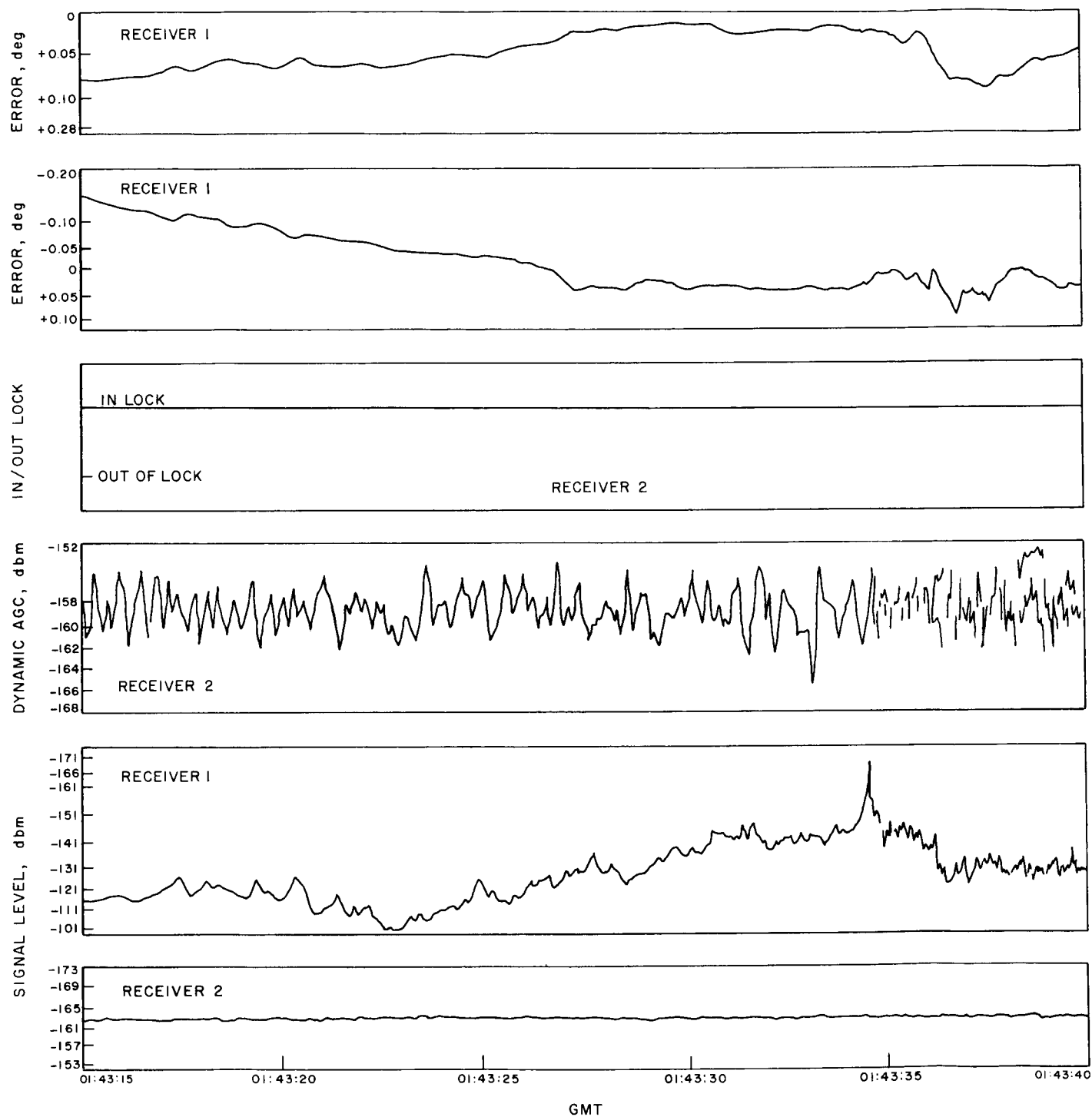


Fig. 9. Representative analog results of valid test runs

On only one run (Run 5, with an antenna elevation of 37 deg) did Receiver 2 drop lock on the *Mariner IV* signal, and then only for 0.3 sec. This run was the first

of three in which the whole aircraft was sighted on the TV screen, but there was no indication that the telemetry demodulator dropped synchronization lock.

The TDH record of nondestructive doppler count showed that the 1-sec doppler count was steady throughout every run. The TDH record for Run 5 is presented in Table 1. It may be noted that the noncumulative doppler count is steady, except for a slight increasing trend caused by motion of the spacecraft.

The DIS record of Receiver 2 dynamic AGC suffered from the disadvantage of a fixed $\frac{1}{2}$ -sec sampling interval. However, these records are consistent with the AIS records of the same quantity, and indicate that the masking effect of the aircraft could result in a drop in received signal strength of up to 7 db.

Data resulting from the different runs are listed in Table 2.

7. Summary

The following is a summary of results of the exercise:

- (1) A part of the aircraft was sighted on the TV screen in 15 of the 24 runs attempted.
- (2) On 5 of the runs the aircraft passed within 0.01 deg of the center of the beam.
- (3) On only one run did the *Mariner IV* receiver drop out of lock, and then only for 0.3 sec.
- (4) On no run did the telemetry demodulator drop synchronization lock.
- (5) On no run did the doppler count show any significant variation arising from the masking effect of the aircraft.
- (6) When the aircraft passed through the center of the beam the drop in *Mariner IV* signal strength was about 5 db.

8. Conclusion

It is concluded that the passing of the DC3 aircraft through the beam and the associated masking of the received *Mariner IV* signal did not significantly affect the capability of DSIF-42 to receive full tracking and telemetry data from the spacecraft.

Table 1. TDH record, Run 5

Event	Day	GMT	Doppler	HA	Dec	Non-Accumulative doppler
	252	01:52:34	6982013381	305674	345628	
	252	01:52:35	6984383742	305678	345628	
	252	01:52:36	6986754102	305680	345628	
	252	01:52:37	6989124463	305684	345628	
	252	01:52:38	6991494825	305690	345628	
	252	01:52:39	6993865186	305694	345628	
	252	01:52:40	6996235547	305798	345628	
	252	01:52:41	6998605909	305702	345628	
	252	01:52:42	7000976271	305706	345628	
	252	01:52:43	7003346633	305710	345628	
	252	01:52:44	7005716995	305714	345628	
	252	01:52:45	7008087359	305718	345628	
	252	01:52:46	7010457721	305722	345628	
	252	01:52:47	7012828085	305726	345628	
	252	01:52:48	7015198448	305730	345628	
	252	01:52:49	7017568812	305734	345628	
	252	01:52:50	7019939177	305740	345628	
	252	01:52:51	7022309541	305744	345628	
	252	01:52:52	7024679905	305748	345628	
	252	01:52:53	7027050269	305752	345628	
	252	01:52:54	7029420635	305756	345628	
	252	01:52:55	7031790999	305760	345628	
	252	01:52:56	7034161365	305764	345628	
	252	01:52:57	7036531729	305768	345628	
	252	01:52:58	7038902095	305772	345628	
	252	01:52:59	7041272461	305778	345628	2370366
	252	01:53:00	7043642827	305780	345628	2370366
	252	01:53:01	7046013195	305784	345628	2370368
	252	01:53:02	7048383561	305790	345628	2370366
Aircraft Contact →	252	01:53:03	7050753929	305794	345628	2370368
	252	01:53:04	7053124295	305798	345628	2370366
	252	01:53:05	7055494662	305800	345628	2370367
	252	01:53:06	7057865029	305804	345628	2370367
	252	01:53:07	7060235397	305808	345628	2370368
	252	01:53:08	7062605765	305814	345628	2370368
	252	01:53:09	7064976133	305818	345628	2370368
	252	01:53:10	7067346501	305822	345628	2370368
	252	01:53:11	7069716869	305826	345628	
Stop Run 5 →	252	01:53:12	7072087239	305830	345628	
	252	01:53:13	70764763	305834	345628	
	252	01:54:02	7190605937	306036	345628	
	252	01:55:02	7332829111	306290	345628	
	252	01:56:02	7475053142	306534	345628	
Start Run 6 →	252	01:57:02	7617278019	306784	345628	
	252	01:57:16	7650463941	306844	345628	
	252	01:57:17	7652834367	306848	345628	
	252	01:57:18	7655204792	306852	345628	

Table 2. Exercise result data

Run No.	Aircraft altitude, k ft	Antenna azimuth, deg	Aircraft run-in times, GMT			TV screen	
			Over Murrumbidgee or ridge	in beam (TV)	Over antenna	Sighted	Appraisal of run
1	1	085	01:28:28	01:28:58	01:29:07	No	—
2	1	084	01:33:00	01:33:32	01:33:40	No	—
3	1	083	01:42:44	01:43:21	01:43:28	Port wing NW of boresight	Good
4	1	082	01:47:35	01:48:14	01:48:20	Port wing tip NW of boresight	—
5	1	081	01:52:28	01:53:04	01:53:10	Complete aircraft on boresight	Excellent
6	1	080	01:57:13	01:57:45	01:57:50	Port wing tip NW of boresight	—
7	1	079	02:01:49	02:02:26	02:02:32	No	—
8	1	079	02:06:44	02:07:23	02:07:28	Complete aircraft on boresight	Excellent
9	1	078	02:11:22	02:12:00	02:12:08	Port wing and engine NW of boresight	Good
10	3	077	02:19:24	02:19:50	02:20:15	No	—
11	3	075	02:28:50	02:29:33	02:29:46	No	—
12	1	358	05:37:50	05:38:37	05:38:40	Port wing tip W of boresight	—
13	1	354	05:42:04	05:43:02	05:43:05	Port wing tip W of boresight	—
14	1	350	05:46:44	05:47:48	05:47:50	Starboard wing, engine E of boresight	Good
15	1	346	05:51:02	05:51:54	05:51:55	No	—
16	1	343	05:54:55	05:56:06	05:56:10	Complete aircraft on boresight	Excellent
17	1	342	05:59:17	06:00:09	06:00:10	Port wing, engine, body just W of boresight	Very good
18	2	339	06:04:14	06:05:00	06:05:02	Port wing and engine W of boresight	Good
19	2	336	—	—	06:09:15	No	—
20	2	333	06:12:24	06:13:29	06:13:30	No	—
21	1.5	330	06:21:09	06:22:14	06:22:15	Starboard wing E of boresight	Good
22	1.5	327	06:26:15	06:26:55	06:26:56	Starboard wing tip E of boresight	—
23	1.5	325	06:29:30	06:30:18	06:30:19	Port wing W of boresight	Good
24	1.5	323	06:33:32	06:34:10	06:34:11	No	—

Analog instrumentation record								TDH record of doppler count	DIS record (based on 1/2 sec samples) of rcvr 2 dynamic AGC
Contact time, GMT	Rcvr 1 signal level, dbm	HA error, deg	DEC error, deg	Rcvr 2 dynamic AGC dbm	Period of rcvr 2 dynamic AGC disturbance, sec	Rcvr 3 signal level, dbm	Rcvr 2 out of lock, sec		
01:29:02	-136	—	—	-160 mean	—	-163	—	Steady	—
Transponder attenuator being removed during this run									
01:43:22	-101	+0.02	0	-162 dip	0.4	-163	—	Steady	—
01:48:18	-124	—	—	-158 mean	—	-163	—	Steady	—
01:53:05	> -101	-0.01	-0.01	« -168 dip	0.6	-164	0.3	Steady	—
01:57:00	-104	—	—	-158 mean	—	-162	—	Steady	—
02:02:28	-111	—	—	-158 mean	—	-163	—	Steady	—
02:07:23	> -101	0	0	< -168 dip	0.5	-164	—	Steady	5-db dip, -158 dbm mean
02:12:00	> -101	+0.04	-0.02	< -168 dip	0.3	-163	—	Steady	4-db dip, -158 dbm mean
02:20:00	—	—	—	-158 mean	—	-163	—	Steady	—
02:29:37	—	—	—	-158 mean	—	-163	—	Steady	—
05:38:38	-115	—	—	-162 mean	—	-162	—	Steady	5-db dip, -158 dbm mean
05:43:05	-115	—	—	-158 mean	—	-163	—	Steady	—
05:47:49	-103	—	—	-166 dip	0.2	-163	—	Steady	—
—	—	—	—	—	—	—	—	Steady	—
05:56:10	-101	+0.01	0	-168 dip	0.4	-163	—	Steady	7-db dip, -158 dbm mean
06:00:10	-101	0	+0.01	-164 dip	0.3	-163	—	Steady	4-db dip, -158 dbm mean
06:05:00	-105	0	0	-167 dip	0.2	-163	—	Steady	5-db dip, -158 dbm mean
—	—	—	—	—	—	—	—	Steady	4-db dip, -158 dbm mean
—	—	—	—	—	—	—	—	Steady	4-db dip, -158 dbm mean
06:22:15	-106	0	-0.01	-164 dip	0.1	-163	—	Steady	3-db dip, -158 dbm mean
—	—	—	—	—	—	—	—	Steady	—
06:30:18	-101	+0.03	0	-159 dip	0.2	-162	—	Steady	—
06:34:10	-115	—	—	-158 dip	0.1	-163	—	Steady	—